DOCTOR OF PHILOSOPHY

Turbulence control of the properties and flux of suspended matter in a tide-stirred shelf sea

Sykes, Peter

Award date:
2008

Awarding institution:
Bangor University

Turbulence Control of the Properties and Flux of Suspended Matter in a Tide-Stirred Shelf Sea

A thesis submitted in accordance with the requirements of the University of Wales for the degree of Doctor of Philosophy

By Peter A. Sykes

University of Wales, Bangor,
School of Ocean Sciences,
Menai Bridge,
Gwynedd, LL59 5AB
U.K.

May 2008

Abstract.

Turbulence and sediment interactions have been studied widely over recent years, this work being mainly carried out in estuarine environments. Due to the development of instrumentation and processing techniques it is now possible to obtain good quality measurements of turbulence and sediment properties on the same temporal and spatial scales over reasonably long durations. Therefore, this study was designed to investigate the turbulence and sediment interactions over numerous tidal cycles at a shelf sea site. To this end the variation in suspended particulate matter (SPM) volume concentration, mass concentration and size, in conjunction with turbulent kinetic energy data, was investigated at a high energy tide-stirred site in the Irish Sea. The study site was located off the north-west coast of Anglesey and was notable for the presence of a turbid patch.

Initial conclusions drawn from harmonic analysis, entropy analysis, and graphs of particle numbers indicated that possible sediment dynamics mechanisms controlling SPM magnitude and variation at the site were: resuspension, aggregation, disaggregation and advection of the turbid patch. It was found that the range of sediment sizes present at the site could be described by 2 characteristic sediment size populations: one fine (~50μm diameter) and one coarse (150μm).

Two models were developed within the study to test these findings upon the 2 characteristic sediment size populations. The first, an advection model, which included no vertical mixing, was able to reproduce the underlying signal present within the observations (both in terms of magnitude and variability). This model was then incorporated into the second model which included turbulent vertical mixing, settling, erosion (resuspension) due to tidally generated shear stresses and turbulence controlled aggregation and disaggregation.

The full sediment dynamics model reproduced the variability and magnitude of the observations reasonably well. Small scale variability was also replicated by the model.

Sensitivity analysis was then performed on the model to quantify the relative importance of each of the sediment dynamics processes at the study site. Results showed that for both size populations the 2 mechanisms controlling the magnitude of the SPM mass concentrations are erosion (resuspension) and aggregation/disaggregation, erosion being dominant for the coarse population and aggregation/disaggregation being dominant for the fine population. In terms of the variability, advection is by far the dominant mechanism for controlling the coarse population. Aggregation/disaggregation and advection control most of the variability in the fine population at this site.

Acknowledgements.

My sincere thanks must go to my supervisors, Colin Jago, Sarah Jones and Tom Rippeth for all their help during my PhD. They have been a constant source of guidance, support and encouragement without which I would not have been able to produce this thesis.

I would also like to say a special thanks to Dave Bowers for his time and assistance with the modelling process. In addition, thanks must go to Ole Mikkelsen for his assistance with the entropy analysis, Philip Wiles for his assistance with the ADCP data and Matthew Palmer for his help with the FLY data.

A big thanks must go to Ben Powell for his technical support and friendship during both the cruises and throughout my PhD. My sincere thanks also go to Anne Hammerstein and Ray Wilton for their technical support and the Captain and crew of the RV Prince Madog.

Special thanks go to Elizabeth Kyte for all her help and friendship throughout my PhD.

Thanks have to go to all the people who supported me both intellectually and socially during my PhD: Neil Fisher, Katherine Ellis, Barbara Berx, Graham Worley and Caroline Duce.

I must also thank my parents and family for their support.

During this PhD I have been financially supported by NERC, for which I am grateful for this opportunity to study.

Contents.

Abstract. ii
Acknowledgements. iv
List of Figures. viii
List of Tables xi
Chapter 1 1
Introduction. 1
1.1 Background and Motivation for Study. 1
1.2 Aims Of The Project 2
1.3 Thesis Structure 3
1.4 The Site. 3
1.4.1 Location. 3
1.4.2 Turbid Patch. 4
1.5 Originality. 6
Chapter 2 7
Turbulence. 7
2.1 Introduction. 7
2.2 Reynolds Numbers. 9
2.3 Reynolds Stresses 10
2.4 Shear Stress. 12
2.5 The Bottom Boundary Layer. 14
2.6 The Drag Coefficient. 15
Chapter 3 17
Suspended Sediments. 17
3.1 Introduction. 17
3.2 Erosion and Resuspension of SPM. 18
3.2.1 Cohesive Sediment 18
3.2.2 Non-Cohesive Sediment. 20
3.3 Deposition of SPM – Settling Velocity. 21
3.4 Aggregates and Flocs 22
3.5 Summary. 29
Chapter 4 30
The Experiment. 30
4.1 Introduction. 30
4.2 The Experiment. 30
4.2.1 Hydrodynamic Description. 30
4.2.2 The Programme and Deployed Instrumentation. 31
4.3 Instrumentation. 34
4.3.1 The ADCP. 34
4.3.1.1 Description. 34
4.3.1.2 Velocity Measurements. 34
4.3.1.3 Turbulence Measurements. 35
4.3.1.4 Errors And Uncertainties. 36
4.3.2 The FLY. 37
4.3.2.1 Description. 37
4.3.2.2 Turbulence Measurements. 38

4.3.3 The LISST-100C.....39
4.3.3.1 Description.....39
4.3.3.2 Particle Size/Concentration Measurements.....40
4.3.3.3 Calibration and Processing Techniques.....41
4.3.3.4 Errors And Uncertainties.....42
4.3.4 The CTD.....43
4.3.4.1 Description.....43
4.3.4.2 The Fluorometer.....44
4.3.4.3 The Transmissometer.....45
4.3.5 Gravimetric Analysis.....46
Chapter 5.....48
Results.....48
5.1 Introduction.....48
5.2 The Gradient.....48
5.2.1 Volume Concentration and Median Diameter.....48
5.2.2 Mass Concentration.....50
5.2.3 Temperature, Salinity and Chlorophyll.....53
5.3 The Time Series.....54
5.3.1 Velocity.....54
5.3.2 Turbulence.....57
5.3.3 SPM Results.....59
5.3.4 Gravimetric Data.....60
5.4 Summary.....61
Chapter 6.....62
Analysis and Discussion.....62
6.1 Introduction.....62
6.2 Harmonic Analysis.....62
6.2.1 Introduction.....62
6.2.2 Velocity.....62
6.2.3 SPM.....63
6.3 Entropy Analysis.....65
6.4 Particle Numbers.....68
6.4.1 Description.....68
6.4.2 Fine – 53.7μm.....70
6.4.2.1 Maxima.....70
6.4.2.2 Minima.....72
6.4.3 Coarse – 157μm.....72
6.4.3.1 Maxima.....72
6.4.3.2 Minima.....73
6.4.4 Total Particle Numbers.....73
6.5 Particle Fluxes.....75
6.6 Summary.....76
Chapter 7.....78
Modelling.....78
7.1 Introduction.....78
7.2 Advection Model.....79
7.2.1 Description.....79
7.2.2 Ship Position Corrected Model.....80

7.2.3 Model Results.....81
7.3 Sediment Dynamics Model. 84
7.3.1 Description. 84
7.3.2 Model Results.....89
7.3.3 Sensitivity Analysis.....93
7.3.3.1 The Tuneable Parameters.....93
7.3.3.2 The Model Components.....97
7.3.3.2.1 Advection Component.....97
7.3.3.2.2 Aggregation & Disaggregation Component.....99
7.3.3.2.3 Resuspension (Erosion) Component. 101
Chapter 8.....104
Summary and Discussion.....104
8.1 Discussion. 104
8.2 Future Work. 112
References. 116

List of Figures.

Figure 1.01	Location of observational site	4
Figure 1.02	Satellite image of observational site	5
Figure 3.01	The relationship between floc modal diameter, mass concentration and shear stress	27
Figure 4.01	Map of the transect sampling locations	32
Figure 4.02	The ADCP	34
Figure 4.03	The FLY	37
Figure 4.04	The LISST-100C	39
Figure 4.05	Internal of LISST-100C	40
Figure 4.06	CTD deployment	43
Figure 4.07	A Niskin bottle	46
Figure 5.01	Variation and gradients in SPM volume concentration and median SPM diameter	49
Figure 5.02	Gradient in mass concentration calculated by gravimetric analysis	51
Figure 5.03	Transmissometer calibration plot	51
Figure 5.04	Gradient in mass concentration using the calibrated transmissometer	52
Figure 5.05	Gradient in salinity	53
Figure 5.06	Gradient in temperature	53
Figure 5.07	Gradient in chlorophyll concentration	54
Figure 5.08	Time series of free surface, depth averaged velocity, tidal excursion, TKE production and dissipation	56
Figure 5.09	Vertical structure time series of TKE production and turbulent dissipation	58
Figure 5.10	Depth averaged time series of volume concentration and median SPM diameter	59
Figure 5.11	Time series of mass concentration at 3 depths	60

Figure 6.01	Harmonic analysis results	64
Figure 6.02	Grouped size distribution spectra from the LISST	67
Figure 6.03	Time series of spectral groups produced by entropy analysis and time series of median SPM diameter	68
Figure 6.04	Time series of number of particles in 53.7 μm and 157μm size classes	69/70
Figure 6.05	Time series of total particle numbers	74
Figure 6.06	Net flux of fine and coarse particles over 2 tidal cycles	76
Figure 7.01	Schematic of the ship position corrected advection model	81
Figure 7.02	Results of advection model compared to observations	82
Figure 7.03	Schematic describing the model components for 2 size classes	88
Figure 7.04	Profiles of observed and modelled fine mass concentration	90
Figure 7.05	Profiles of observed and modelled coarse mass concentration	91
Figure 7.06	Results of sediment dynamics model compared to observations	92
Figure 7.07	Results of sensitivity analysis (variability)	94
Figure 7.08	Results of sensitivity analysis (magnitude)	95
Figure 7.09	Model results compared to observations with advection component turned off	98
Figure 7.10	Model results compared to observations with the aggregation/disaggregation component turned off	100
Figure 7.11	Model results compared to observations with the erosion component turned off	103
Figure 8.01	Relative importance of the 3 main model components upon variability and magnitude	111

Figure 8.02	Observed median SPM diameters in June 2004	114
Figure 8.03	Observed median SPM diameters in February 2004	115

List of Tables.

Table 4.01	Inventory of the data collected with each instrument	33
Table 8.01	Relative importance of the 3 main model components upon variability and magnitude	110

Chapter 1

Introduction.

1.1 Background and Motivation for Study.

A shelf sea is the stretch of water that extends from the shorelines of our coasts to the shelf break at the edge of the continental shelf and such a shelf sea is the critical interface between the terrestrial and the oceanic environments. Shelf seas are characterised by shallow waters, typically of about 50 to 200 metres in depth.

Although, by area, the shelf seas only constitute 8% of the world's oceans (Thomas et al. 2004), they are an extremely important part of our environment as they are used extensively for a variety of applications, e.g. as a food source, for the disposal and dispersal of wastes, for recreation, as a source of materials and minerals etc. They are the most energetic part of the oceans in relation to currents (tidal, wind-driven, density-driven etc.) with 2.6TW of the total global tidal energy flux (3.5TW) being dissipated in the bottom boundary layers of the shelf seas (Munk and Wunsch, 1998). As a result they are highly active in terms of transport and re-working of sediments and nutrients, in relation to biological production (10-30%) and in relation to biological growth (Wollast, 1998). Therefore, a high level of understanding of how the shelf sea system functions and the possible effects that anthropological, as well as natural activity, have upon the system is necessary in order for us to manage the shelf seas correctly.

The process of sediment transport as a whole in our shelf seas is of general importance as it is an important mechanism in many processes within the shelf seas. Sediment transport controls the erosion of our coasts and beaches as well as controlling the in-filling of our harbours and estuaries. The magnitude of suspended sediment concentration within the water column has consequences for the water clarity and also the light levels, which in turn affects biological processes. Sediment transport is also an important mechanism by which

pollutants are removed from or distributed around our coastal waters which consequently can affect how pollutants enter the food chain. Another topical importance of sediment transport is the role it plays in the draw down and storage of carbon dioxide from the atmosphere (Ittekkot et al., 1992).

The main source of energy within the shelf seas is that brought about by the forcing of the tide on and off the shelf every tidal cycle (2.6TW of the total 3.6TW) with the energy input of wind being approximately 1TW globally (Munk and Wunsch, 1998, Wunsch, 1998). The tides can create strong tidal currents in certain parts of the shelf, which have consequences for sediment transport, erosion and deposition mechanisms.

As a result of these currents, turbulence is produced throughout the water column and normally greatest at the bed due to the friction of the flow over the bed known as bed shear stress (see Chapter 2). The magnitude of the turbulence is dependent upon a number of factors: 1) the magnitude of the current velocity involved, 2) the roughness of the bed over which the flow passes, 3) the viscosity of the fluid in which the turbulence is created and any factors that may affect the viscosity.

Therefore, if sediment transport mechanisms are to be fully understood there is a need for investigation into the turbulent environment and the interplay between this and the suspended sediment so that modelling and management of the shelf seas may be carried out effectively.

1.2 Aims Of The Project.

The aim of this project was to improve the understanding of the interactions between tidally driven turbulence and suspended sediments within the water column of a typical shelf sea environment. To this end a good quality dataset of turbulence and suspended sediment parameters was collected at a high energy site in the Irish Sea on comparable spatial and temporal scales. This has allowed

qualitative and quantitative conclusions to be drawn between the 2 properties. This dataset has then been used to develop a model which simulates turbulence/velocity driven sediment transport. The model includes the main processes which appear to be taking place at the site. The results from this model have then been compared with the collected dataset for calibration and conclusions have been drawn about the relative influence of various sediment transport mechanisms upon the suspended sediment.

1.3 Thesis Structure.

In the next subsection (1.4) an introduction to the study area will be outlined, including a description of its location, the general hydrodynamic situation and any interesting features of the area. Chapter 2 provides an introduction to present turbulence theory and chapter 3 provides an introduction to suspended sediment theory along with descriptions of important sediment dynamics mechanisms as well as theories on turbulence and suspended sediment interactions. Chapter 4 provides a description of the observational programme followed by an outline of the deployed instrumentation and data processing techniques. In chapter 5 the initial results are presented followed by analysis and initial discussions in chapter 6. Chapter 7 then describes 2 models developed and presents the results of these models with conclusions and discussions outlined in chapter 8.

1.4 The Site.

1.4.1 Location.

A site off the north-west coast of Anglesey, Wales (UK), was selected; its exact location was 53°28'N 4°32'W. The site location is positioned such that it may be influenced by processes in the Irish Sea as well as Liverpool Bay (Fig. 1.01).

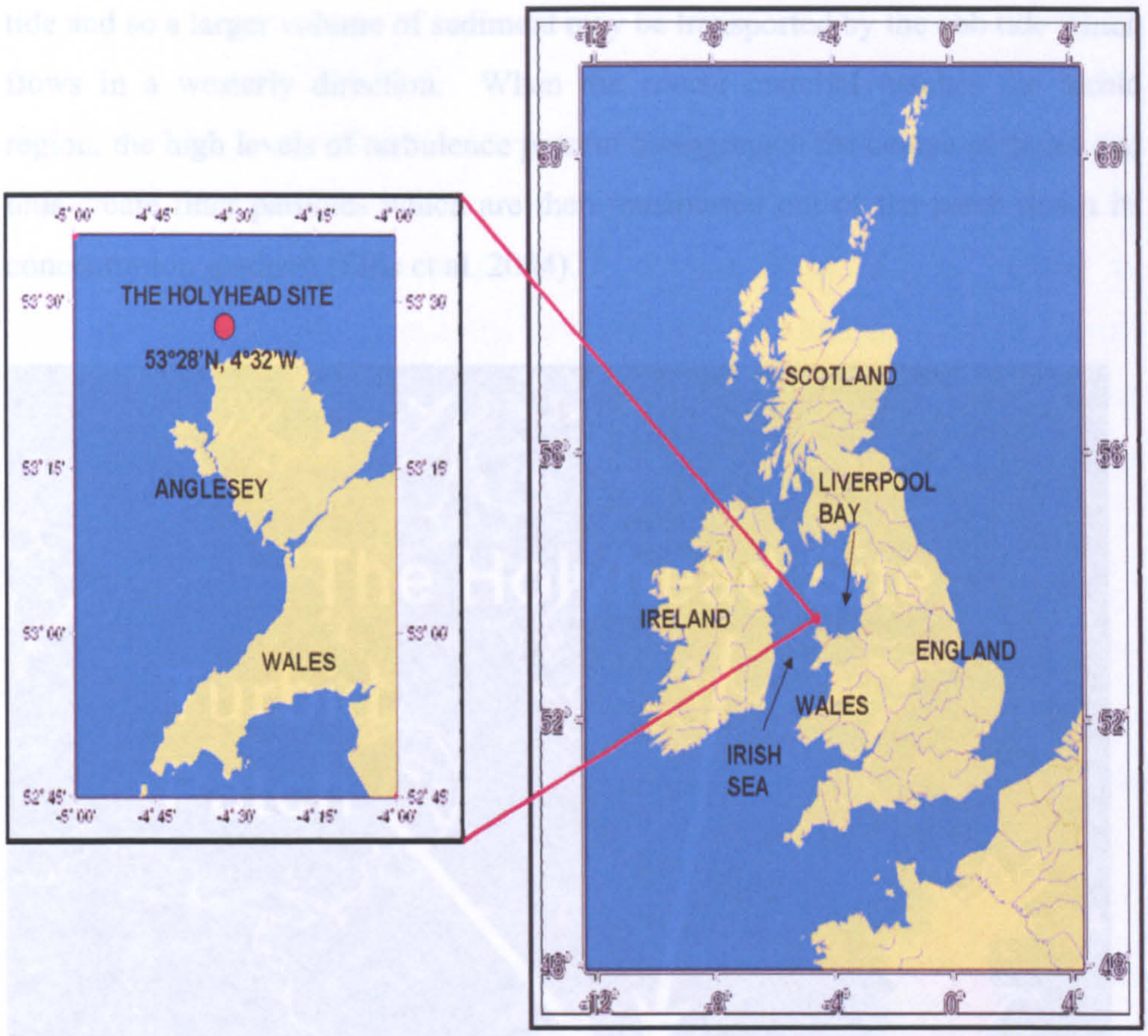

Fig. 1.01 The location of the observational site (courtesy of http://woodshole.er.usgs.gov/mapit/index.html)

This site was selected as other authors have found it to be of interest in terms of turbulence and sediments (Ellis et al., 2004; Bowers et al., 2002, 2005) as it is a high energy site with relatively high sediment concentrations.

1.4.2 Turbid Patch.

It has also been observed in the vicinity of the site that a turbid patch is present (Fig. 1.02). This patch is maintained by the dynamics of the area (Ellis et al. 2004; Bowers et al., 2005). Coarse material from Liverpool Bay is transported out to the location of the maxima down a concentration gradient of sediment. In addition, due to the tidal asymmetry, a westward volume flux of material occurs towards the turbid patch. The ebb tide lasts for a greater duration than the flood

tide and so a larger volume of sediment may be transported by the ebb tide which flows in a westerly direction. When the coarse material reaches the turbid region, the high levels of turbulence present disaggregate the coarse particles and thus create finer particles which are then transported out of the patch down its concentration gradient (Ellis et al. 2004).

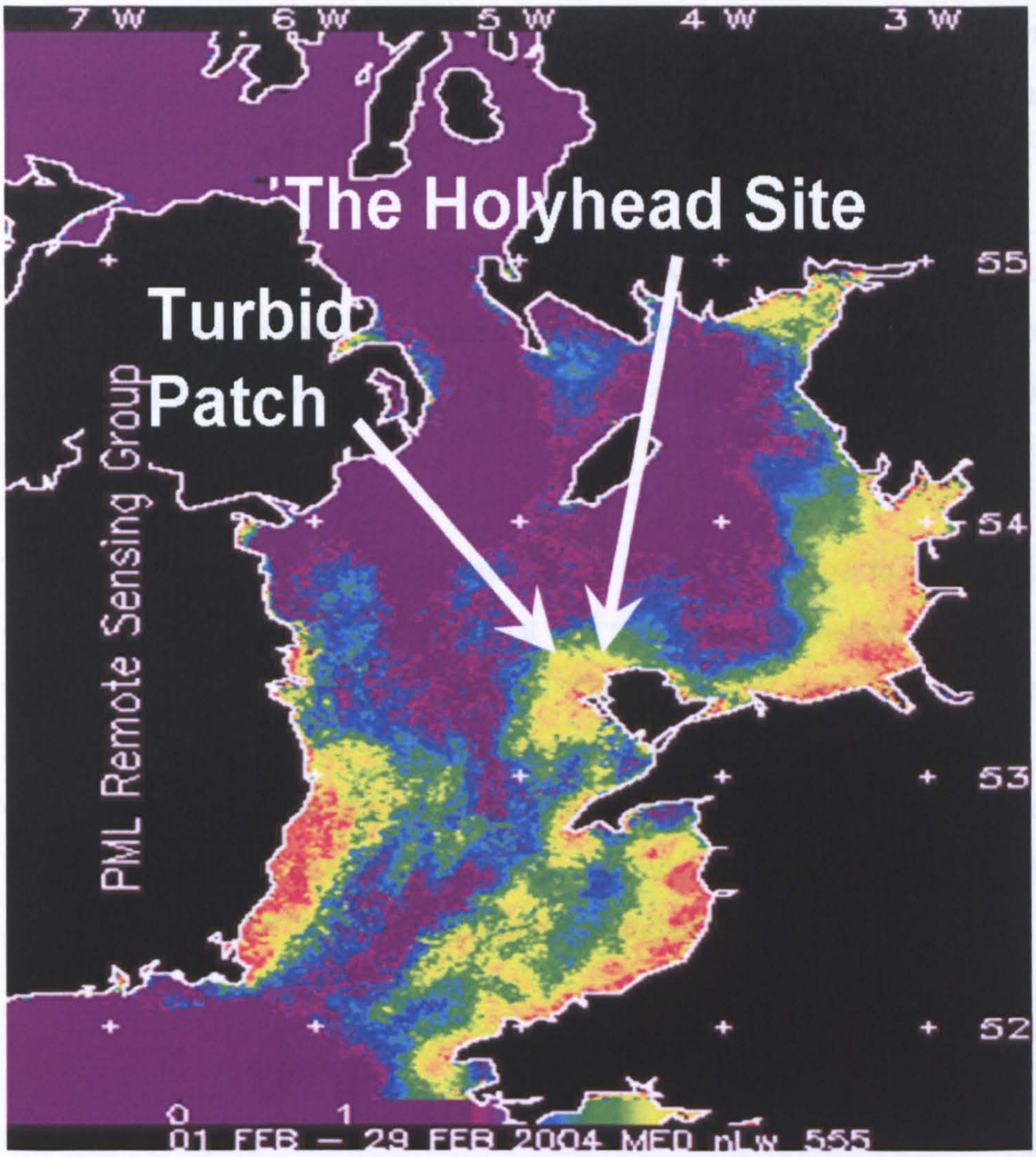

Fig. 1.02 The location of the turbid patch (seen here in orange/red) in relation to the observational site from a SeaWiFS composite image of the Irish Sea showing normalised water leaving radiance at 555nm for February 2004 (courtesy of the NERC, PML Remote Sensing Group and RSDAS).

1.5 Originality.

Previous studies in this area have shown the existence of a self-maintaining gradient in suspended sediment properties due to the local variations in tidal and turbulent conditions (Ellis et al. 2004; Bowers et al., 2005). Other studies elsewhere have found correlations between sediment mechanisms and turbulence parameters such as resuspension, aggregation/disaggregation, settling etc (Kawanisi and Yokosi, 1997; Bowers, 2003; Bowers et al., 2005; Fugate and Friedrichs, 2002, 2003).

Therefore, the hypothesis to be tested is whether the characteristics and variability of the suspended sediment at this site are dominated by resuspension and disaggregation mechanisms as a result of the high levels of turbulence present at the site.

This study differs from others carried out in this area due to the quality and quantity of measurements of turbulent and sediment parameters taken in situ on the same temporal and spatial scales. The associated model development has incorporated a range of sediment transport processes in order to qualify and quantify the variations in suspended sediment at a fixed location in a shelf sea. Further sensitivity analysis has been carried out in order to indicate the significance of both "empirical" parameters and discrete processes.

Chapter 2

Turbulence.

2.1 Introduction.

Turbulence is a common phenomenon in the environment which can be easily observed on a daily basis. Be it lurching experienced during a flight in an aircraft or the swirling waters behind a rock in a fast flowing river, these events are turbulent and governed by the processes of turbulence.

Unfortunately, turbulence is one of the most complicated types of fluid motion to study; however, it is an extremely important property of flow to investigate as most flows in nature are turbulent (Bradshaw, 1971). Clifford, French and Hardisty (1993) commented that turbulence is one of the least studied and understood phenomena in the earth sciences; this hinders the development of realistic, physically based, models of sediment transport both in the atmosphere and in the world's oceans. Therefore, if we wish to be able to understand and even predict the fluid dynamics of nature, be it atmospheric flows of weather patterns or currents and eddies in the oceans, then we must study and increase our knowledge of the nature of turbulence and its consequences.

An early pioneer of turbulence theory was the physicist Geoffrey I Taylor who introduced the concept of a mixing length in understanding evolution of turbulence. He also introduced the idea of a correlation function of turbulent diffusion. This explains the motion of a particle in relation to a random walk. Initially, particles diffuse away (by turbulence) from their source in proportion to time. Only when the patch size is much larger than the largest scale eddy do the particles diffuse in proportion to the square root of time, i.e. by Fickian diffusion (Taylor, 1921). Taylor later produced papers on the statistical theory of turbulence and these formed the basis for the future statistical approach taken.

Two other key contributors to the understanding of turbulence were Prandtl (1925) and von Karman (1930). Together during the mid/late 1920's they furthered Taylor's work on mixing lengths to produce mixing length theory, one of the most notable of the semi-empirical theories of turbulence.

Richardson (1922) proposed the theory that energy is transferred from large to small scale eddies and then is ultimately dissipated by viscous dissipation. This formed the basis of what became known as the spectral energy cascade.

Before the mathematics and the physics of turbulence are investigated, it is necessary to establish the formal characteristics of turbulent flows. Turbulence is not a feature of a given fluid; rather it is a feature of fluid flows. All turbulent flows are random, chaotic or irregular, in nature. Thus turbulent flow study has to be of a statistical approach rather than a deterministic approach in which the output is determined by the input. Turbulent flows also possess high levels of three-dimensional, fluctuating vorticity as turbulence is three-dimensional and rotational. The vorticity structures observed are eddies which vary in size. The energy contained within these eddies is passed down from the large scale eddies to the small scale eddies by nonlinear interactions until the energy is dissipated by viscous dissipation. This process is known as vortex stretching and it is the method by which three-dimensional (not two-dimensional) flows maintain their vorticity. Turbulent motions induce diffusion, thus rapid mixing can occur and there are increased rates of heat, mass and momentum transfer. These rates of transfer can be many orders of magnitude greater than the rates of transfer due to molecular diffusion. This is possibly one of the most important features of turbulence and it is this feature that makes the study of turbulence and turbulent flows very important.

All turbulent flows are dissipative; the viscous shear stress within the turbulent flow increases the internal energy of the fluid but decreases the overall kinetic energy of the turbulence (see section 2.4). This process is carried out during vortex stretching. As a result, turbulent flows require a continuous input of

energy to oppose the effects of the viscous stresses in order to maintain the turbulence. If this energy supply is non-existent or insufficient then the turbulence rapidly decays and turbulent flow would become laminar flow. Turbulent flows occur at high Reynolds numbers (see section 2.2). For the turbulence to be maintained the Reynolds number must remain above a particular value.

2.2 Reynolds Numbers.

Reynolds (1883) was one of the earliest experimenters and researchers of turbulence. He carried out pipe flow experiments which showed that turbulence occurred once a parameter exceeded a critical value. This parameter is what became known as the Reynolds number. Thus, the Reynolds number of a flow is used to determine whether the flow is laminar (constant with depth) or turbulent. The Reynolds number is a dimensionless parameter that compares the inertia forces with the viscous forces. However, this can cause confusion when the Reynolds numbers are high because the viscous and other diffusion effects take place on smaller length scales than the inertia effects. Therefore, it is less confusing to think of Reynolds numbers as a ratio of a turbulence time scale to a molecular time scale (Tennekes and Lumley, 1972):

$$R_e = \frac{VL}{\upsilon} \qquad (Eq.\ 2.01)$$

where: V = a velocity scale,

L = a length scale,

υ = kinematic viscosity = dynamic (absolute) viscosity (μ) / density (ρ).

The critical Reynolds number for the onset of turbulence is dependent upon the situation in which the flow occurs; within circular pipes the critical Reynolds number is typically between 2000 and 3000 (Kanda, 1999).

2.3 Reynolds Stresses.

Reynolds also developed the idea of decomposing a turbulent velocity flow into a mean component, $\bar{u}$, which slowly varies with time and a more rapidly fluctuating, time-dependent component, u'. This method of decomposition was termed the Reynolds decomposition in honour of Osborne Reynolds himself and has been extended to other properties of turbulent flows such as temperature, pressure etc.

Applying the Reynolds decomposition to the velocity variable as mentioned previously gives the velocity at any particular time as: $u_i = \bar{u}_i + u_i'$. By definition the time mean of the velocity (or turbulent) fluctuations is equal to zero, i.e.: $\overline{u_i'} = 0$.

The development of the Navier-Stokes equations was an extremely important result. The Navier-Stokes equations express Newton's second law for a Newtonian fluid (a fluid with a constant viscosity regardless of shear). Eq. 2.02 shows the Navier-Stokes equation for flow in the x direction.

$$\frac{\partial u_i}{\partial t} + u_j \frac{\partial u_i}{\partial x_j} = -\frac{1}{\rho}\frac{\partial p}{\partial x_i} + \upsilon \frac{\partial^2 u_i}{\partial x_i \partial x_j} \qquad (Eq.\ 2.02)$$

where: t = a time scale,

ρ = density of seawater (~1025 gm^{-3})

p = pressure

u = the velocity component in the x-direction

i,j,k = the i,j,k dimensions.

The Navier-Stokes equations (Eq. 2.02) may now be written in terms of the flow decompositions so that after averaging we obtain an equation that includes the turbulent fluctuations (Eq. 2.03). When the Navier-Stokes equations take this form they are known as the Reynolds equations.

$$\frac{\partial \bar{u}_i}{\partial t} + \bar{u}_j \frac{\partial \bar{u}_i}{\partial x_j} = -\frac{1}{\rho}\frac{\partial \bar{p}}{\partial x_i} + \upsilon \frac{\partial^2 \bar{u}_i}{\partial x_j^2} - \frac{\partial}{\partial x_j}\overline{(u_i' u_j')}. \qquad (Eq.\ 2.03)$$

The final term of this equation describes the action of the turbulent fluctuations on the mean flow. The right-hand side of the Reynolds equation may also be written in the form:

$$-\frac{1}{\rho}\frac{\partial \bar{p}}{\partial x_i}+\frac{1}{\rho}\frac{\partial}{\partial x_j}\left[\mu\frac{\partial \bar{u}_i}{\partial x_j}-\rho\overline{(u_i'u_j')}\right]. \qquad \textit{(Eq. 2.04)}$$

It can be seen then that the Reynolds decompositions give rise to additional turbulent stresses upon the mean flow of the form: $-\rho\overline{(u_i'u_j')}$. These stresses are known as Reynolds stresses. They arise due to the fact that, although the time mean of the turbulent fluctuations is zero by definition, the time mean of their squares and mixed products is not (Clifford, French and Hardisty, 1993). These stresses occur in all three dimensions and so they are present in the Reynolds equations for each direction. These terms are typically larger than the viscous terms. The Reynolds stresses describe the turbulent flux of momentum and consist of one normal and two tangential turbulent stresses for each direction (Campbell, 1996). Using the Cartesian velocity components u, v and z to represent the velocity in the x, y and z directions, the nine components of Reynolds stress are presented in Eq. 2.05.

$$\begin{aligned}
&\text{x direction}: -\rho\overline{(u')^2}, -\rho\overline{(u'v')}, -\rho\overline{(u'w')}\\
&\text{y direction}: -\rho\overline{(v')^2}, -\rho\overline{(v'u')}, -\rho\overline{(v'w')} \qquad \textit{(Eq. 2.05)}\\
&\text{z direction}: -\rho\overline{(w')^2}, -\rho\overline{(w'u')}, -\rho\overline{(w'v')}
\end{aligned}$$

where: u = velocity component in the x-direction,

v = velocity component in the y-direction,

w = velocity component in the z-direction.

This can be expressed in tensor form (Eq. 2.06) and is called the Reynolds stress tensor (Kundu, 1990). For turbulence generated by shear predominantly along the x-axis, it is usual that the r.m.s. values u', v' and w' of the three velocity components decrease with respect to one another, i.e. $u' > v' > w'$ (Soulsby, 1981).

$$\begin{bmatrix} -\rho\overline{(u')^2} & -\rho\overline{u'v'} & -\rho\overline{u'w'} \\ -\rho\overline{u'v'} & -\rho\overline{(v')^2} & -\rho\overline{v'w'} \\ -\rho\overline{u'w'} & -\rho\overline{v'w'} & -\rho\overline{(w')^2} \end{bmatrix} \qquad (Eq.\ 2.06)$$

2.4 Shear Stress.

In most natural flows the production of turbulence (i.e. turbulent kinetic energy or TKE) is through shear of the mean flow known as shear stress (Michallot and Mory, 2004). Shear stress is produced as a result of two adjacent fluid layers flowing over one another (i.e. parallel) with different flow rates, i.e. the difference (or shear) in velocity with height. The symbol to denote shear stress is τ. Shear stress is present throughout the water column if the fluid flow is not uniform with depth, and so is generated between infinitesimal layers throughout the water column.

Often the most important shear stresses are the stresses produced as a result of a tidal flow flowing over the stationary bed; these stresses are known as bed shear stresses. Bed shear stress is defined as the frictional force exerted by the flow per unit area of bed and is represented by the symbol τ_b. When the current, and therefore the stress, reaches a critical or threshold value, then some of the bed material may be eroded and carried up into suspension by the flow. Thus a suspended sediment layer is formed (see chapter 3). The value at which the erosion is initiated is called the threshold or critical bed shear stress and is represented by the symbol τ_c.

The bed shear stress has a number of different formulations. One such formulation for the bed shear stress in laminar flow is to relate it to the velocity gradient, i.e. (Soulsby, 1997):

$$\tau_b = \rho\nu \left.\frac{\partial u}{\partial z}\right|_{z=0} \qquad (Eq.\ 2.07)$$

Another formulation of the bed shear stress in turbulent flow is the quadratic drag law:

$$\tau_b = \rho\, C_D \overline{U}^2 \qquad (Eq.\ 2.08)$$

where: C_D = the drag coefficient (see section 2.6)

$\overline{U}$ = depth-averaged velocity.

The bed shear stress may be expressed in turbulent flows in terms of the Reynolds stress (Soulsby, 1981; Kim et al., 2000; Fugate and Friedrichs, 2003):

$$\tau_{xz} = -\rho\, \overline{u'w'} = \rho\, K_{xz} \frac{\partial \overline{u}}{\partial z} \qquad (Eq.\ 2.09)$$

where: $K_{xz} = \kappa\, u_* z$ = a height-independent eddy viscosity

κ = von Karman's constant = 0.40.

Another way of defining the bed shear stress is through the relationship of the friction velocity (or shear velocity), u_*, (Adams and Weatherly, 1981):

$$\tau_b \equiv \rho\, u_*^2 \qquad (Eq.\ 2.10)$$

where: u_* = friction velocity.

The friction velocity is purely mathematical as it does not correspond to a 'real' velocity in the flow, although it can be related to the turbulent fluctuations in the real velocity components (Soulsby, 1997); it characterises the shear at the boundary. It is commonly calculated by rearrangement of Eq. 2.10. Near the bed, for turbulent flow the friction velocity can also be estimated using the near bed Reynolds stress (Soulsby, 1983; Kim et al., 2000; Fugate and Friedrichs, 2002; Voulgaris and Meyers, 2004):

$$u_* = \sqrt{-\overline{u'w'}}\,. \qquad (Eq.\ 2.11)$$

For non-cohesive sediments, i.e. sands, there exists just one critical bed shear stress for a sediment of a given grain size. However, for the cohesive sediments, i.e. muds, there are two critical values: one is the critical value for the initial erosion of the sediment; the other is a value for the onset of deposition.

Bottom shear stress and turbulence are key parameters for moving the sediment and keeping it in suspension (Fredsøe and Deigaard, 1992; Michallot and Mory, 2004), and it is these parameters which control the mechanism known as resuspension (see section 3.2).

2.5 The Bottom Boundary Layer.

The bottom boundary layer (BBL) is the region above the bed where the flow is measurably slower than the free stream mean velocity in the overlying water (Jumars, 1993). The velocity of the flow rapidly decreases to zero within the bottom boundary layer. The top of the bottom boundary layer is defined as being where the velocity approximately equals the free stream velocity or where $u(z,t) = 0.99u_\infty(t)$ (with $u_\infty(t)$ being the free stream velocity), (Nielsen, 1992, Jumars, 1993).

This layer can be thought of as a two-layer system: an inner layer which has strong velocity shear close to the bed, and an Ekman-like outer layer which comprises the remainder of the boundary layer. In the overlapping region between these two layers the velocity profile is logarithmic and for a vertically uniform density field is given as (Adams and Weatherly, 1981):

$$\bar{u} = \frac{u_*}{\kappa} \ln \frac{z}{z_0} \qquad (Eq.\ 2.12)$$

where: z_0 = the bed roughness length.

The roughness length, z_0, is related directly to the equivalent bed roughness k_s in the rough regime by (Nowell, Jumars and Eckman, 1980):

$$z_0 = k_s / 30 \qquad (Eq.\ 2.13)$$

In the context of flat granular beds k_s is commonly known as the Nikuradse roughness and many empirical expressions for k_s have been suggested; for a flat sandy bed k_s may range between $1.25D_{35}$ (Ackers and White, 1973) to $5.1D_{84}$ (Mahmood, 1971), Einstein and Barbarossa (1952) used $k_s = D_{65}$ whereas

Engelund and Hansen (1967) modified this to $2D_{65}$, Hey (1979) used $3.5D_{84}$ and $2.5D_{50}$ is also commonly used (Raudkivi, 1998). D_{35}, D_{50} and D_{85} are the lower, median and upper particle diameters respectively.

In the smooth regime, the roughness length is related to the shear velocity and the viscosity (Nowell, Jumars and Eckman, 1980):

$$z_0 = \nu / 9u_* \qquad (Eq.\ 2.14)$$

When considering sediment transport possibly the most important part of the water column is the bottom boundary layer. In this region of the water column there is a significant amount of interaction between the flow and the bed.

2.6 The Drag Coefficient.

In order to estimate hydrodynamic resistance of a suspended particle, knowledge of the drag coefficient is required (Li and Ganczarczyk, 1989; Wu and Lee, 1998). The drag coefficient is a function of the Reynolds number and the particle sphericity (Tambo and Watanabe, 1979; Namer and Ganczarczyk, 1993) and can therefore be expressed by the general form:

$$C_D = S/R_e \qquad (Eq.\ 2.15)$$

where: S = sphericity

$$R_e = \rho VL/\mu$$

μ = dynamic (absolute) viscosity ~ 1.08×10^{-3} Pa.s (at 20C) for water.

The drag coefficient, C_D, for a non-porous sphere in laminar flow is governed by (Eq. 2.16).

$$C_D = 24/R_e \qquad (Eq.\ 2.16)$$

This expression for the drag coefficient is widely accepted for cases when $R_e < 1$. However, it is also thought that it may still be acceptable for cases when $R_e > 1$, i.e. $100 > R_e > 1$ for porous flocs (Wu and Lee, 1998; Xia et al., 2004). Bushell et al. (2002) showed that the porosity of a floc can reduce the drag by allowing advection of the suspending medium through the floc structure. Increased porosity of a floc decreases its effective density.

Green and McCave (1995) found that, at a study site in the eastern Irish Sea, the mean drag coefficient at the bed was 0.0025. This is a value that has been widely used (Soulsby, 1983; Ziervogel and Bohling, 2003).

Chapter 3

Suspended Sediments.

3.1 Introduction.

The sea bed of the shelf seas consists of a variety of sediments. The sediments differ depending upon their size, their mineralogical composition, their density, the source from which they originated, their degree of cohesiveness and their shape.

Many of the characteristics of the sediments found at a particular location are dependent upon the magnitude of the tidal currents, the wave activity and the presence of any other currents. In areas of strong currents and/or wave activity the sediments consist of mainly sands and gravels known as non-cohesive sediments; and at locations of weak currents/wave activity there is a predominance of silts, clays and muds, known as cohesive sediments.

Sediments may be brought into suspension from the bed or they may begin by being in suspension if they are wind-borne. Suspended sediments (also known as seston or suspended particulate matter - SPM) are important carriers of trace metals, radionuclides and organic pollutants owing to their adsorptive capacity (Xia et al., 2004). For many contaminants, transport in particulate form constitutes up to 70% of the total transport (Eisma and Irion, 1988). As a result of this, pollutants in the sediments may become incorporated into the food web (Klamer et al., 1990) and so damage flora and fauna.

There are four sources of particulate matter found within the oceans: 1) land-borne sediment (from river discharge, coastal erosion, wind-borne etc.), 2) the sea bed itself, 3) primary production (and other biological processes) (Meade, 1972) and 4) anthropogenic (such as sewage discharge, industrial waste, tipping etc.).

The particulates in suspension, i.e. the SPM, can be single grain particles or they may have formed aggregates or flocs. Single grained particles and aggregates have different properties and behaviour. In addition SPM can be either inorganic particles (i.e. weathered rock fragments) or organic particles (either living or dead biological material) or a mixture of both.

3.2 Erosion and Resuspension of SPM.

It has already been commented that stresses at the sea bed, i.e. bed shear stresses, are an important consequence of turbulence and so it follows that a significant proportion of the sedimentary material found within the water column (in high energy regimes) originates from 'localised' bed erosion.

The mechanisms for erosion and resuspension of SPM depend upon whether the sediment is cohesive (muds) or non-cohesive (sands).

3.2.1 Cohesive Sediment.

There are a number of erosion mechanisms that may take place at a bed comprised of cohesive sediment. Mehta (1991) identified four of these methods of erosion. These are:

1. **surface erosion,** whereby particles are removed from the surface by the weakening of the attractive bonds between the particles
2. **mass erosion,** whereby parts of the bed are stripped away as a whole
3. **bed fluidisation,** whereby a muddy bed becomes more fluid than particle based
4. **entrainment of fluidised mud,** whereby the fluidised bed "diffuses" into the water column.

In terms of a critical bed shear stress for the erosion of cohesive sediment there is at present no general agreement upon a general value for this threshold as the critical value is likely to be site specific (Le Hir et al., 2007). However, Le Hir et

al. (2007) stated that for a consolidating bed the critical stress is between 0.1 and 1Pa; but, for a consolidated bed the critical bed stress may be a factor of 10 greater.

Another important parameter to consider in terms of bed erosion is the erosion rate (erodibility) or flux (E). Many formulations for this have been suggested by various authors, however there is little agreement upon the appropriate formulation as knowledge of the erosion rate of sediment is poor (Le Hir et al., 2007).

The erodibility of cohesive sediment is much more complicated than the erodibility of non-cohesive sediment as it depends upon the stage of consolidation of bed material. There are three stages:

1) for freshly deposited cohesive sediment (or fluid mud), there is no critical erodibility and so the erosion is calculated as an entrainment of sediment by the water above,

$$\text{e.g. } E = V_e C_{mud} \qquad (Eq.\ 3.01)$$

where: V_e = the entrainment velocity (a function of a Richardson number that quantifies the intensity of stratification (Odd and Cooper, 1989)

C_{mud} = the dry density of the surface sediment.

2) for consolidating mud, an expression which accounts for a rapid limitation of the erosion rate as the critical bed shear stress (τ_c) increases with depth was suggested by Parchure and Mehta (1985):

$$E = E_0 \exp\left(\alpha[\tau_b - \tau_c(z)]^{\beta}\right) \qquad (Eq.\ 3.02)$$

where: E_0 = a function of sediment density (ρ_s) and median SPM diameter (D_{50})

α,β = empirical constants.

3) For fully consolidated beds the Partheniades law is used:

e.g. $E = E_0\left(\frac{\tau_b}{\tau_c} - 1\right)$ *(Eq. 3.03)*

3.2.2 Non-Cohesive Sediment.

In terms of non-cohesive sediments, the main erosion mechanism is surface erosion. This is controlled by the bed shear stresses as mentioned previously (Chapter 2.4).

The critical bed shear stress for the initiation of movement (i.e. erosion) can be approximated by Eq. 3.04 as stated by Soulsby (1997) and Le Hir et al. (2007).

$$\tau_c = g(\rho_s - \rho)D_{50}\left\{\frac{0.3}{1+1.2D_*} + 0.055[1 - \exp(-0.02D_*)]\right\} \qquad \textit{(Eq. 3.04)}$$

where: g = acceleration due to gravity ~ $9.81 ms^{-2}$

D_* = the dimensionless particle size = $\left[g(\rho_s/\rho - 1)/\nu^2\right]^{1/3} D_{50}$

ν = kinematic viscosity

Again, the other important parameter to consider in terms of bed erosion is the erosion rate or flux (E). Some studies use a linear expression of the form in Eq. 3.05 (van Leussen and Winterwerp, 1990; Sanford et al., 1991), others use a power law approach as in Eq. 3.06 (Lick, 1982; Lavelle et al., 1984), however, the expressions are generally written in the form of Eq. 3.07 (Aldridge et al., 2003; Le Hir et al., 2007).

$$E = M(\tau_b - \tau_c) \qquad \textit{(Eq. 3.05)}$$

$$E = M(\tau_b - \tau_c)^n \qquad \textit{(Eq. 3.06)}$$

$$E = E_0 T^\gamma \qquad \textit{(Eq. 3.07)}$$

where: M, n, γ = empirical constants

T = the excess shear stress = $\left(\tau_b / \tau_c\right) - 1$.

3.3 Deposition of SPM – Settling Velocity.

SPM may remain in suspension for as long as the velocity remains above the particular critical bed shear stress value (and for a while after the flow falls below this value). If the current velocity decreases below this value then the SPM will settle out of suspension under gravity at a rate known as the settling/fall velocity, w_s. This is defined as the terminal velocity attained when the grain (or particle) is settling in an extended (non-turbulent) fluid under the action of gravity (Fredsøe and Deigaard, 1992).

As density determines how buoyant a particle is in a fluid then density must also play a role in the determination of the particle's settling velocity. An expression for settling velocity stated by Fredsøe and Deigaard (1992) is:

$$w_s = \sqrt{\frac{4(s-1)gd}{3C_D}} \qquad (Eq.\ 3.08)$$

where: $s = \frac{\rho_s}{\rho}$,

γ_s = specific gravity,

γ = specific gravity of water at 4°C (relative density)

g = acceleration due to gravity ~ $9.81 ms^{-2}$

d = diameter of settling particle.

A common formulation for settling velocity however, is Stokes law (Eq. 3.09).

$$w_s = \frac{(\rho_s - \rho)gd^2}{18\mu} \qquad (Eq.\ 3.09)$$

The settling velocity characteristics can also be estimated indirectly through analytical techniques (Glenn and Grant, 1987; Lynch and Agrawal, 1991; Kawanisi and Yokosi, 1997; Fugate and Friedrichs, 2002, 2003). This is done using the common assumption of a lowest order sediment concentration balance between gravitational settling and upward turbulent diffusion. The settling velocity can be solved for by rearrangement of the equation for volume

concentration, C_n, as stated from the conservation of mass for particles of size class n (Lynch and Agrawal, 1991):

$$\frac{\partial C_n}{\partial t} = w_{sn}\frac{\partial C_n}{\partial z} - \frac{\partial}{\partial z}\left(K_{xz}\frac{\partial C_n}{\partial z}\right)$$

$$\Rightarrow w_{sn} = \frac{\partial C_n/\partial t + \partial/\partial z\left(K_{xz}\,\partial C_n/\partial z\right)}{\partial C_n/\partial z} \qquad (Eq.\ 3.10)$$

where: w_{sn} = settling velocity for particle size n

$K_{xz} = \kappa\, u_* z$ = a height-dependent eddy viscosity

$K_{xz}\dfrac{\partial C_n}{\partial z}$ = the concentration diffusive term

$w_{sn}\dfrac{\partial C_n}{\partial z}$ = the concentration settling term.

Following the work of Fugate and Friedrichs (2002, 2003) and Dyer et al. (2004), it is possible to estimate the concentration diffusive term near the bed using the Reynolds diffusive flux, i.e.:

$$K_{xz}\frac{\partial C_n}{\partial z} \equiv \overline{w'C_n'} \qquad (Eq.\ 3.11)$$

Settling times of particles can be drastically modified by levels of instantaneous bursts of turbulence, produced at the bed, diffusing up through the water column.

3.4 Aggregates and Flocs.

Whilst sediment is in suspension, individual particles may collide with each other and become connected. This is the process of aggregation. The aggregates maintain this connection either through van der Waals attraction (Kranck, 1973; Trent et al., 1978; Bale and Morris, 1987; Eisma, 1991a) or due to, for example, mucus produced from biological processes (van Leussen, 1997). In fact, living organisms are often very closely associated with aggregates (Zabawa, 1978; Eisma, 1986).

A large proportion of the work done into the investigation of aggregates has been carried out in estuarine systems where sedimentation plays an important role in the management and usage of the estuary (Eisma et al., 1980; Dyer, 1989; Chen et al., 1994; Law et al., 1997; Manning and Dyer, 1999; Knebel et al., 1999; Lunven and Gentien, 2000; Fugate and Friedrichs, 2002, 2003; Dyer et al., 2004).

Some methods by which aggregation may take place are (Winterwerp, 1998, 2002):

1. Brownian motion causing particles to collide to form aggregates,
2. particles with large settling velocities overtake particles with low settling velocities; collisions between these particles may result in aggregation (a process known as differential settling), and
3. turbulent motions causing particles carried by eddies to collide and form aggregates (or to be broken up), the process known as fluid shear.

Brownian motion is due to the thermal energy of the fluid and so is random in nature. It is generally only significant for particles <1μm in diameter (Lick et al., 1993). Studies show that in estuaries and coastal regions, flocculation by Brownian motion is negligible (O'Melia, 1980; McCave, 1984). The effects of fluid shear are proportional to the turbulence and so are important in high-energy zones. As collisions due to fluid shear decrease, differential settling becomes the dominant mechanism (Lick et al., 1993).

The concentration of SPM in the water and the degree of turbulent shear may be related to the aggregate size due to their effects on particle encounter frequency (Dyer, 1989; Berhane et al., 1997).

Fugate and Friedrichs (2003) state that the important factors determining aggregation are: SPM concentration, turbulent shear in the water column, differential settling of the particles and the amount of sticky organic compounds within the water (Eisma et al., 1991b).

Flocculants (better known as flocs) are produced as a result of an aggregation process known as flocculation. Most of the suspended particulate matter in rivers, lakes and oceans exists in the form of flocs (Eisma, 1986; Lick et al., 1993). Research in estuaries shows that suspended fine-grained sediment is predominantly in flocculated form (Gibbs et al., 1989; Milligan et al., 2001).

Flocs are aggregates which are loosely held together and have a high level of water content. A proposed definition for a floc is a highly porous, fractal-like aggregate made of many primary particles that exhibit a fractal dimension ranging between 1.4 and 2.8 (Li and Ganczarczyk, 1989, 1990, 1992; Jiang and Logan, 1991). The fractal dimension is a measure of how compact an aggregate is; an entirely compacted aggregate, such as a coalesced sphere, has a fractal dimension of 3 (Meakin, 1988; Wiesner, 1992). The scale for fractal dimensions is: $1 \leq D \leq 3$, where D = fractal dimension. Kranenberg (1994) and Winterwerp (2002) state an expression for the fractal dimension, n_f, as:

$$n_f = \lim_{L \to \infty} \frac{\ln(N(L))}{\ln(L)} \qquad (Eq.\ 3.12)$$

where: L = linear size of the growing object,

N = number of primary (seed) objects.

As the flocs consist of some particulate matter and a large quantity of water, they correspondingly have lower densities than a solid particle of the equivalent size. In fact, Tambo and Watanabe (1979) state that as the diameter of a floc increases the density of the floc decreases, i.e. an inverse relationship.

As a result, the dynamics of aggregates are different to that of solid particles. In the experiments of Tambo and Watanabe (1979), due to the sphericity and the low Reynolds numbers of the low density flocs they decided that the drag coefficient as mentioned earlier (Eq. 2.16) would be too low and would be more closely approximated by the following expression to account for the lower Reynolds numbers of the flocs:

$$C_D = {}^{45}/_{R_e} \qquad (Eq.\ 3.13)$$

With this increased drag coefficient and the flocs' low density the settling velocity of the floc is also affected. In the experiments of Namer and Ganczarczyk (1993), they concluded that the settling velocity of the aggregates in their study had power law coefficients lower than that predicted by Stokes' law, therefore Stokes' Law is not applicable.

A number of authors have investigated the relationship between floc diameter and floc settling velocity. The relationship is found to be non-linear. Gibbs (1985) conducted laboratory and field experiments in Chesapeake Bay into the relationship of floc diameter and settling velocity. His work showed a non-Stokes relationship and he formulated the following empirical expression for floc settling velocity (cm/s):

$$w_s = 1.73 D_f^{\,0.78} \qquad (Eq.\ 3.14)$$

where: D_f = floc diameter (cm).

Other contributors in this area are Dyer et al. (1996). They took in-situ measurements of estuarine floc settling velocities and formulated the following empirical relationship between floc size and settling velocity (mm/s):

$$w_s = 0.00093 D_f^{\,1.31} \qquad (Eq.\ 3.15)$$

where: D_f = floc diameter (μm).

Another similar study was carried out by Sternberg et al. (1999) who again used in-situ observations of settling velocity. They produced the following empirical relation for floc settling velocity (mm/s):

$$w_s = 0.0002 D_e^{\,1.54} \qquad (Eq.\ 3.16)$$

where: D_e = the elliptical nominal diameter (μm) ≡ the diameter of a sphere with projected cross-sectional area equal to the area of an ellipse with the measured semi-axes of the particles $= D_e = 2(ac)^{1/2}$,

a = particle width/2 (μm),

c = particle length/2 (μm).

The most important factor controlling aggregation, disaggregation and aggregate dynamics and the dominant collision mechanism is thought to be the fluid shear (Berhane et al., 1997), i.e. the turbulent motions and the turbulent kinetic energy (TKE) of the fluid. This is thought to be the case except during periods of slack current velocities when differential settling may be responsible for the most floc formation (van Leussen, 1988; Fugate and Friedrichs, 2003) and the clearing of the water column.

The turbulent motions within the water column can increase the collision probabilities of the particles in suspension, thereby promoting aggregation and thus floc growth (Eisma, 1986; Xia et al., 2004).

The fluid/turbulent shear is known to be a factor in limiting the size of the flocs. In addition to promoting floc growth, due to the weakness of the flocs, the magnitude of the turbulence may be such that it breaks the flocs apart. This has been observed by many authors (McCave, 1984; Hill et al., 1992; Chen et al., 1994; Manning and Dyer, 1999; Hill et al., 2001; Fugate and Friedrichs, 2003; Ellis et al., 2004). For example, in the experiments of Berhane et al. (1997), they observed that the floc size was indeed related to current velocity and thus turbulent shear. They stated that the floc size increased with increasing velocity and turbulence up to a critical value (floc growth stage) and then decreased as the current velocity and turbulence continued to increase (floc break-up stage).

Some authors (e.g. Alldredge et al., 1990; Hill et al., 2001) have found only a weak floc size dependency on the shear stress at times of low to medium turbulence, which suggests that turbulence may not be the limiting floc size at low to medium stress.

Dyer (1989) produced a conceptual plot showing the interlinking relationships between floc diameter, shear stress and mass concentration (Fig. 3.01) for his work carried out in estuaries. This shows an initial increase in floc size with increasing shear stress followed by a peak at a particular stress after which floc size decreases with increasing shear stress.

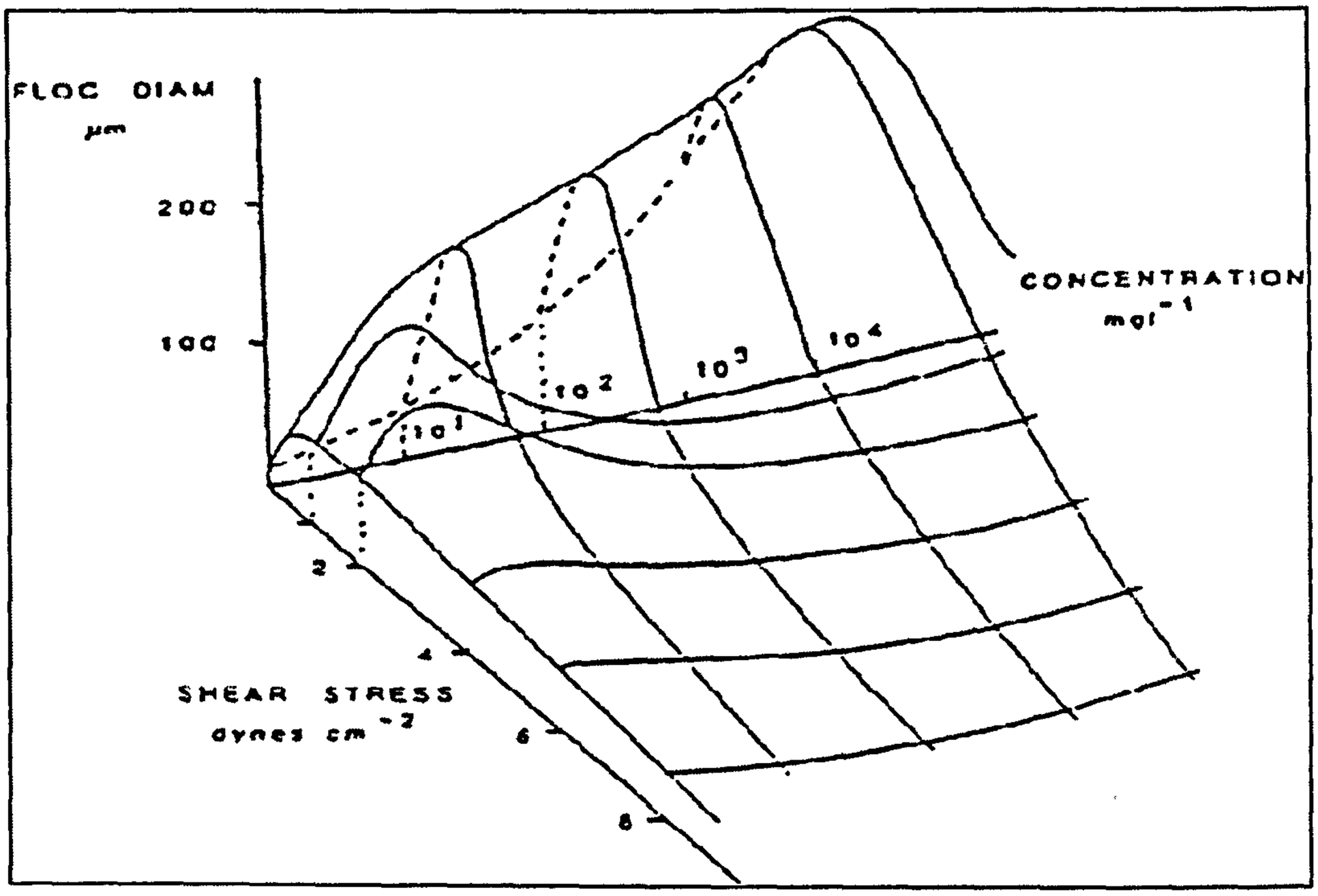

Fig. 3.01 A schematic diagram showing the relationship between floc modal diameter, mass concentration and shear stress (Dyer, 1989).

It has been suggested that the Kolmogorov microscale (λ), the size of the smallest turbulent eddies found in the water, should approximate the maximum size that a floc can attain before being torn apart by the turbulent motions (van Leussen, 1988, 1997; Berhane et al., 1997; Fugate and Friedrichs, 2003). The Kolmogorov microscale is defined by assuming that TKE production is equal to TKE dissipation (e.g. Hill et al., 1992; Fugate and Friedrichs, 2003):

$$\lambda = \left(\frac{\nu^3}{\varepsilon}\right)^{1/4} \qquad (Eq.\ 3.17)$$

where: ν = kinematic viscosity,

ε = dissipation rate of TKE.

Therefore, increases in TKE production/dissipation results in decreasing Kolmogorov microscales. Berhane et al. (1997) found that flocs may reach a maximum diameter that is half the magnitude of the Kolmogorov microscale.

It has been proposed that the opposing effects of increased encounter frequency and increased shear upon particles may determine an equilibrium particle/floc size for a particular concentration and turbulence level (Chen et al., 1994; Fugate and Friedrichs, 2003).

In addition to the fluid shear there are the stresses induced by sinking to consider. As SPM falls through the water it experiences stress which it is thought can also play a part in limiting floc size. At times and in regimes of low turbulent shear, particles/flocs may be maintained at a constant size by the drag force produced by their sinking (Hill et al., 2001; Fugate and Friedrichs, 2003). However, others believe that the stresses induced by sinking of a floc always limit the size of that floc (e.g. Hill et al, 2001).

Turbulence is also known to limit floc and particle size in the bottom boundary layer (Stow and Bowen, 1980; Krank and Milligan, 1992; Hill et al., 2001). The turbulence in the near bed region may suspend or resuspend bed material, or settling SPM. If the material is loose flocs or aggregates then the turbulent shear will immediately disaggregate them (Fugate and Friedrichs, 2003).

Not only does the turbulence affect the sediment but the sediment affects the turbulence. When flocs are present in suspension within the water column they absorb energy from the flow (Dyer et al., 2004) as they are disrupted, collide or interact. This gives rise to an increase in effective viscosity which in turn can dampen the turbulence level as a greater fraction of the shear stress is carried by the effective viscosity. Dyer et al. (2004) states that the physical conditions governing this process in high SPM concentrations are not well understood as there are few field measurements of turbulence in these conditions.

3.5 Summary.

The current knowledge and understanding about turbulence is that turbulence in most natural flows is produced by shear stresses within the flow, and in particular at the interface of the flow and a stationary bed. As a result of these bed shear stresses, sediment is eroded from the bed if the shear stresses achieve a critical value. The sediment may then be mixed up through the water column by turbulent vertical mixing. It is widely accepted that turbulence can maintain high concentrations of sediment in steady state suspension (Chen et al., 1994; Michallot and Mory, 2004). However, more detailed relationships between these two properties are less well understood. Once the sediment is in suspension it is known as suspended particulate matter (SPM) or simply suspended sediment. If the upward mixing decreases, then SPM will settle out under gravity. Another process that may occur whilst sediment is suspended is aggregation/disaggregation. Aggregation is the process by which individual or smaller aggregates join together to form larger aggregates or flocs. Under differing conditions turbulence may either promote aggregation or encourage disaggregation (where aggregates are broken apart). As a result of aggregation/disaggregation, the size distribution of the suspended sediment may be modified at different times during a tidal cycle due to the differing turbulent conditions. In addition, as a result of aggregation/disaggregation and upward diffusing turbulence, settling times of populations of SPM in the water column are modified.

Chapter 4.

The Experiment.

4.1 Introduction.

In this chapter a description of the hydrodynamic conditions occurring at the site is presented which is then followed by a description of the observational programme performed at the site.

Descriptions of the instrumentation deployed are outlined. Included in the descriptions are the equations employed during processing along with the processing techniques and a brief outline of any errors and uncertainties.

4.2 The Experiment.

4.2.1 Hydrodynamic Description.

A cruise was undertaken to the study site aboard the RV Prince Madog between the 12 and 15 February 2004. The site was chosen as it lies in a region of high tidal velocities and with a patch of higher turbidity nearby. February was chosen for the cruise as levels of biology were low and so the results should not have been influenced by biological activity. Therefore, only physical processes should have been controlling the sediment transport. The aim of this cruise was to collect a 54 hour time series of good quality turbulence and SPM measurements covering the whole water column over the desired time period.

The tidal ellipse was negligible and so the tide can be assumed to be rectilinear aligned east-west across the study site. Although the tides were decreasing from springs to neaps, the tidal currents (more specifically the east velocity component being the major velocity component) were still high, typically reaching $1.5ms^{-1}$ on the flood phase of the tide. The tidal excursion at the site at the beginning of

the observational period was approximately 12km in the near bed region and approximately 17km at the surface.

Weather conditions were favourable as there were relatively weak winds for the duration of the observations and the sea state was calm.

4.2.2 The Programme and Deployed Instrumentation.

An upward looking 600KHz Acoustic Doppler Current Profiler (ADCP) was deployed on the seabed in approximately 40m water depth at the site. The bin sizes were 1.09m and the ADCP sampled the water column from approximately 2.5m above the sea bed. The ADCP was moored in-situ until the suite of observations was completed.

To measure the horizontal gradients at the site a transect was first performed along a line east to west across the site (Fig. 4.01). The timing of the casts was determined by estimating the time at which low water would occur at each of the cast locations so that the measurements were always being taken at low water. The purpose of this was to minimise if not remove the influence of time variation in the measurements taken along the gradient. Vertical profiles were performed at each cast with the CTD which had a LISST-100C attached to the CTD frame. In addition water samples for gravimetric analysis were collected, providing a detailed dataset of the gradient in suspended sediment properties across the site.

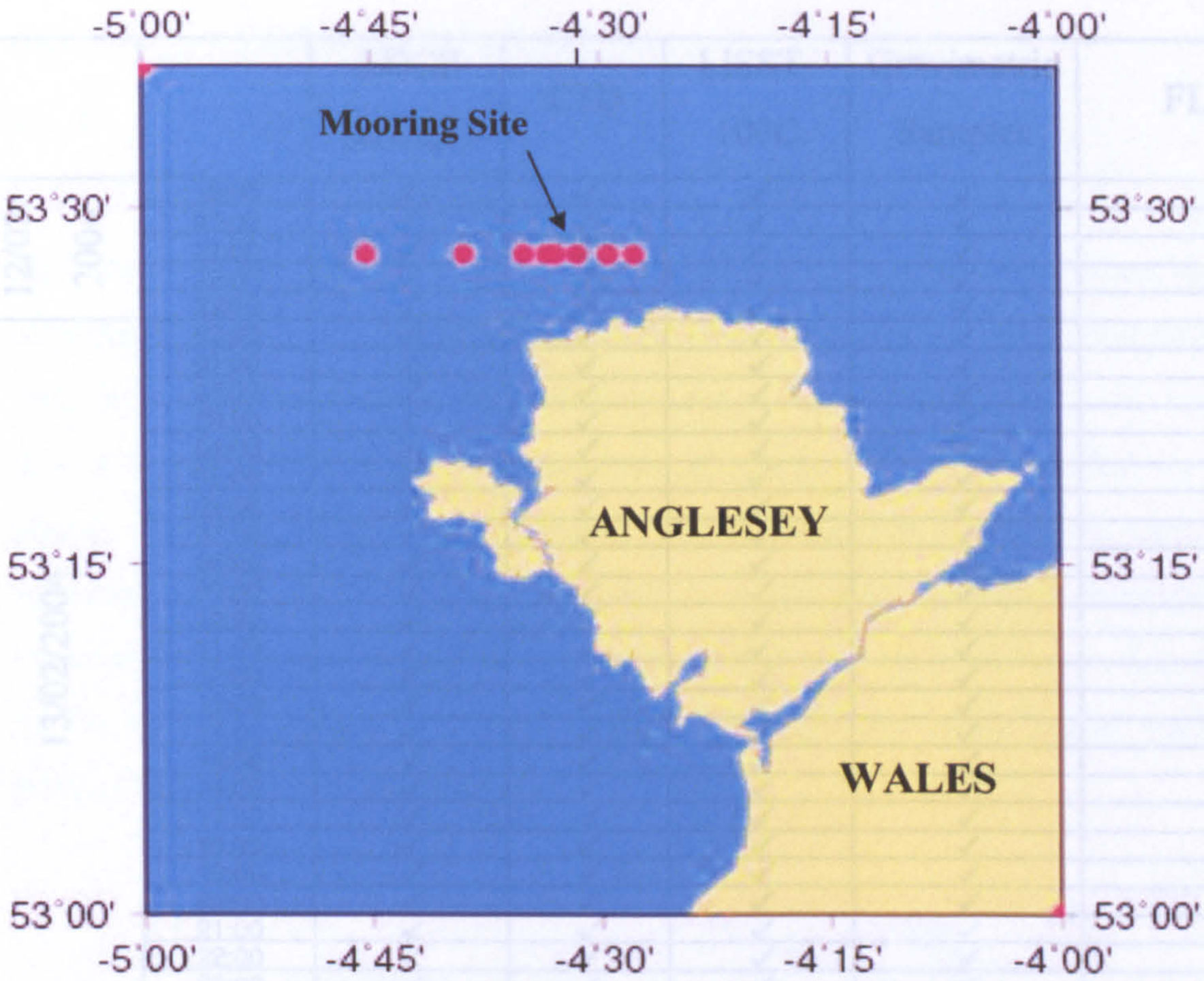

Fig. 4.01 A map of the sampling positions during the transect; the mooring site is highlighted.

Once the transect had been completed the ship steamed back to the study site and a 54 hour tidal station was carried out adjacent to the mooring site. This tidal station consisted of hourly CTD casts together with LISST profiles and water samples for gravimetric analysis. In addition, profiles of the rate of dissipation of turbulent kinetic energy, ε, were collected over the last 2 tidal cycles (25 hours) of the observations using a loosely tethered FLY microstructure profiler. Full details of the timings of the measurements are given in Table 4.01.

		ADCP (u,v,τ,P)	CTD	LISST-100C	Gravimetric Samples	FLY
12/02/2004	19:00	✓	✓	✓	✓	
	20:00	✓	✓	✓	✓	
	21:00	✓	✓	✓	✓	
	22:00	✓	✓	✓	✓	
	23:00	✓	✓	✓	✓	
13/02/2004	00:00	✓	✓	✓	✓	
	01:00	✓	✓	✓	✓	
	02:00	✓	✓	✓	✓	
	03:00	✓	✓	✓	✓	
	04:00	✓	✓	✓	✓	
	05:00	✓	✓	✓	✓	
	06:00	✓	✓	✓	✓	
	07:00	✓	✓	✓	✓	
	08:00	✓	✓	✓	✓	
	09:00	✓	✓	✓	✓	
	10:00	✓	✓	✓	✓	
	11:00	✓	✓	✓	✓	
	12:00	✓	✓	✓	✓	
	13:00	✓	✓	✓	✓	
	14:00	✓	✓	✓	✓	
	15:00	✓	✓	✓	✓	
	16:00	✓	✓	✓	✓	
	17:00	✓	✓	✓	✓	
	18:00	✓	✓	✓	✓	
	19:00	✓	✓	✓	✓	
	20:00	✓	✓	✓	✓	
	21:00	✓	✓	✓	✓	
	22:00	✓	✓	✓	✓	
	23:00	✓	✓	✓	✓	
14/02/2004	00:00	✓	✓	✓	✓	
	01:00	✓	✓	✓	✓	
	02:00	✓	✓	✓	✓	
	03:00	✓	✓	✓	✓	
	04:00	✓	✓	✓	✓	
	05:00	✓	✓	✓	✓	
	06:00	✓	✓	✓	✓	
	07:00	✓	✓	✓		✓✓✓✓✓✓✓✓
	08:00	✓	✓	✓		✓✓✓✓✓✓✓✓
	09:00	✓	✓	✓		✓✓✓✓✓✓✓✓
	10:00	✓	✓	✓		✓✓✓✓✓✓✓✓
	11:00	✓	✓	✓		✓✓✓✓✓✓✓✓
	12:00	✓	✓	✓		✓✓✓✓✓✓✓✓
	13:00	✓	✓	✓		✓✓✓✓✓✓✓✓
	14:00	✓	✓	✓		✓✓✓✓✓✓✓✓
	15:00	✓	✓	✓		✓✓✓✓✓✓✓✓
	16:00	✓	✓	✓		✓✓✓✓✓✓✓✓
	17:00	✓	✓	✓		✓✓✓✓✓✓✓✓
	18:00	✓	✓	✓		✓✓✓✓✓✓✓✓
	19:00	✓	✓	✓		✓✓✓✓✓✓✓✓
	20:00	✓	✓	✓		✓✓✓✓✓✓✓✓
	21:00	✓	✓	✓		✓✓✓✓✓✓✓✓
	22:00	✓	✓	✓		✓✓✓✓✓✓✓✓
	23:00	✓	✓	✓		✓✓✓✓✓✓✓✓
15/02/2004	00:00	✓	✓	✓		✓✓✓✓✓✓✓✓
	01:00	✓	✓	✓		✓✓✓✓✓✓✓✓
	02:00	✓	✓	✓		✓✓✓✓✓✓✓✓
	03:00	✓	✓	✓		✓✓✓✓✓✓✓✓
	04:00	✓	✓	✓		✓✓✓✓✓✓✓✓
	05:00	✓	✓	✓		✓✓✓✓✓✓✓✓
	06:00	✓	✓	✓		✓✓✓✓✓✓✓✓
	07:00	✓	✓	✓		✓✓✓✓✓✓✓✓
	08:00	✓	✓	✓		✓✓✓✓✓✓✓✓
	09:00	✓	✓	✓		✓✓✓✓✓✓✓✓
	10:00		✓	✓		✓✓✓✓✓✓✓✓
	11:00		✓	✓		✓✓✓✓✓✓✓✓
	12:00		✓	✓		✓✓✓✓✓✓✓✓

Table 4.01 An inventory of the data collected with each instrument. ✓ = one deployment, except for the ADCP which was sampling continuously.

4.3 Instrumentation.

4.3.1 The ADCP.

4.3.1.1 Description.

The "Acoustic Doppler Current Profiler" (ADCP) is an in-situ instrument that uses the Doppler shift of sound scattered by particles within the water column in order to estimate profiles of water velocity (Fig. 4.02). The instrument can have 3, 4 or 5 sensors which emit an acoustic signal at a specific frequency (known as pings). The instrument then "listens" to the backscattered signal from various scatterers within the water column, such as suspended sediments, biological material etc. The received signal is Doppler shifted relative to the mean velocity of the scatterers within the beam. Range gating of the return signal allows profiles of velocity to be constructed.

Fig. 4.02 An RDI workhorse sentinel ADCP as used in this experiment (courtesy of http://www.rdinstruments.com).

4.3.1.2 Velocity Measurements.

The ADCP used takes measurements along 4 beams which in the case of this experiment are tilted at an angle $\theta = 20°$ from a single axis that forms the centreline of the instrument. The orientation of the ADCP beams are logged by

the ADCP's compass so that they can be rotated to north, south, east and west during processing. With beam 3 oriented in the north direction, then the velocity along each beam is given by the following expressions (Lu and Lueck, 1999a):

$$\begin{aligned} b_1 &= u_1 \sin\theta + w_1 \cos\theta \\ b_2 &= -u_2 \sin\theta + w_2 \cos\theta \\ b_3 &= v_3 \sin\theta + w_3 \cos\theta \\ b_4 &= -v_4 \sin\theta + w_4 \cos\theta \end{aligned} \qquad \textit{(Eq. 4.01)}$$

where: b_i = along beam velocity (with i = beam number = 1, 2, 3, 4),

u_i, v_i, w_i = velocity in the east, north and vertical respectively in beam *i*.

For this experiment, the ADCP was setup as follows:

1. number of bins = 45
2. bin size = 1.09m
3. distance to first bin = height of frame + distance of first bin length
   = 0.45m + 2.14m
   = 2.59m
4. pings per ensemble = 1
5. time per ping = 1s

4.3.1.3 Turbulence Measurements.

ADCPs can also be used to measure profiles of turbulence by calculating estimates of the Reynolds stresses (as mentioned earlier) within the water column. These Reynolds stresses are calculated by application of the variance method on the acoustic beam data outlined by Lohrmann et al. (1989); Rippeth et al. (2002) and Simpson et al. (2004). By assuming that the flow field is homogenous over the beam spread so that the statistics of the turbulence are the same for all four beams (Lu and Lueck, 1999b), and the ADCP stands flat on the seabed (Stacey et al., 1999; Rippeth et al., 2003), the estimates of the Reynolds stresses in the x and y directions are given by:

$$\frac{\tau_x}{\rho} = \overline{u'w'} = \frac{\overline{b_1'^2} - \overline{b_2'^2}}{2\sin 2\theta}$$
$$\frac{\tau_y}{\rho} = \overline{v'w'} = \frac{\overline{b_3'^2} - \overline{b_4'^2}}{2\sin 2\theta} \qquad \textit{(Eq. 4.02)}$$

where: τ = shear stress.

The rate of turbulent kinetic energy (TKE) production, i.e. the rate at which energy is transferred from the mean flow to turbulent energy, is estimated by taking the product of the Reynolds stress and the velocity shear. This leads to the turbulent kinetic energy production equation (Rippeth et al., 2001; Simpson et al., 2004):

$$P = -\tau_x \frac{\partial \bar{u}}{\partial z} - \tau_y \frac{\partial \bar{v}}{\partial z} = -\rho\left(\overline{u'w'}\frac{\partial \bar{u}}{\partial z} + \overline{v'w'}\frac{\partial \bar{v}}{\partial z}\right) \qquad \textit{(Eq. 4.03)}$$

4.3.1.4 Errors And Uncertainties.

Uncertainties in the Reynolds stress and TKE production estimates using the variance method have been investigated by Williams and Simpson (2004). It was found that for weak flows the uncertainties in the Reynolds stress estimates arise mainly from instrument noise and that this uncertainty is proportional to the square of the standard deviation of the velocity. This results in an uncertainty in the calculated TKE production rate which is proportional to the cube of the standard deviation of the velocity. A possible solution to this is to increase the ping rate of the ADCP.

Conversely, for stronger flows the uncertainties arise mainly from the number of individual velocity measurements taken over which the variance is then calculated. This may be alleviated again by increasing the ping rate. For further reading on this subject the reader is referred to Williams and Simpson (2004).

The assumption that the ADCP stands flat on the bed is an important one so that the ADCP is orientated with the mean streamlines. If this is not the case then the

estimates of the TKE production rate may be inaccurate. In this study, upon examination of the pitch and roll sensors onboard the ADCP it was found that the ADCP was indeed flat on the bed and so the errors associated with misalignment of the ADCP can be regarded as being minimal.

4.3.2 The FLY.

4.3.2.1 Description.

A direct method for the measurement of TKE dissipation rate (ε) is to utilise a free-fall microstructure profiler known as a FLY ("Fast Light Yo-Yo"), Fig. 4.03, (Dewey et al., 1987). This type of instrument has been developed over the years and has been used in other turbulence investigations (Knight et al., 2002; Fisher et al., 2002).

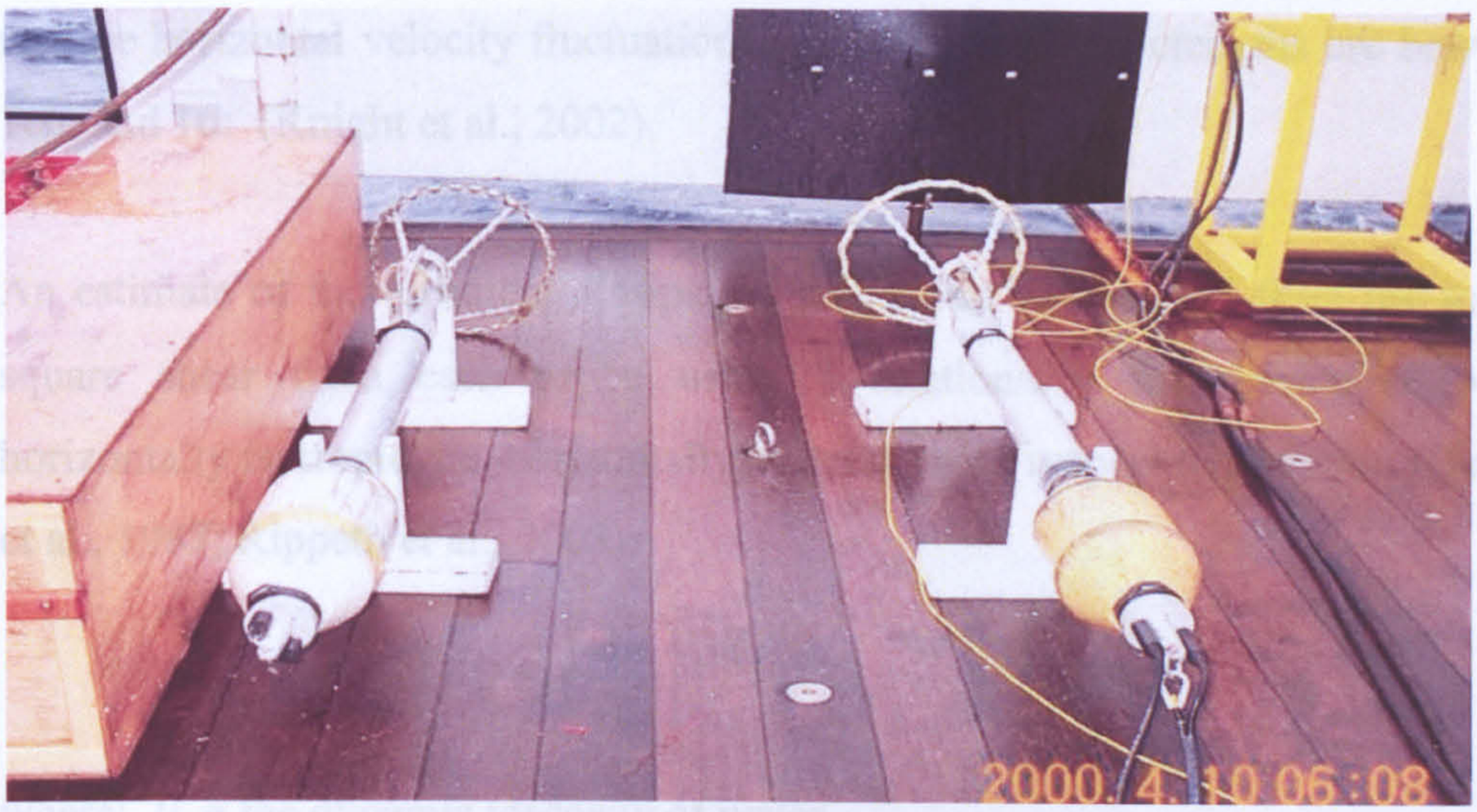

Fig. 4.03 The FLY onboard the RV Prince Madog.

As the instrument falls through the water column it measures velocity shear, pressure, temperature and conductivity. The optimal fall speed of the instrument is between 0.70 and 0.80ms^{-1} which allows for approximately 95% of the dissipation spectrum to be observed.

There is a guard at the base of the instrument to protect the sensors; however, data collection is possible to within 15cm of the bed. Data is therefore available from the bed up to approximately 5m of the surface. The data in the surface 5m of water must be discarded as there may be interference from the turbulence of the ship's wake.

4.3.2.2 Turbulence Measurements.

The measurements of shear are obtained from components of horizontal velocity by two piezoelectric shear sensors that protrude from the base of the profiler. These sensors measure the force exerted on them by the flow which is in turn proportional to the horizontal velocity. The velocity shear is then found by differentiation of the force. The sensors sample at a frequency of 280Hz and can resolve horizontal velocity fluctuations whose vertical wavelengths are between 1cm and 1m (Knight et al., 2002).

An estimate of the turbulent dissipation rate ε can be obtained from the mean-square shear from each probe using a relationship for turbulence being horizontally isotropic, i.e. horizontally invariant with respect to direction (Dewey et al., 1987; Rippeth et al., 2003):

$$\varepsilon = 7.5\mu\left(\frac{\partial \bar{u}}{\partial z}\right)^2 \qquad (Eq.\ 4.04)$$

where: μ = the dynamic viscosity of water.

This result is similar to the eddy diffusivity concept (McLean and Yean, 1987) which states that the Reynolds stresses are related to the mean velocity shear by use of an eddy viscosity coefficient (Lohrmann et al., 1990), e.g.

$$-\overline{u'w'} = A\frac{\partial \bar{u}}{\partial z},$$

$$-\overline{v'w'} = A\frac{\partial \bar{v}}{\partial z}$$

where: A = the eddy viscosity coefficient.

The are 3 different forms that the expression for A can take; the first is that A is a function of depth (Jordon and Baker, 1980), the second is that A is a simple function of time and depth such as in terms of the bottom stress (McLean and Yean, 1987) and the third is that A depends on the actual flow field such as through the TKE production and/or dissipation (Mellor and Yamada, 1974).

The uncertainty in the individual estimates of the TKE dissipation rate (ε) may be potentially 50% of the mean and is mainly due to the uncertainty in the fall speed estimates of the instrument (Simpson et al. 1996).

4.3.3 The LISST-100C.

4.3.3.1 Description.

In recent years an optical instrument known as a LISST-100C instrument (Laser In-Situ Scattering and Transmissometry), has been developed by Sequoia Scientific (Fig. 4.04). This instrument is used in situ and measures particle volume concentration in 32 size classes. As the instrument is in-situ, delicate flocs and aggregates are not broken up into finer particles thus providing more realistic particle size distributions and spectra than other methods which rely on collected samples.

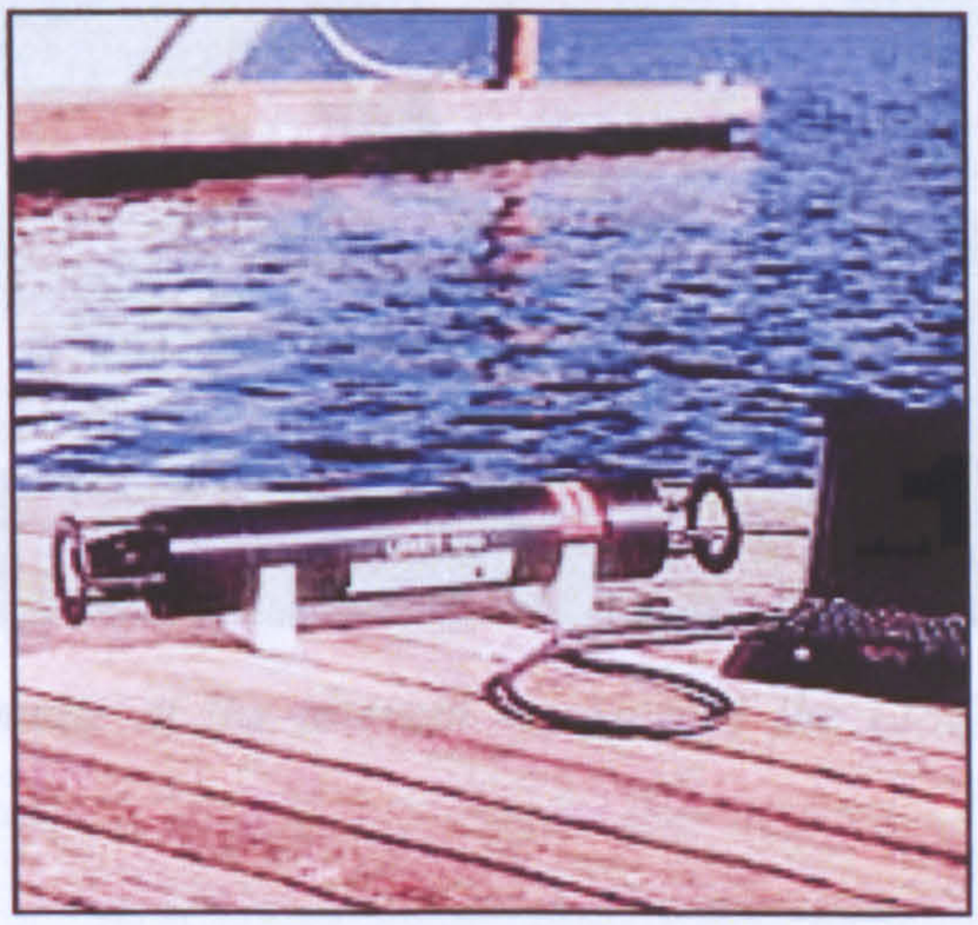

Fig. 4.04 The LISST-100C (courtesy of http://www.sequoiasci.com).

4.3.3.2 Particle Size/Concentration Measurements.

The LISST emits a beam of high intensity laser light from its light source which is a 3mW visible diode laser which operates at 670nm. The beam is collimated and made circular by lenses and prisms in front of the light source. This beam of light then travels through the seawater along a path length of known distance. Any scatterers present within the seawater scatter the beam which is then refocused and received at the other end of the path length. Unscattered light is focussed into a spot in the centre of a ring of detectors. Light that has been scattered is focussed onto a particular detector ring, which one being determined by the amount the light has been scattered and therefore determined by the size of the scattering particle. The instrument then collates the data collected for 32 different size classes, and stores it internally (Fig. 4.05). The operating size range of the LISST is 2.5 to 500µm.

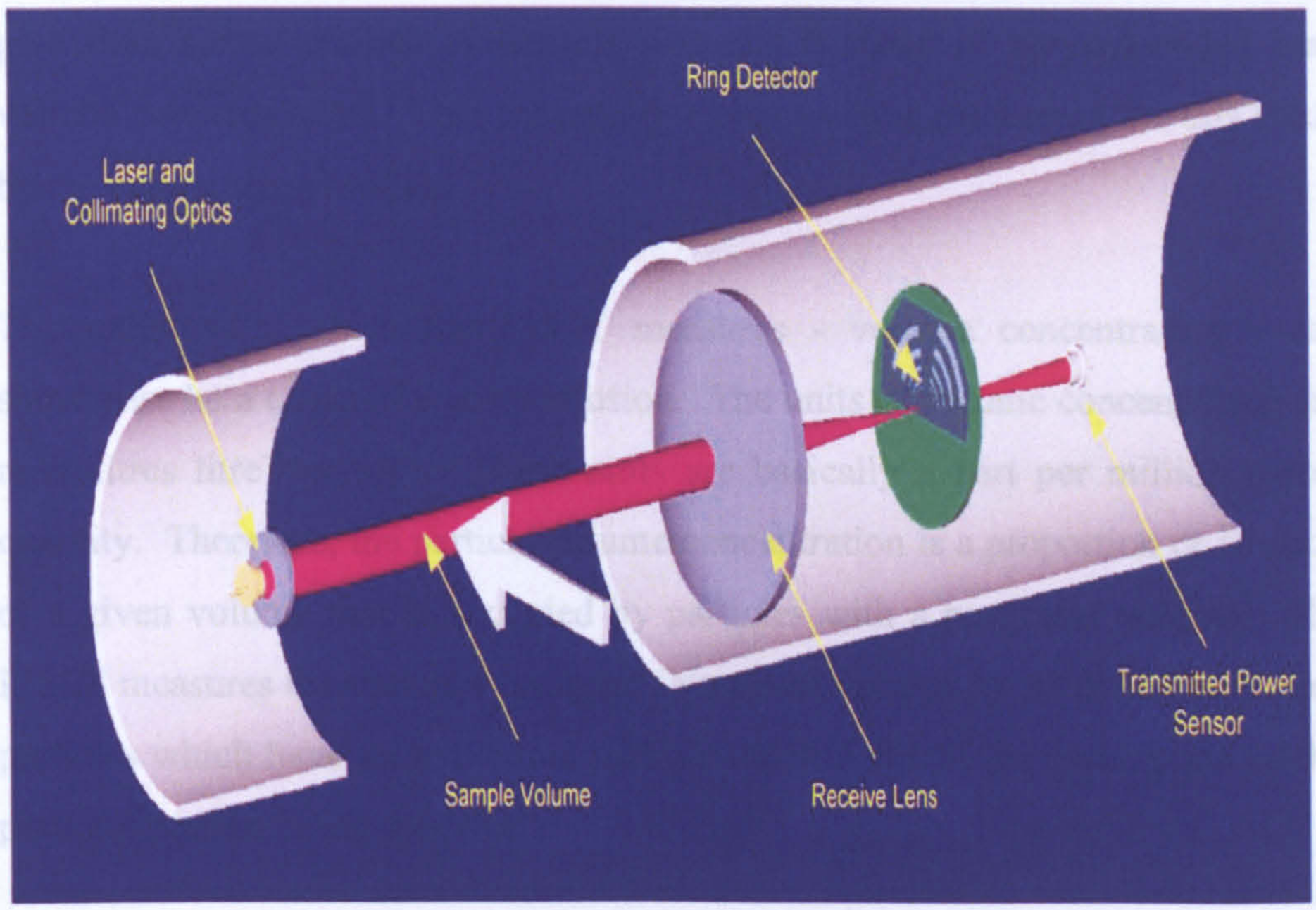

Fig. 4.05 A schematic of the internal working of the LISST (courtesy of the LISST-100C manual).

4.3.3.3 Calibration and Processing Techniques.

Once the data has been offloaded from the instrument, the data is converted from binary files into real data using the LISST software supplied by the manufacturer Sequoia Scientific.

Normal practice is to run a *z-scat* prior to use. This involves attaching a water bath to the LISST and filling it with distilled (pure) water. Measurements are then taken and saved as a background particle distribution scattering file. This is then deducted from the data collected during an observational period to remove the background noise.

The resulting data is then de-spiked of any erroneous data points, bin-averaged into 1 metre bins using both the up and down casts and separated into casts to give time series profiles of particle size distributions of the suspended load volume concentrations. This processing technique was performed for this study by the author using Matlab.

The units, with which the LISST measures - volume concentration - can sometimes be a cause of some confusion. The units of volume concentration are microlitres $litre^{-1}$ or $\mu l l^{-1}$. These units are basically a part per million (ppm) quantity. Therefore, the particle volume concentration is a proportion or fraction of a given volume that is occupied by particles with a particular volume. The LISST measures the volumes occupied in a given volume by 32 differently sized particles which have an individual particle volume due to the assumption of the particles present being spherical.

Thus the mass of particles is not taken into account in the measurements. As a result, a high volume concentration can consist of a large volume occupied by a few large particles, or it can be a large volume occupied by many small particles.

In other words, during the analysis of the data from the LISST it is necessary to process both the volume concentration data and the median size data in order to

infer the behaviour and characteristics of the suspended sediments. Further description of this instrument and its operation can be found in Agrawal and Pottsmith (1994, 2000), Traykovski et al (1999) and Ellis et al. (2004).

The total volume concentration of the SPM is calculated by summation of the volume concentrations of each of the 32 size classes at a given time and height, i.e.

$$V(z,t) = \sum_{i=1} v_i(z,t) \qquad (Eq.\ 4.04)$$

where: $V(z,t)$ = total volume concentration at height z and time t.

$v_i(z,t)$ = volume concentration of size class i, (i = 1,..,32) at height z and time t.

The median diameters are calculated using a weighted-mean calculation.

4.3.3.4 Errors And Uncertainties.

Errors in the size distribution and hence the median SPM diameter data may result from the assumption about the shape of the particles present, i.e. the assumption that they are spheres. In reality, the suspended sediments possess many different and often none-uniform shapes.

A number of authors have suggested that the scattered light of natural particles may be significantly different from that of equivalent spheres e.g. Mühlenweg and Hirleman (1998), Pedocchi and García (2006). Fischbach et al. (1985) comments that non-spherical particles create different diffraction patterns from spherical particles of equivalent size.

Jones (1987) and Al-Chalabi and Jones (1993) suggested that over a limited range of irregular sizes and for angles close to the forward direction, the scattered light patterns artificially produced a broader size distribution.

Pedocchi and García (2006) concluded that the size distribution obtained using a procedure involving assumptions of sphericity could give poor estimations. They also stated that Sequoia Scientific were aware of the situation and are working to improve it.

Therefore, these shape effects must be kept in mind whilst analysing and interpreting the data. For further reading on this issue the reader is referred to Pedocchi and García (2006).

4.3.4 The CTD.

4.3.4.1 Description.

The CTD (Conductivity Temperature Depth) system involves a frame connected to a wire which is lowered through the water column. As it does so sensors for temperature, salinity and pressure take readings. The CTD used for this study was a Sea-Bird CTD 9Plus (Fig. 4.06).

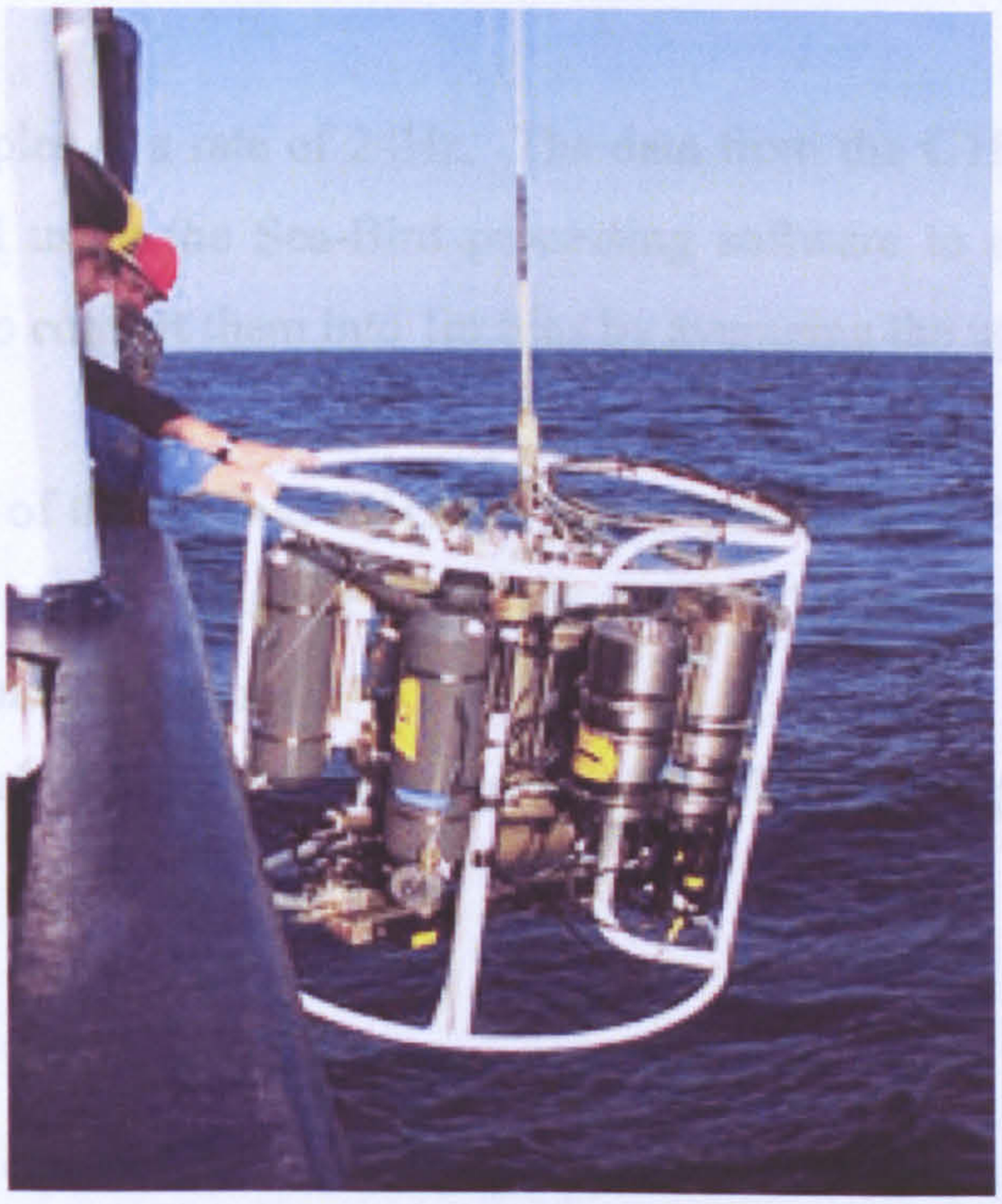

Fig. 4.06 The CTD frame being deployed from the RV Prince Madog.

The CTD can measure parameters from up to 8 auxiliary sensors. As this is the case it is common for more instruments to be attached to the CTD frame so that a whole range of measurements can be taken by the same system. Such measurements include:

1. a Rosette sampler of Niskin bottles to take water samples for analysis of suspended sediments, chlorophyll, yellow substance etc
2. LISST instruments to measure transmittance, SPM volume concentration and SPM median diameter
3. a fluorometer to measure phytoplankton fluorescence.
4. a transmissometer which can be used for calibration of the LISST-100C and which may be calibrated to measure mass concentration
5. dissolved oxygen
6. pH
7. sound velocity.
8. density
9. .....etc.

The CTD samples at a rate of 24Hz. The data from the CTD are collected and then processed using the Sea-Bird processing software to output the required variables and to convert them into 1m bins by averaging the up and down casts.

The resolution of the CTD at 24Hz for temperature is 0.0002C, for conductivity is 0.00004 S/m and for pressure is 0.001% of the full scale range (values courtesy of the SBE 9*plus* CTD manual:
http://www.seabird.com/pdf_documents/manuals/9plus_008.pdf).

4.3.4.2 The Fluorometer.

Fluorescence can be used as a proxy for chlorophyll concentration as photosynthesising algae emit light. In fact about 1% of the light absorbed by a photosynthesising cell within the algae is re-emitted as fluorescence (Kirk, 1994).

An empirical calibration (Mikkelsen, personal correspondence) to convert units of volts, measured by the fluorometer, to chlorophyll (mgl^{-1}), can be used to estimate the actual chlorophyll concentration range (see the equation below).

$$Chl = 173.35V - 1.7305 \qquad (Eq.\ 4.05)$$

where: Chl = chlorophyll concentration (mgl^{-1})

V = voltage as measured by the fluorometer.

The R^2 of this empirical calibration is 0.92. The calibration is the result of a regression between in-situ chlorophyll measurements with in-situ fluorometer measurements at various locations around the Irish Sea. Therefore, it is reasonable to assume that it is a suitable calibration to use. This calibration had to be used as no other chlorophyll data was collected during this cruise.

4.3.4.3 The Transmissometer.

The transmissometer functions in a very similar manner to the LISST-100C. A beam of collimated light is emitted across a path of known length. Opposite the transmitter is a receiver where the scattered light is focused on to a detector. The data from the transmissometer attached to the CTD gives values in volts. These values may then be converted to beam attenuation values and then into SPM concentrations. The conversion of volts to beam attenuation is given by Eq. 4.06:

$$Beam\ Attenuation = \frac{1}{r}\ln\left(\frac{V}{V_0}\right) \qquad (Eq.\ 4.06)$$

where: r = path length (m)

V = measured volts

V_0 = reference level voltage

The beam attenuation coefficient is linearly proportional to the concentration of suspended material in the water if the particles are of uniform size and composition (Moody et al., 1987). Therefore, the mass concentration data collected as a result of the gravimetric analysis (Chapter 4.3.5) may be plotted

against the corresponding beam attenuation values from the transmissometer in order to determine a calibration for the transmissometer. The voltages from the transmissometer can then be converted to SPM mass concentration.

4.3.5 Gravimetric Analysis.

Gravimetric analysis is performed as it is the method by which the mass concentration of the total suspended sediment load is estimated. In the laboratory, prior to a cruise, GF/F microfilters with a measuring diameter of 0.4μm are washed in distilled water and then dried in an oven at 80C overnight. Once removed from the oven the filter papers are weighed using a high precision balance that measures to 0.00001g (or 0.001mg). The filters are then stored in tin dishes inside plastic wallets.

Water samples are collected during a cruise using Niskin bottles (Fig. 4.07) attached to the CTD frame. The caps on either end of the bottles are remotely released by an onboard computer at a required depth so that they snap shut and collect a sample of water from the desired depth.

Fig. 4.07 A Niskin bottle which is used to collect water samples for gravimetric analysis.

Once back on board a known volume (usually between 1 and 2 litres) of the water samples collected is filtered through the pre-washed, pre-dried and pre-weighed GF/F microfilters. After filtration the filters are replaced into their tin dishes and plastic wallets and then frozen for later analysis in the laboratory. In the laboratory the samples are again dried in an oven at 80C overnight and then reweighed using the high precision balance. The initial weight is then deducted from the final weight to give the total weight. The total weight is divided by the known volume of water sample sampled (in litres) to give the mass concentration of the total suspended sediments present in the sample of water taken at a particular location and time.

4.4 Summary.

The range of instrumentation used during the research cruise has been presented and processing techniques have been described in this chapter. These processing protocols have been used utilising numerous Matlab scripts written by the author to produce the results presented in the following chapters.

Chapter 5.

Results.

5.1 Introduction.

In this chapter the data collected from the deployed instrumentation during the observational program are presented. Data collected during the west-east transect across the study site are presented and described (see Fig. 4.01 for a map of the transect). The results of the turbulence properties at the site are presented and described, and with initial comments made. This is followed by time series of the suspended sediment properties. Descriptions of the time series are given with remarks made about possible correlations with the turbulence data.

5.2 The Gradient.

5.2.1 Volume Concentration and Median Diameter.

A transect along the major axis (i.e. west to east) was carried out across the study site (Fig. 4.01) at low water (i.e. when the tidal velocities were at a minimum) in order to determine the local gradients present in suspended sediment properties, salinity, temperature and chlorophyll concentration. The data has been plotted using axes of distance from the mooring (x) and height above the bed (y). Height above the bed was calculated utilising the altimeter incorporated in the CTD. The height of the water surface from the bed at each cast was found from the altimeter data; the depth values from the profiling instruments were then deducted from this surface height to convert depth to height above the bed.

The results of the suspended sediment observations collected by the LISST-100C shows a gradient in both the suspended sediment concentration and the suspended sediment characteristics (see Fig. 5.01).

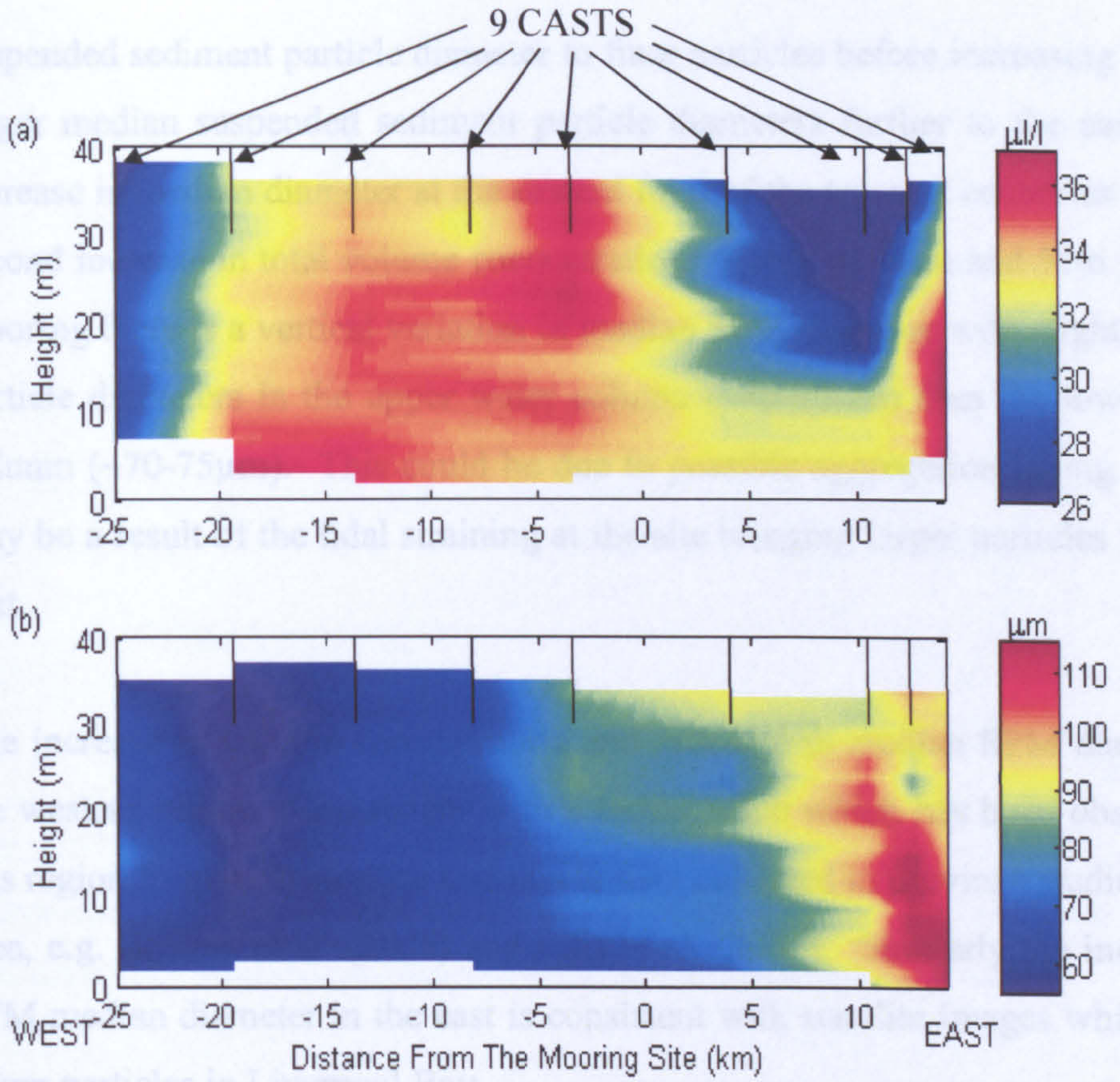

Fig. 5.01 Variations and resulting gradients in (a) SPM total volume concentration and in (b) SPM median diameter across the observational site. The site is located at 0 on the x-axis with the black lines and arrows indicating the positions at which 9 casts were taken.

Fig. 5.01(a) shows the total volume concentration of suspended sediment with distance from the mooring site. Moving from west to east (Irish Sea to Liverpool Bay) across the site results in an increase in suspended sediment volume concentration, this then decreases east of the mooring site before there is another increase further to the east. Between the mooring (0km) and 10km from the mooring there is a vertical variation in volume concentration with higher volume concentration at the bed (32-34µl/l) than at the surface (~26µl/l).

Fig. 5.01(b), the plot of median SPM diameter with distance from the mooring site, shows that moving from west to east brings about a decrease in the median

suspended sediment particle diameter to finer particles before increasing again to larger median suspended sediment particle diameters further to the east. This increase in median diameter at the eastern limit of the transect coincides with the second increase in total volume concentration. Between -5km and 5km from the mooring there is a vertical variation in median SPM diameter with slightly larger particle diameters in the upper water column (~80-90μm) than the lower water column (~70-75μm). This could be due to possible aggregation taking place or may be a result of the tidal straining at the site bringing larger particles from the east.

The increase in volume concentration and decrease in median SPM diameter in the western region is consistent with a turbid patch which has been observed in this region from both satellite and in situ data collected in previous studies in this area, e.g. Bowers et al. (2005) and Ellis et al. (2004). Similarly the increase in SPM median diameter in the east is consistent with satellite images which show larger particles in Liverpool Bay.

5.2.2 Mass Concentration.

The plot (Fig. 5.02) produced from the results of the gravimetric analysis of collected water samples during the transect clearly shows that there is a gradient in suspended sediment mass concentration across the site.

Similar to the total volume concentration gradient the mass concentrations show an increase when moving eastward from the western extreme of the transect. The mass concentrations decrease in the vicinity of the mooring site before increasing again toward the eastern extremity. This is particularly noticeable in the surface waters. This gradient is again consistent with other observations of the presence of a turbid patch in the western region of this study area.

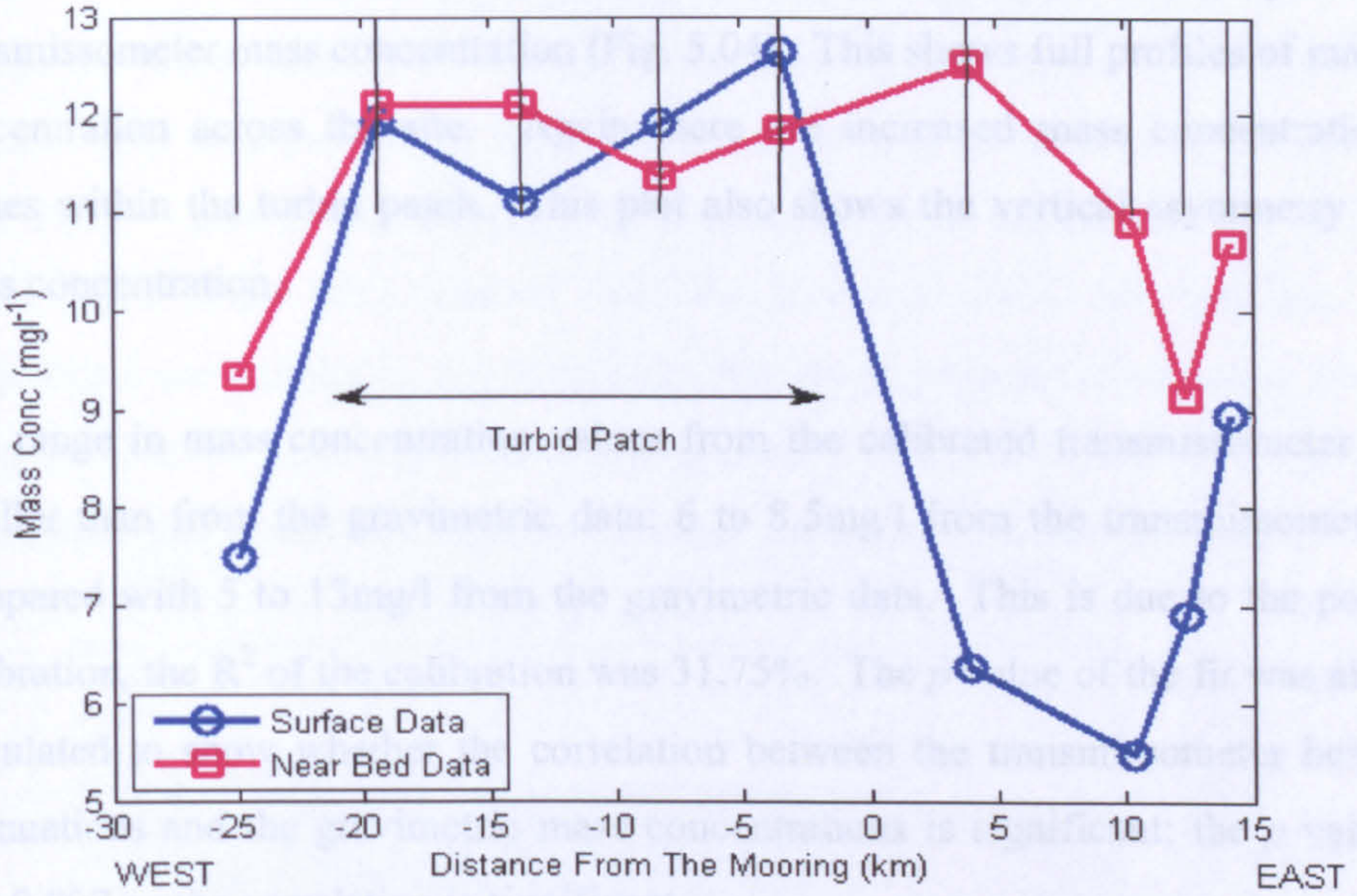

Fig. 5.02 The gradient in mass concentration across the observational site as calculated by gravimetric analysis. The observational site is located at 0 with the black lines showing the positions of 9 casts taken during the transect.

To enhance the detail of the mass concentration gradient located across the site the transmissometer was calibrated against the gravimetric data as described in Chapter 4.3 (Fig. 5.03).

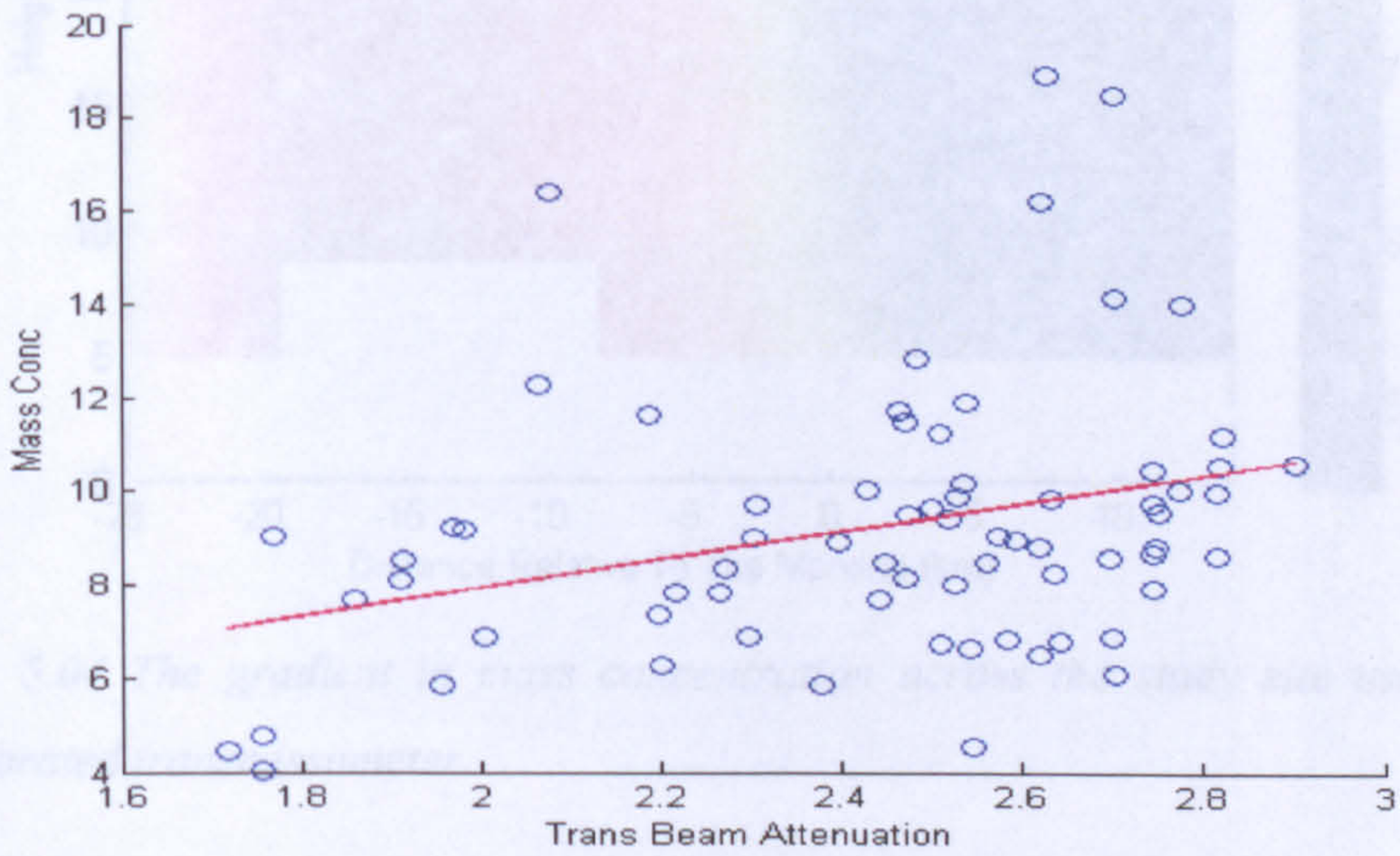

Fig. 5.03 Calibration plot of transmissometer beam attenuation against gravimetric mass concentration.

The calibration coefficients from Fig. 5.03 were used to produce a plot of transmissometer mass concentration (Fig. 5.04). This shows full profiles of mass concentration across the site. Again there are increased mass concentration values within the turbid patch. This plot also shows the vertical asymmetry in mass concentration.

The range in mass concentration values from the calibrated transmissometer is smaller than from the gravimetric data: 6 to 8.5mg/l from the transmissometer compared with 5 to 13mg/l from the gravimetric data. This is due to the poor calibration, the R^2 of the calibration was 31.75%. The *p* value of the fit was also calculated to show whether the correlation between the transmissometer beam attenuations and the gravimetric mass concentrations is significant; the *p* value was 0.007 so the correlation is significant.

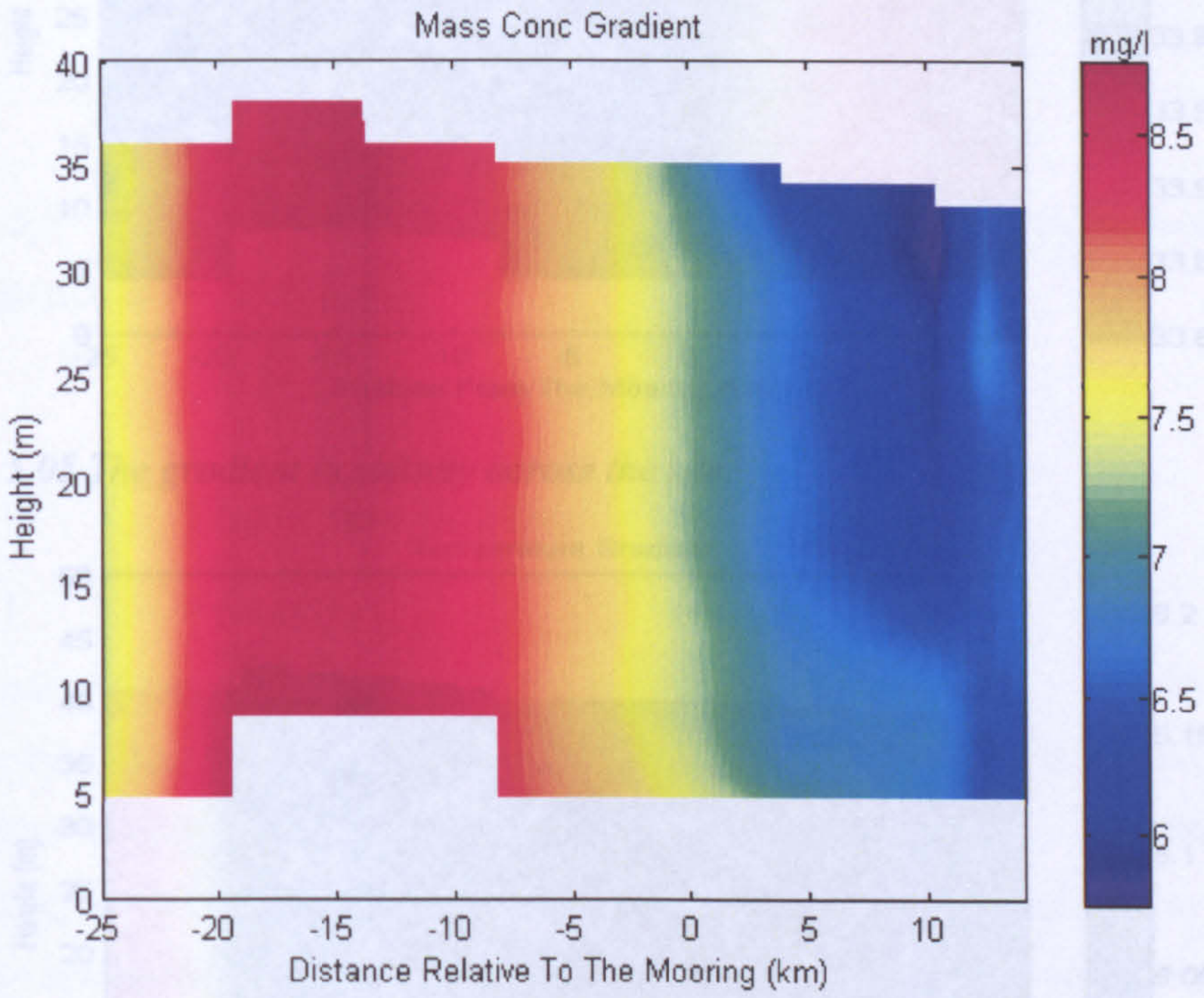

Fig. 5.04 The gradient in mass concentration across the study site using the calibrated transmissometer.

5.2.3 Temperature, Salinity and Chlorophyll

Within the turbid patch (to the west of the mooring site) there is a slight but uniform drop in salinity with higher values of salinity either side of the patch (Fig. 5.05). There is also a slight drop in temperature in the eastern part of the turbid patch (Fig. 5.06) centred over the mooring site. The gradient in temperature and salinity is, however, only very weak, with salinity ranging from about 33.85 to 34 and temperature ranging from 7.95 to 8.2C. Therefore, it can be assumed that conditions are approximately homogenous across the site.

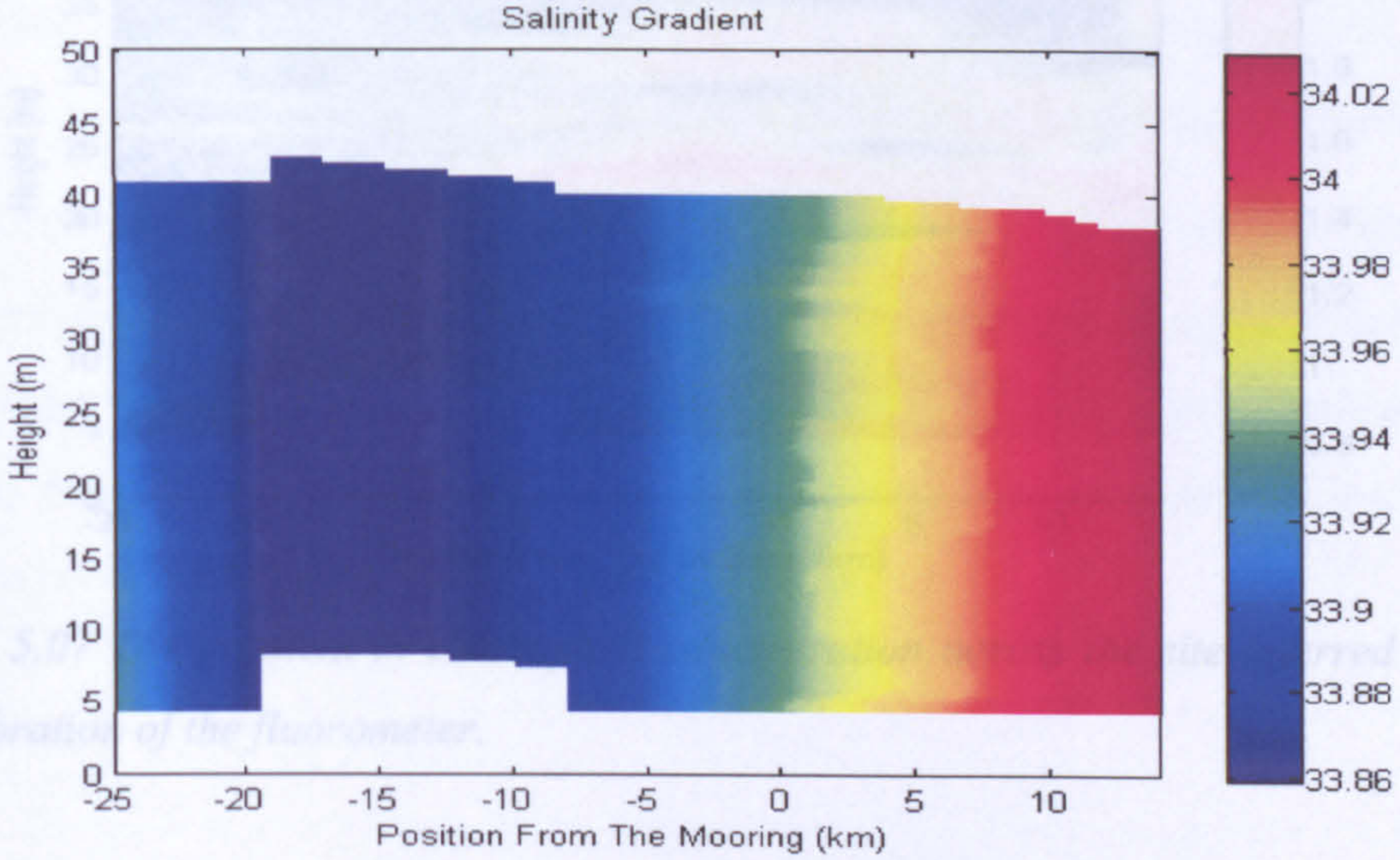

Fig. 5.05 The gradient in salinity across the site.

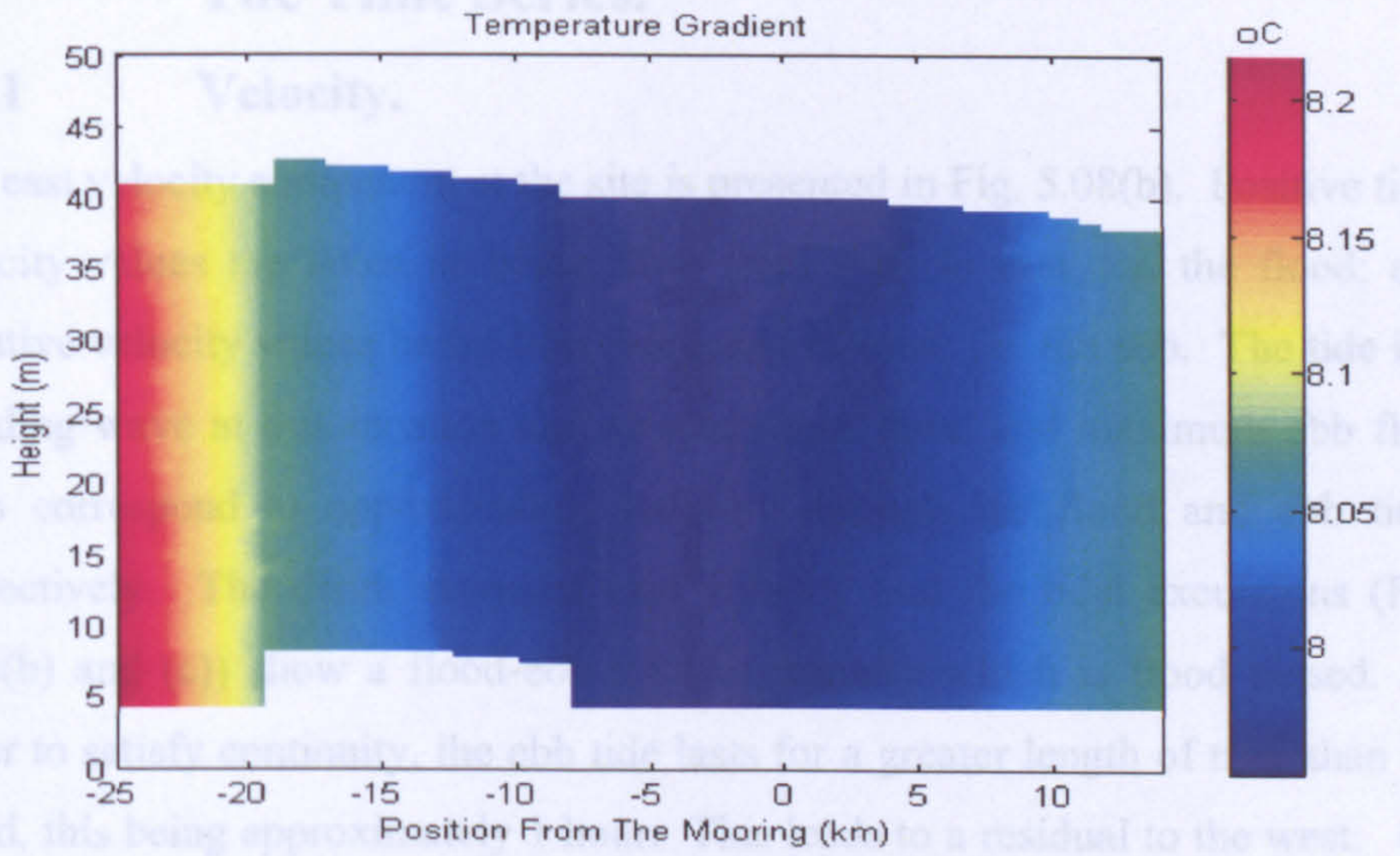

Fig. 5.06 The gradient in temperature across the site.

Applying the calibration discussed in Chapter 4.3.4.2 to the data collected by the fluorometer, the results show that there was little chlorophyll (0.8 to 2.4mgl^{-1}) present within the water column, as would be expected in February. Chlorophyll concentration increases across the site from west to east with higher chlorophyll concentrations being observed towards Liverpool Bay in the east (Fig. 5.07).

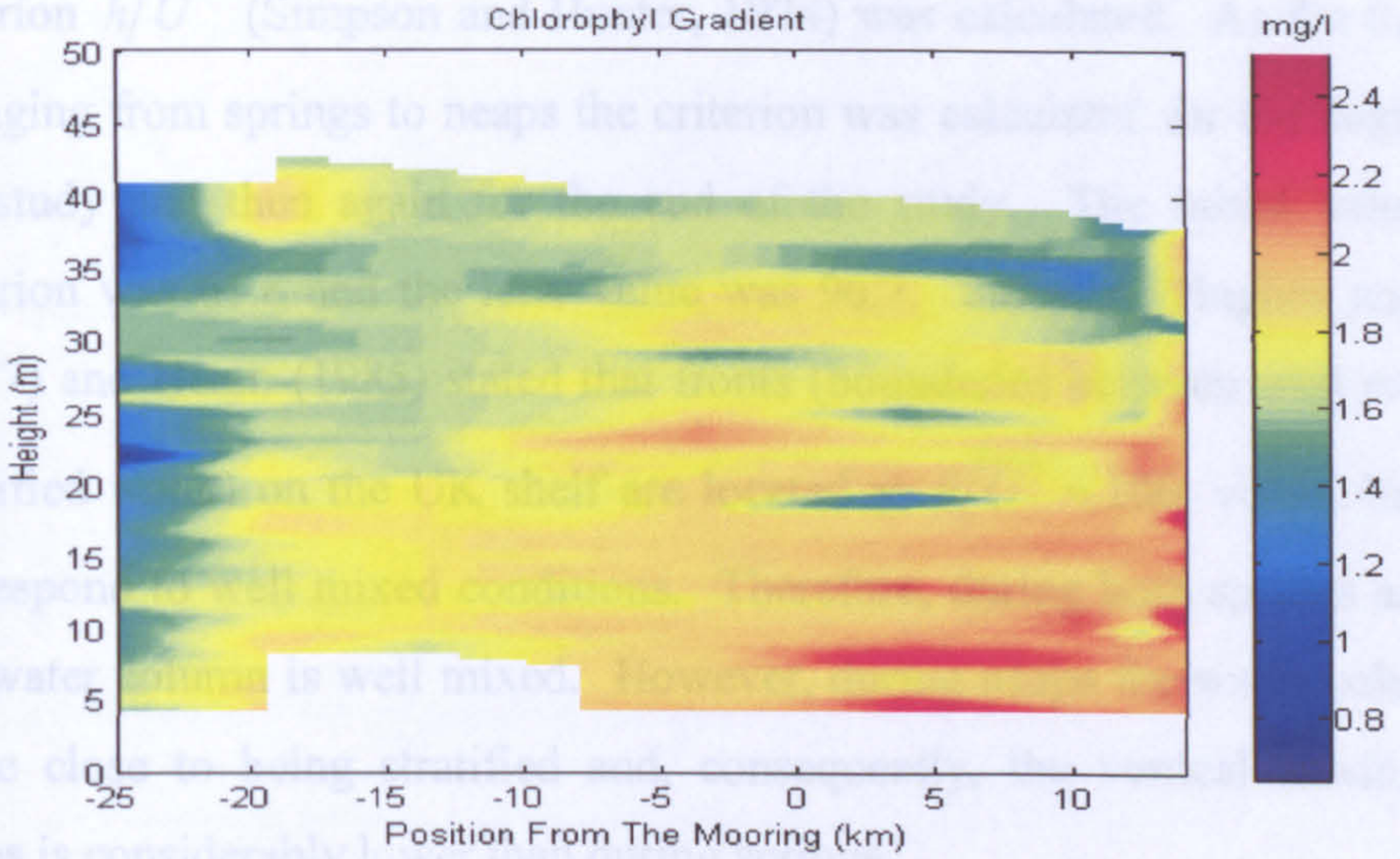

Fig. 5.07 The gradient in chlorophyll concentration across the site inferred by calibration of the fluorometer.

5.3 The Time Series.

5.3.1 Velocity.

The east velocity component at the site is presented in Fig. 5.08(b). Positive tidal velocity values are taken as being flow from west to east, i.e. the flood; and negative velocity values being flow from east to west, i.e. the ebb. The tide is a standing wave at this location and so maximum flood and maximum ebb flow rates correspond to approximately halfway through the flood and ebb tides respectively. The depth averaged east velocity and the tidal excursions (Fig. 5.08(b) and (c)) show a flood-ebb tidal asymmetry which is flood biased. In order to satisfy continuity, the ebb tide lasts for a greater length of time than the flood, this being approximately 1 hour. This leads to a residual to the west. On

account of the vertical shear within the tidal flow, the velocities and therefore the tidal excursions are greater at the surface than at the bed.

In order to quantify how well mixed the water column was the Simpson-Hunter criterion $h/\overline{U}^3$ (Simpson and Hunter, 1974) was calculated. As the tides were changing from springs to neaps the criterion was calculated for the beginning of the study and then again for the end of the study. The initial value of the criterion was 61.8 and the later value was 96.7. Simpson, Hughes and Morris (1977) and Hearn (1985) stated that fronts (boundaries between well mixed and stratified water) on the UK shelf are located at $h/\overline{U}^3 \approx 100$; values below this correspond to well mixed conditions. Therefore, during both springs and neaps the water column is well mixed. However, during neaps the water column may come close to being stratified and, consequently, the vertical mixing during neaps is considerably lower than during springs.

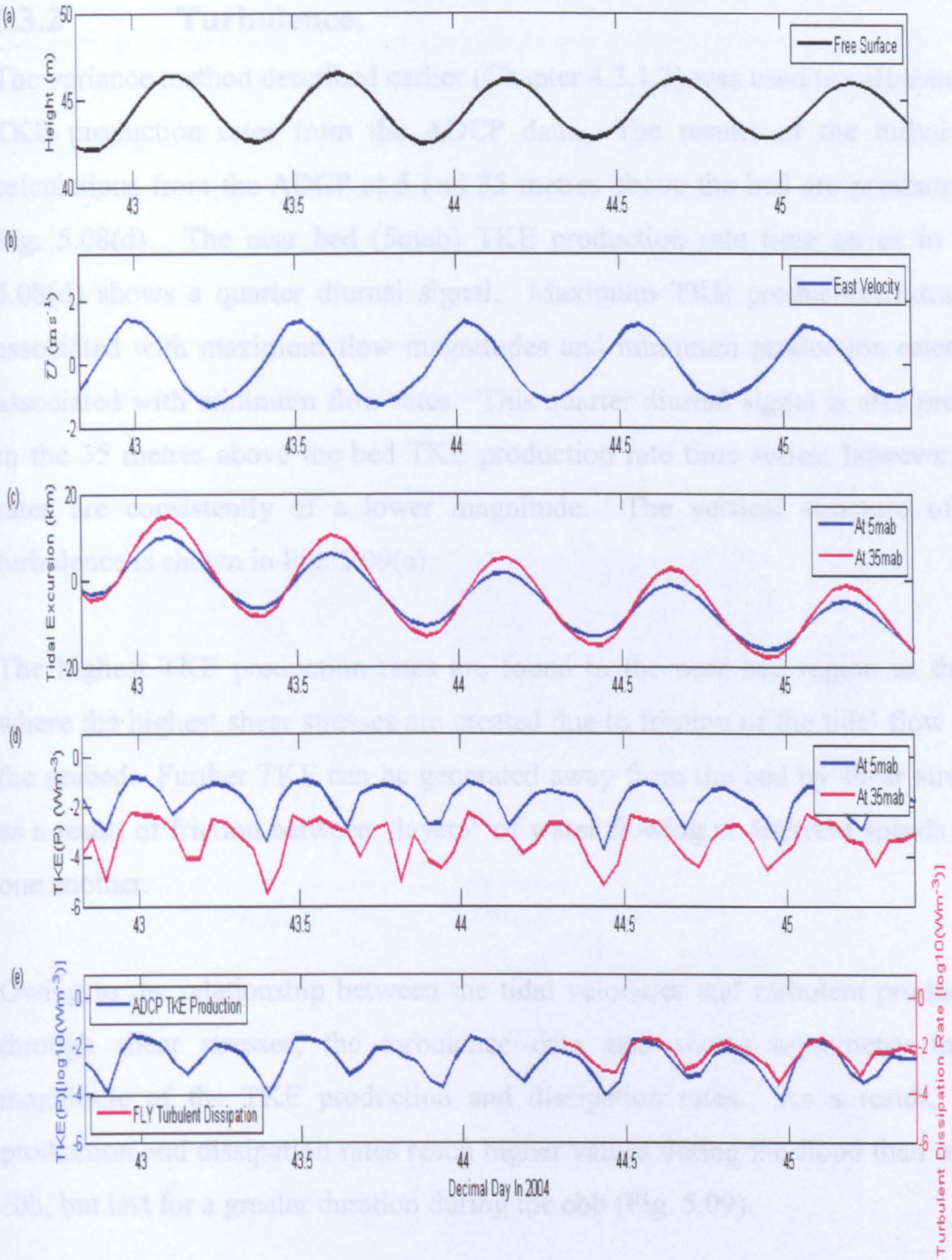

Fig. 5.08 shows at the mooring site (a) the free surface as derived from the ADCP pressure record, (b) the depth averaged east (major) velocity component, (c) the tidal excursion at 5 and 35mab, (d) the turbulent kinetic energy production (TKE) rate at 5 and 35mab and (e) the depth averaged TKE production rate from the ADCP and the depth averaged turbulent dissipation rate from the FLY.

5.3.2 Turbulence.

The variance method described earlier (Chapter 4.3.1.3) was used to calculate the TKE production rates from the ADCP data. The results of the turbulence calculations from the ADCP at 5 and 35 metres above the bed are presented in Fig. 5.08(d). The near bed (5mab) TKE production rate time series in Fig. 5.08(d) shows a quarter diurnal signal. Maximum TKE production rates are associated with maximum flow magnitudes and minimum production rates are associated with minimum flow rates. This quarter diurnal signal is also present in the 35 metres above the bed TKE production rate time series; however, the rates are consistently of a lower magnitude. The vertical structure of the turbulence is shown in Fig. 5.09(a).

The highest TKE production rates are found in the near bed region as this is where the highest shear stresses are created due to friction of the tidal flow with the seabed. Further TKE can be generated away from the bed by shear stresses as a result of friction between "layers" of water flowing at different speeds over one another.

Owing to the relationship between the tidal velocities and turbulent production through shear stresses, the turbulence data also shows asymmetry in the magnitude of the TKE production and dissipation rates. As a result, TKE production and dissipation rates reach higher values during the flood than on the ebb, but last for a greater duration during the ebb (Fig. 5.09).

As the flow decreases to slack water, the TKE production and dissipation rates decrease to levels approaching instrument noise. Intuitively this would be the case because as the tidal flow decreases to zero, the friction between the flow and the bed would correspondingly decrease to zero and so the shear stresses produced also decrease to zero; therefore TKE production and dissipation decrease to zero. The reduction in the magnitude of the turbulence during the observational period will later be shown to alter the behaviour of the sediments within the water column.

In previous studies of turbulence and sediments, assumptions have been made that the TKE production rate is approximately equal to the turbulent dissipation rate. A comparison of the depth averaged TKE production data from the ADCP and the TKE dissipation from the FLY is shown in Fig. 5.08(e). This appears to show that either the ADCP is underestimating or the FLY is overestimating turbulence levels. It is likely to be the former that the ADCP is underestimating potentially due to the fact the ADCP may not be quite orientated with the mean streamlines, as mentioned earlier (Chapter 4.3.1.4). This would introduce errors in the variance method calculations of the TKE production rate.

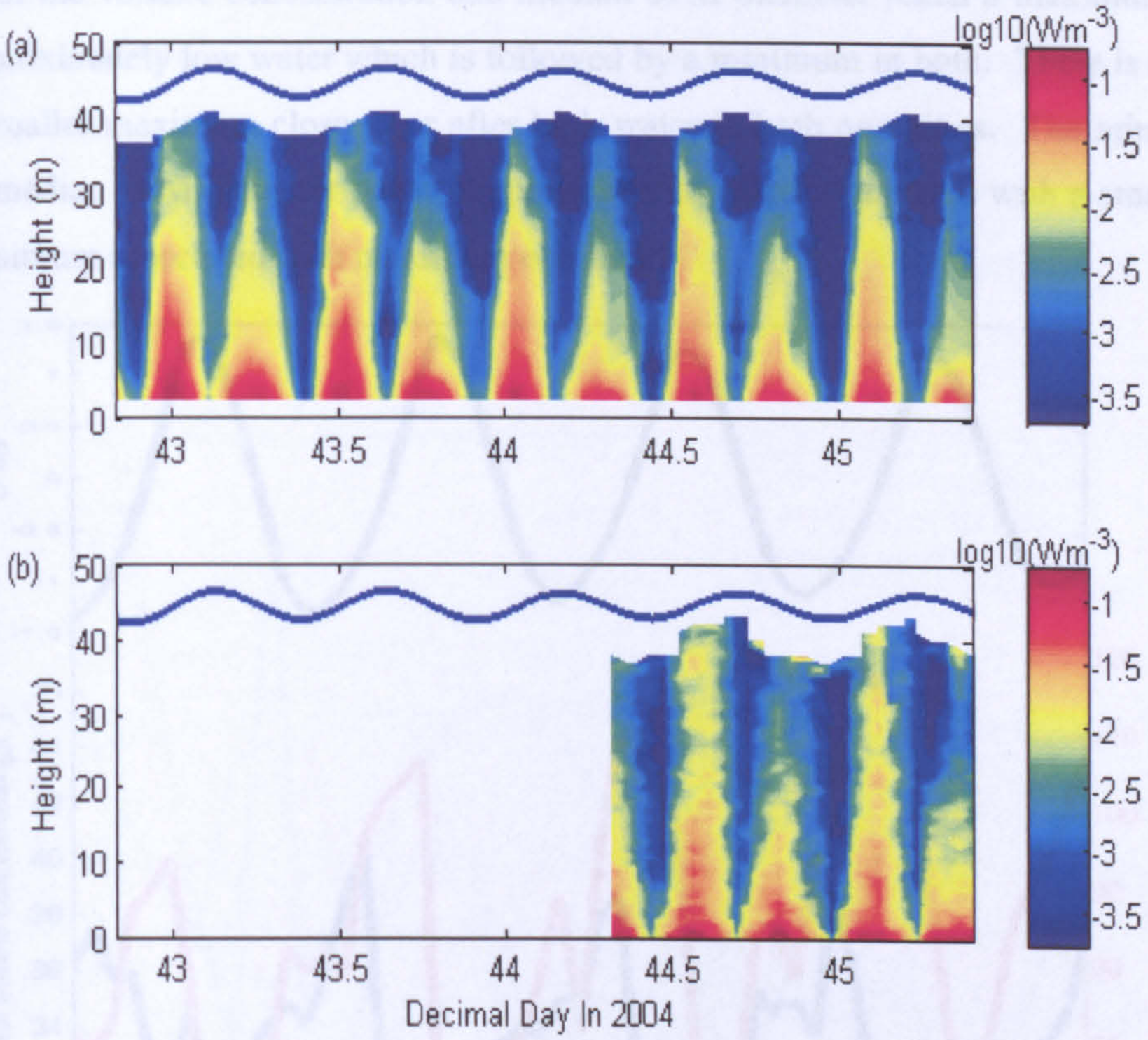

Fig. 5.09 (a) the vertical structure time series of total turbulent kinetic energy (TKE) production rate from the ADCP and (b) the vertical structure time series of turbulent dissipation from the FLY. The advantage of the FLY over the ADCP for turbulence measurements is that the FLY measures down to within 15cm of the bed compared with the 600 KHz ADCP used in this experiment which measures from approximately 2.5 metres above the bed.

5.3.3 SPM Results.

The depth averaged total suspended sediment volume concentration and median suspended sediment particle diameter data are presented in Fig. 5.10. This shows a semi diurnal signal in both the total volume concentration and median SPM diameter which appears to co-vary with velocity. Finer, low volume concentration particles are dominant during the flood tide and larger, higher volume concentration particles dominate during the ebb. Therefore, it appears that fine and coarse suspended sediment concentrations are inversely related.

Both the volume concentration and median SPM diameter reach a maximum at approximately low water which is followed by a minimum in both. There is also a smaller maximum close to or after high water in both quantities. The minima in median SPM diameter occur at approximately maximum flood with a smaller minimum associated with maximum ebb flow.

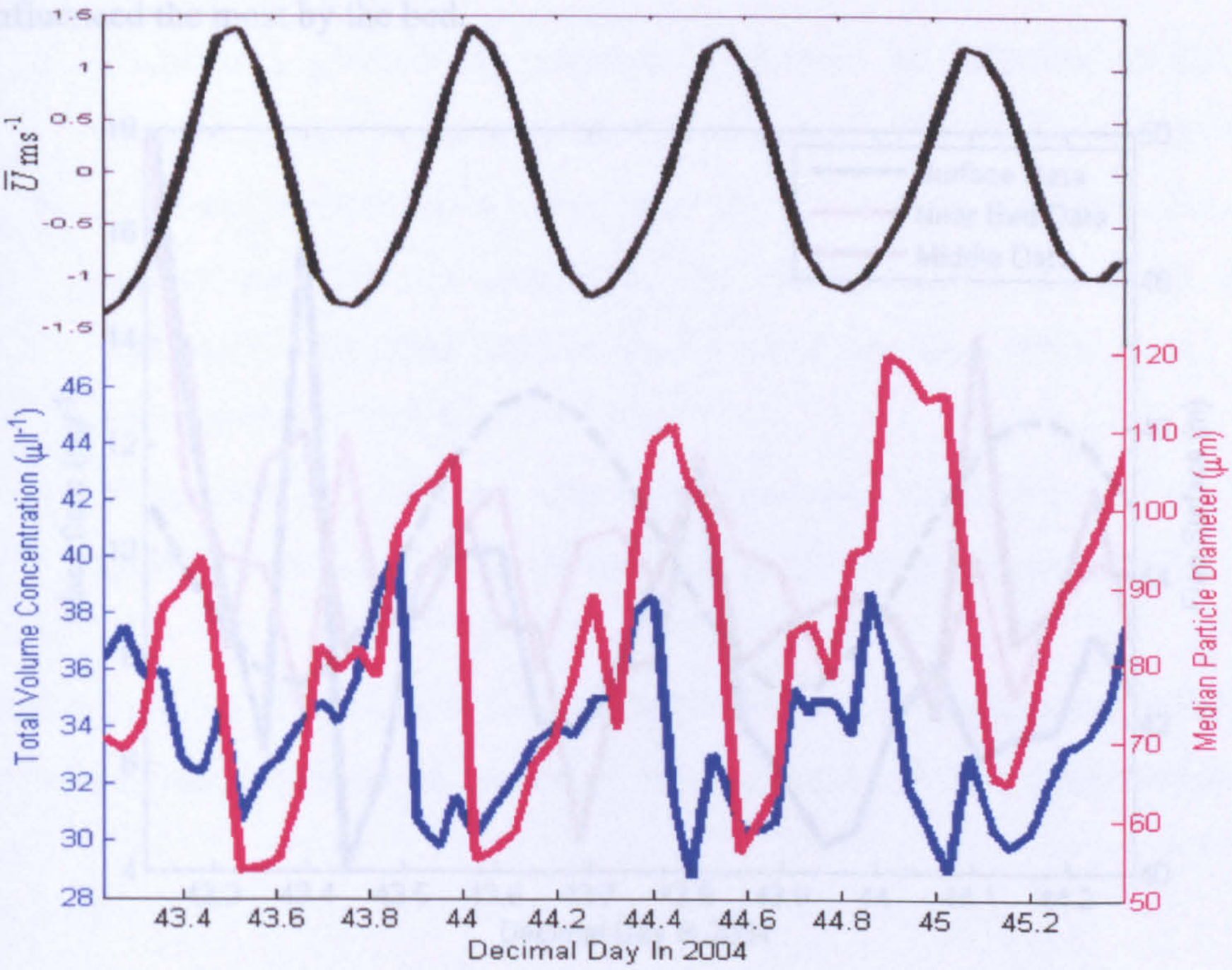

Fig. 5.10 Depth averaged time series of the total volume concentration (blue) and the median SPM diameter (red). The depth averaged east velocity is also plotted (black) to show the phase of the tide (+ve = flood, -ve = ebb).

The range in total suspended sediment volume concentration is generally decreasing as the tides decrease towards neaps, whereas the range in median SPM diameter is generally increasing over the observational period. This could be associated with the decrease in the tidal velocities towards neaps during the study.

5.3.4 Gravimetric Data.

After the first low water of the observational period there is a quarter diurnal signal in mass concentration at all heights (Fig. 5.11); this is approximately in phase with maximum flood and ebb flows. The time series in the near bed region of the water column (red) is much more irregular than in the surface waters and mid waters (blue and purple, respectively) as this is the region of the water column which experiences the highest magnitudes of turbulence and is also influenced the most by the bed.

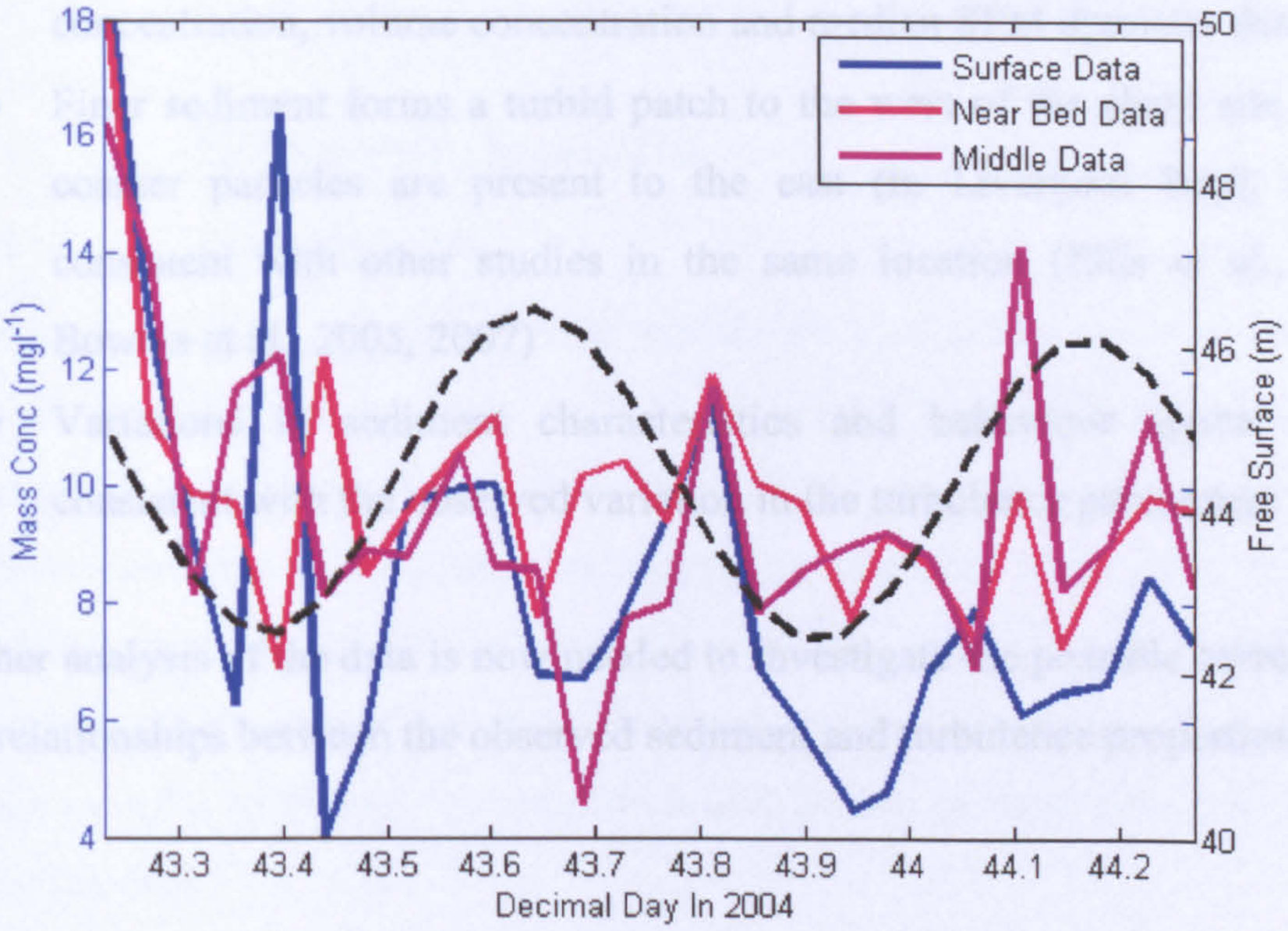

Fig. 5.11 Time series of mass concentrations at bottom (red), middle (magenta) and surface (blue) positions within the water column. The dashed black line is the free surface.

5.4 Summary

In this chapter has been presented:

- Suspended sediment mass concentration, volume concentration and median SPM size data collected from the transect carried out across the study site
- A description of the gradients in temperature, salinity and chlorophyll across the study site
- Velocity, turbulent kinetic energy production and turbulent kinetic energy dissipation time series data
- Suspended sediment volume concentration, median SPM diameter and mass concentration time series data.

The initial results show that:

- There is a gradient in suspended sediment as reflected in the mass concentration, volume concentration and median SPM diameter data
- Finer sediment forms a turbid patch to the west of the study site whilst coarser particles are present to the east (in Liverpool Bay); this is consistent with other studies in the same location (Ellis et al., 2004; Bowers et al., 2005, 2007)
- Variations in sediment characteristics and behaviour appear to be consistent with the observed variation in the turbulence parameters

Further analysis of the data is now needed to investigate the possible correlations and relationships between the observed sediment and turbulence properties.

Chapter 6

Analysis and Discussion.

6.1 Introduction.

In this chapter further analysis of the data is presented in order to discover possible quantitative and qualitative relationships between the hydrodynamics and SPM properties and dynamics at this site.

Harmonic analysis of both the sediment and velocity data is presented followed by a description of the results of entropy analysis performed on the sediment data. Variations in particle numbers for 2 sizes classes are scrutinised followed by the range of total particle numbers.

6.2 Harmonic Analysis.

6.2.1 Introduction.

In order to qualitatively relate SPM variability to the flow regime harmonic analysis is performed on both the velocity data (tidal analysis) and on the sediment data to identify the tidal signal within the SPM time series. The harmonic analysis is performed by dissecting the time series data of the 2 quantities (velocity and SPM volume concentration) using the tidal signals. This is done by regression analysis of the observed data against various tidal harmonic signals in order to identify the amplitude and phases of these tidal components within the data.

6.2.2 Velocity.

Multi-regression harmonic analysis was carried out on the velocity data in order to isolate the 3 main tidal components in the region: M2 (the principal lunar semi-diurnal constituent), M4 (the shallow water overtides of principal lunar

constituent; quarter-diurnal) and K1 (the lunar diurnal constituent). Separation of more constituents was not possible due to the limited length of the data set.

The harmonic analysis of both the east and north velocity components revealed that the quarter-diurnal (M4) amplitude is 11.4% of the semi-diurnal (M2) amplitude and so the tidal flow is dominated by the semi-diurnal (M2) component at this site. The M2 amplitude of the north component is only 17.1% of the M2 amplitude of the east component. This shows that the tide is dominant along the east-west axis at this site. There are phase differences of approximately 0.04, 0.2 and 0.8 hours for the M2, M4 and K1 tidal components respectively between the flow at the bed and at the free surface.

6.2.3 SPM.

In order to consider relationships between the hydrodynamics and the sediment dynamics/properties, harmonic analysis of the 2 main tidal constituents – semi-diurnal (M2) and quarter-diurnal (M4), was performed on the sediment results (Fig. 6.01); the time scale of the phase values are in hours after the first low water. Only the M2 and M4 components were used as these appear to be the main components at this site. Also, separation of more constituents was again not possible due to the limited length of the data.

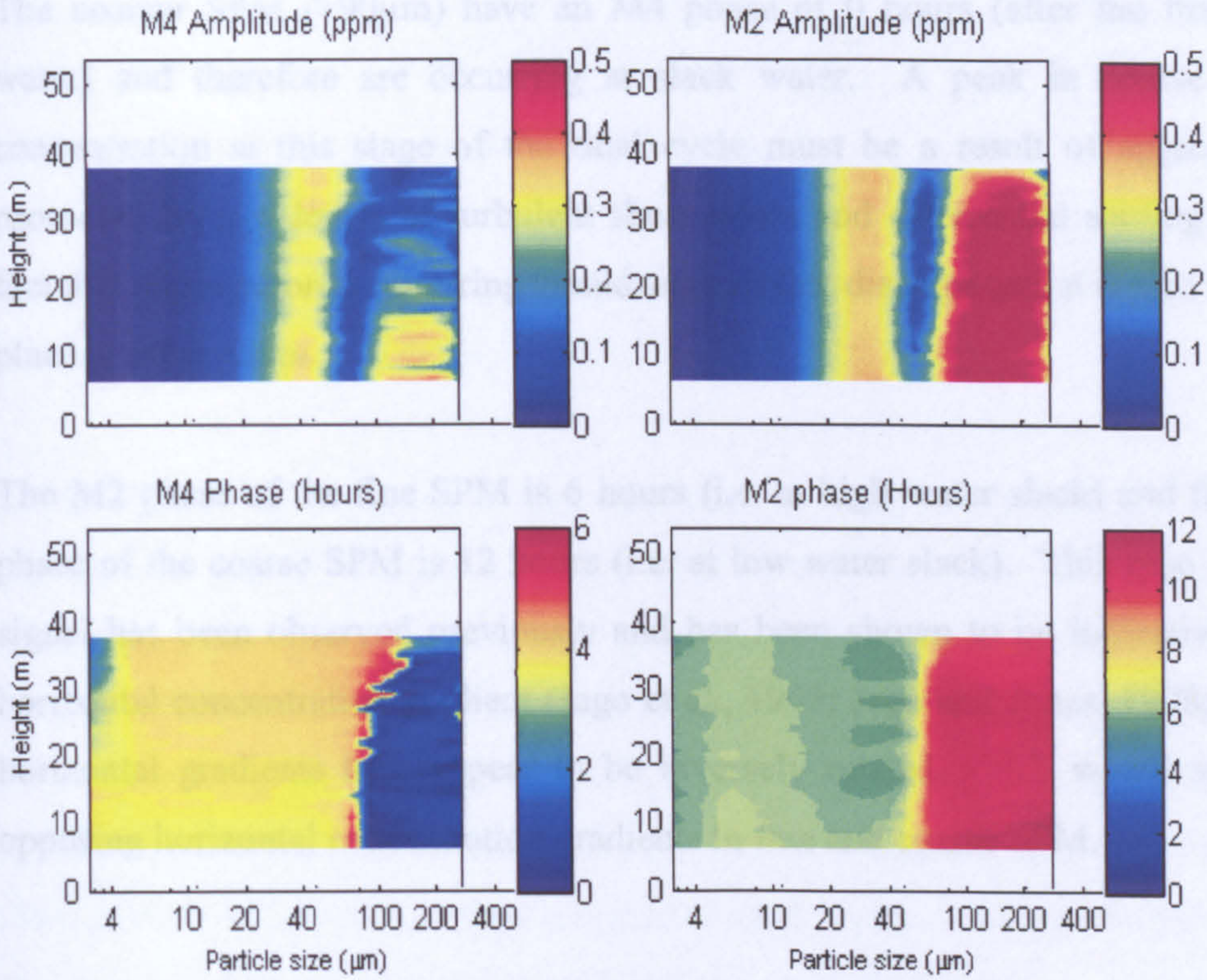

Fig. 6.01 Results of harmonic analysis on the sediment data.

The harmonic analysis shows that amplitudes in both the M2 and M4 components possess peaks centred at approximately 55µm and 150µm. The phase differences in the M2 and M4 components both show a clear size distribution split at approximately 90µm. Therefore, it is reasonable to say that the SPM present at this site consists of 2 distinct characteristic size classes centred around 55 and 150µm.

The finer SPM (<90µm), have an M4 phase of 3 hours (after the first low water) at the bed which increases to 4.5 hours at the surface. Therefore, this occurs at maximum flow and thus maximum stress at the bed which then propagates up through the water column. This feature is consistent with a resuspension event (Jago et. al 2006); however it could also be as a result of disaggregation of large flocs taking place due to the high shear stresses, or alternatively both of these mechanisms.

The coarser SPM (>90μm) have an M4 phase of 0 hours (after the first low water) and therefore are occurring at slack water. A peak in coarse SPM concentration at this stage of the tidal cycle must be a result of aggregation promoted by low levels of turbulent shear stress and differential settling. The fact that aggregation is occurring would suggest that disaggregation is also taking place at other times.

The M2 phase of the fine SPM is 6 hours (i.e. at high water slack) and the M2 phase of the coarse SPM is 12 hours (i.e. at low water slack). This type of M2 signal has been observed previously and has been shown to be indicative of a horizontal concentration gradient (Jago et al., 1993; Jago and Jones, 1998). The horizontal gradients here appear to be inversely related which would suggest opposing horizontal concentration gradients in fine and coarse SPM.

6.3 Entropy Analysis.

Another method of analysis of sediment data is entropy analysis which has been developed by Mikkelsen et al. (2007). The concept of entropy has been developed from information theory in which entropy is related to the randomness of an event or signal and so entropy links the information content of a given signal or event to the randomness of that event. Therefore, if an event is highly random, i.e. has high entropy then the information content of that event is low and vice versa. This translates to particle size by examination of individual size spectra whereby maximum entropy is assigned to a completely flat size spectrum. This is a spectrum where all volume/mass in a size spectrum occurs at the same frequency, i.e. a highly random distribution of matter throughout the size spectrum. Minimum entropy is assigned to a size spectrum which consists of the entire particle volume/mass being found at a single size. The entropy, E, of a given size spectrum with n size bins is given by Eq. 6.01 (Shannon, 1948; Johnston and Semple, 1983).

$$E = -\sum_{i=1}^{n} p_i \log p_i \qquad (Eq.\ 6.01)$$

where: p_i = the proportion of particles in size bin i

The entropy value is then related to an information gain value, I, by Eq. 6.02.

$$I = (\log n) - E \qquad (Eq.\ 6.02)$$

When entropy of a particular size spectrum is maximum (i.e. flat) then the information gain, I, is equal to zero. Thus as the value of I increases so the information content of a given size spectrum increases. With a collection of data, in this case size spectra, the calculations above are performed and then the results can be split into groups. Each group contains a set of similarly shaped spectra which possess similar entropy and information gain values. A characteristic size spectra is then assigned to each group so that the shapes of the size spectra differ between groups rather than within the groups.

This analysis technique was performed on the size spectra collected by the LISST during each profile in order to confirm the presence of the 2 distinct size populations indicated by the harmonic analysis (Fig. 6.02). A point to note about Fig. 6.02 is that due to the bell-shaped curves of the grouped spectra it shows that the LISST is "seeing" the full size distribution of the SPM present as the curves are closed.

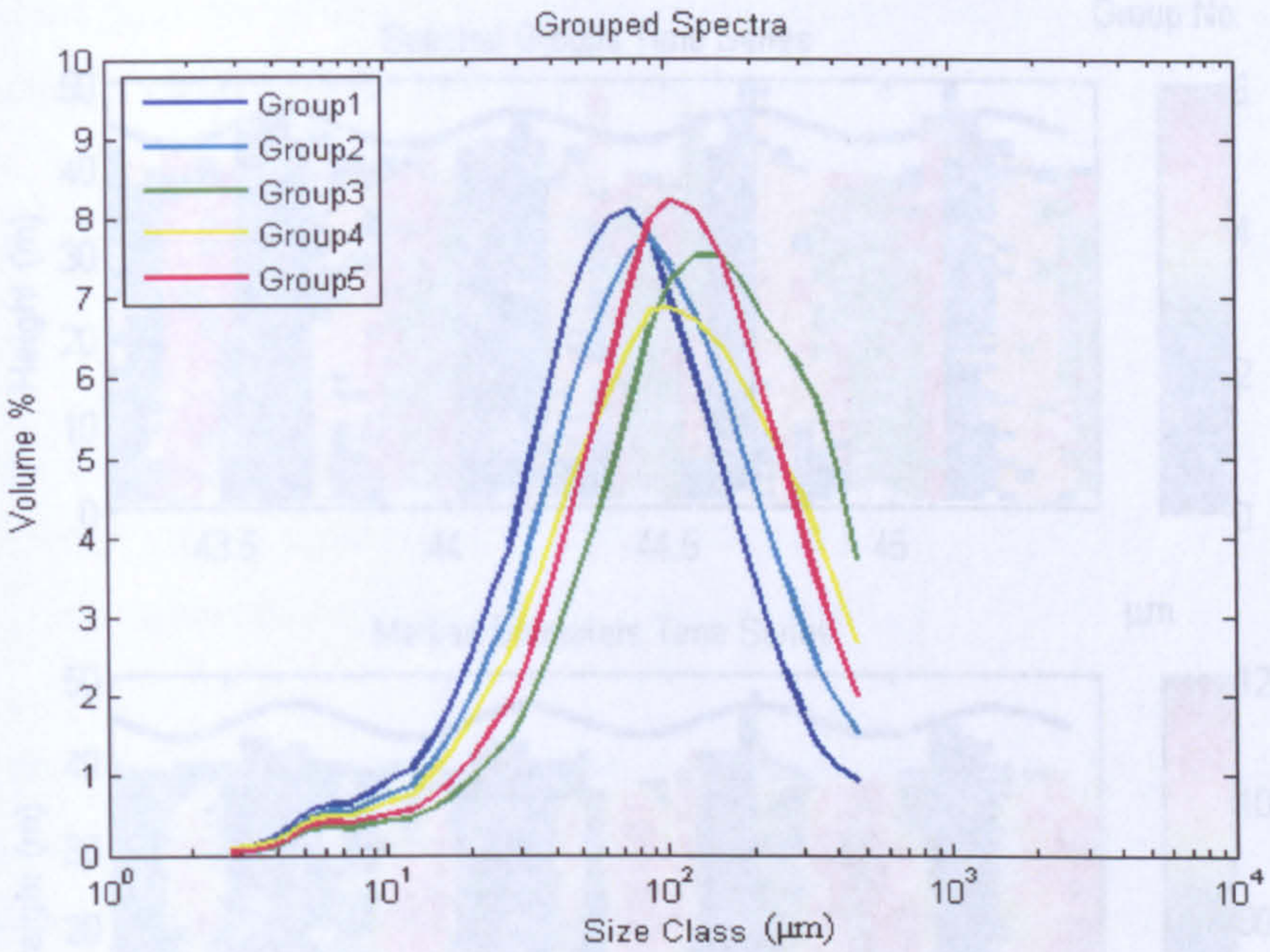

Fig. 6.02 Grouped size distribution spectra from the LISST as output by the entropy analysis.

The results of the grouping process shows that there are 5 characteristic groups within the dataset of size spectra. All 5 groups share a similar spectral shape but each has a peak at a different size class. However, the 5 groups could be grouped further into just 2 groups: a group with a peak at a size class below 100µm and another group with a peak greater than 100µm.

This additional grouping into just 2 characteristic groups is further highlighted upon comparison of the grouped spectra time series with the median SPM diameter time series (Fig. 6.03). From this it can be seen that the 2 blue groups, i.e. groups 1 and 2, are associated with periods of lower median SPM diameter and the remaining groups, i.e. groups 3, 4 and 5, are associated with periods of higher median SPM diameter. This therefore confirms that the SPM at this site can be described by 2 distinct size populations which show an inverse relationship.

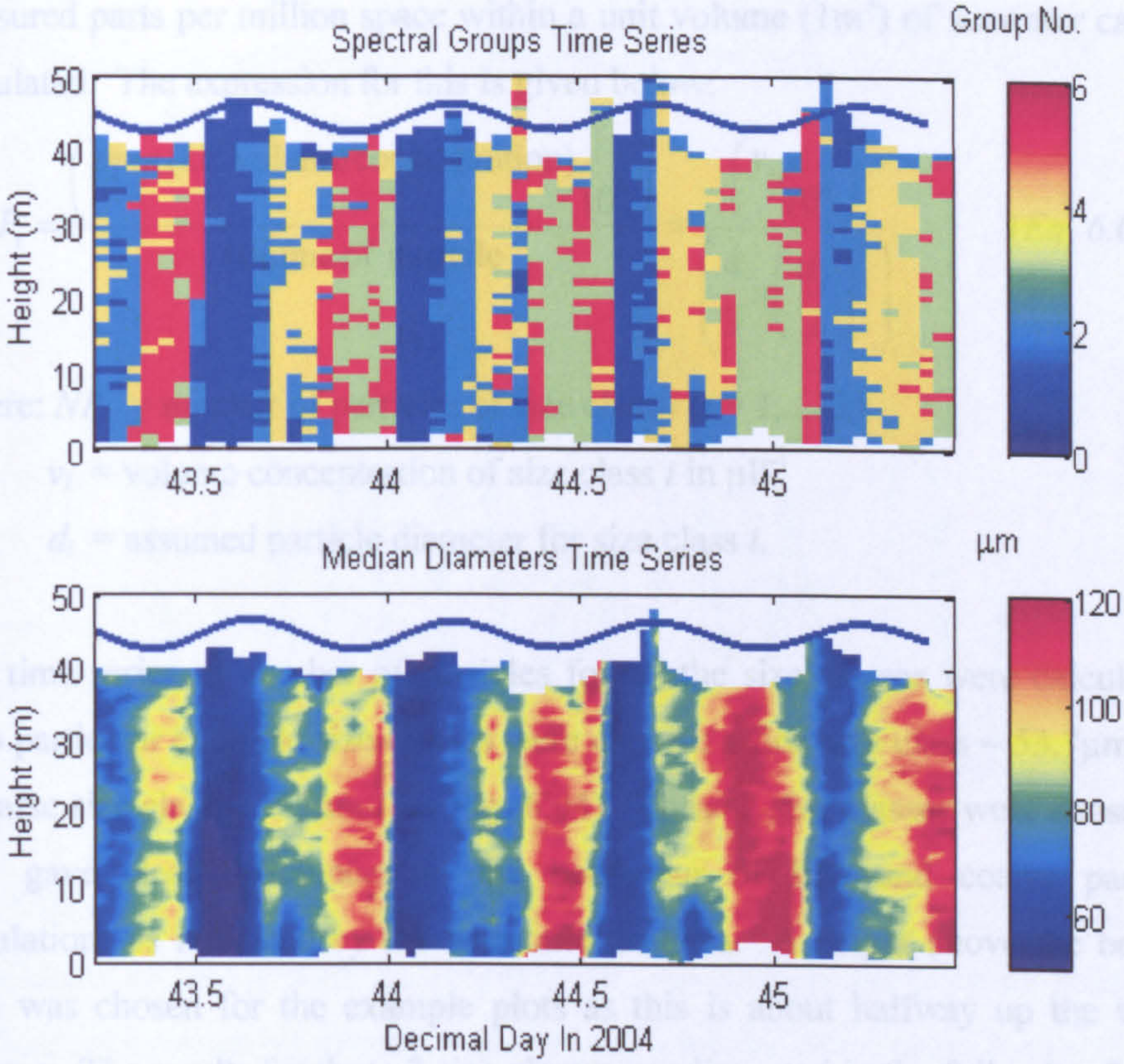

Fig. 6.03 Time series of the spectral groups produced by the entropy analysis compared with the time series of median SPM diameter.

6.4 Particle Numbers.

6.4.1 Description.

The volume concentration data that is produced by the LISST can be used to estimate the number of suspended particles present per cubic metre. This was done as the resulting time series may show more clearly the differences in the variation observed in particular size class behaviour. At each sampling interval the LISST measures the volume concentration of 32 differently sized particles. The units of volume concentration are microlitres per litre ($\mu l l^{-1}$). This is equivalent to a part per million (ppm) measure. In addition, as each of the 32 size classes has an assumed size, they, as a result, have an assumed volume. Therefore, the number of particles, with a particular volume, required to fill the

measured parts per million space within a unit volume ($1m^3$) of seawater can be calculated. The expression for this is given below:

$$NP_i = \frac{\left(ppm \text{ (i.e. volume concentration)} / 10^6 \right)}{\text{volume of particle}} = \frac{\left(v_i / 10^6 \right)}{\left(\frac{4}{3}\pi \left(\frac{d_i}{2} \right)^3 \right)} \qquad (Eq.\ 6.03)$$

Where: NP_i = number of particles of size class i (i = 1,..,32)

v_i = volume concentration of size class i in $\mu l l^{-1}$

d_i = assumed particle diameter for size class i.

The time series of number of particles for all the size classes were calculated. Two particular example size classes were chosen: a fine size class – 53.7μm and a coarse size class – 157μm (see Fig. 6.04). These 2 size classes were chosen as they gave clear differences in the behaviour of fine and coarse particle populations as indicated by the harmonic analysis. A height above the bed of 22m was chosen for the example plots as this is about halfway up the water column. The results for these 2 size classes are discussed in the following 2 sub-sections.

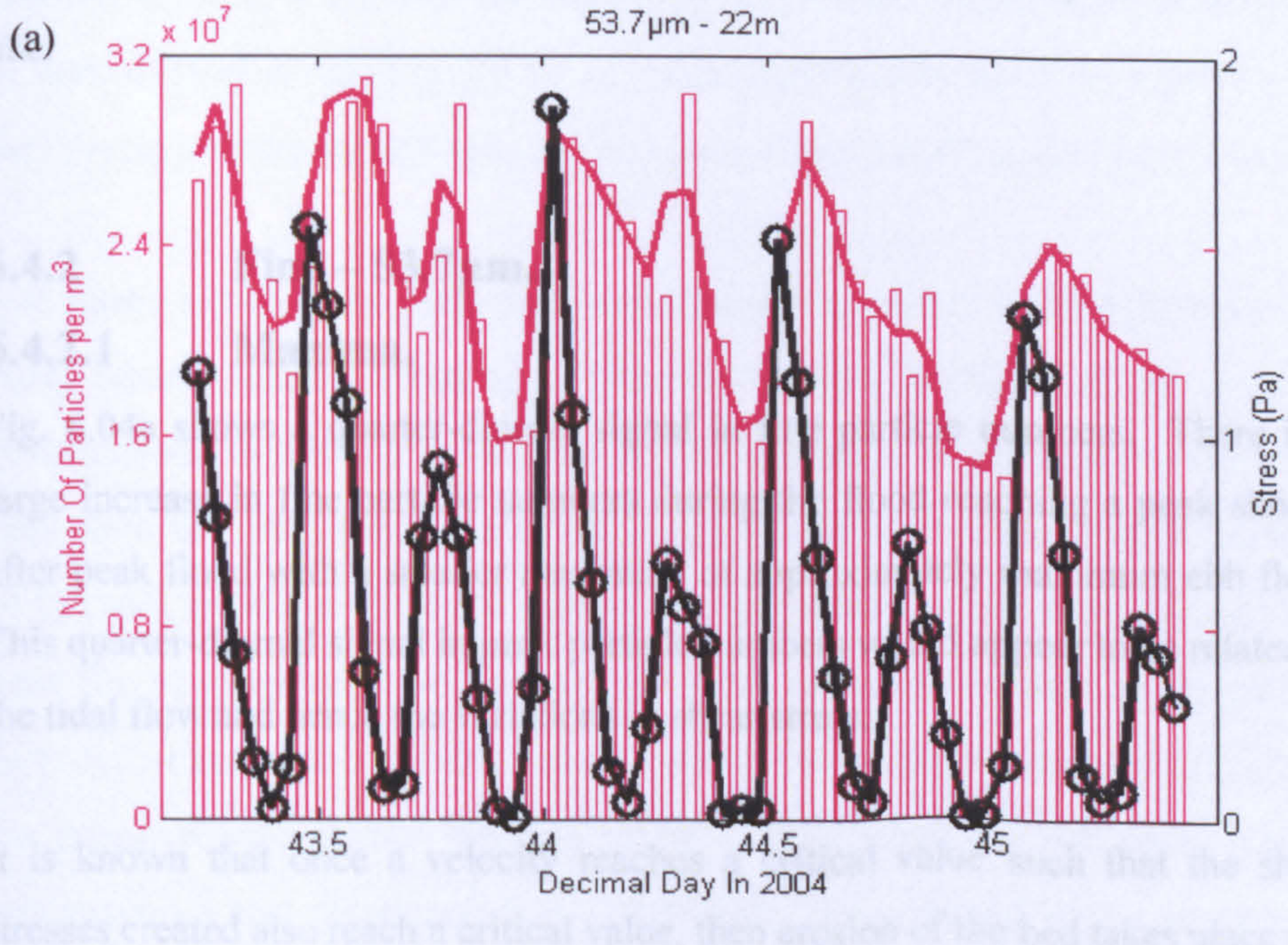

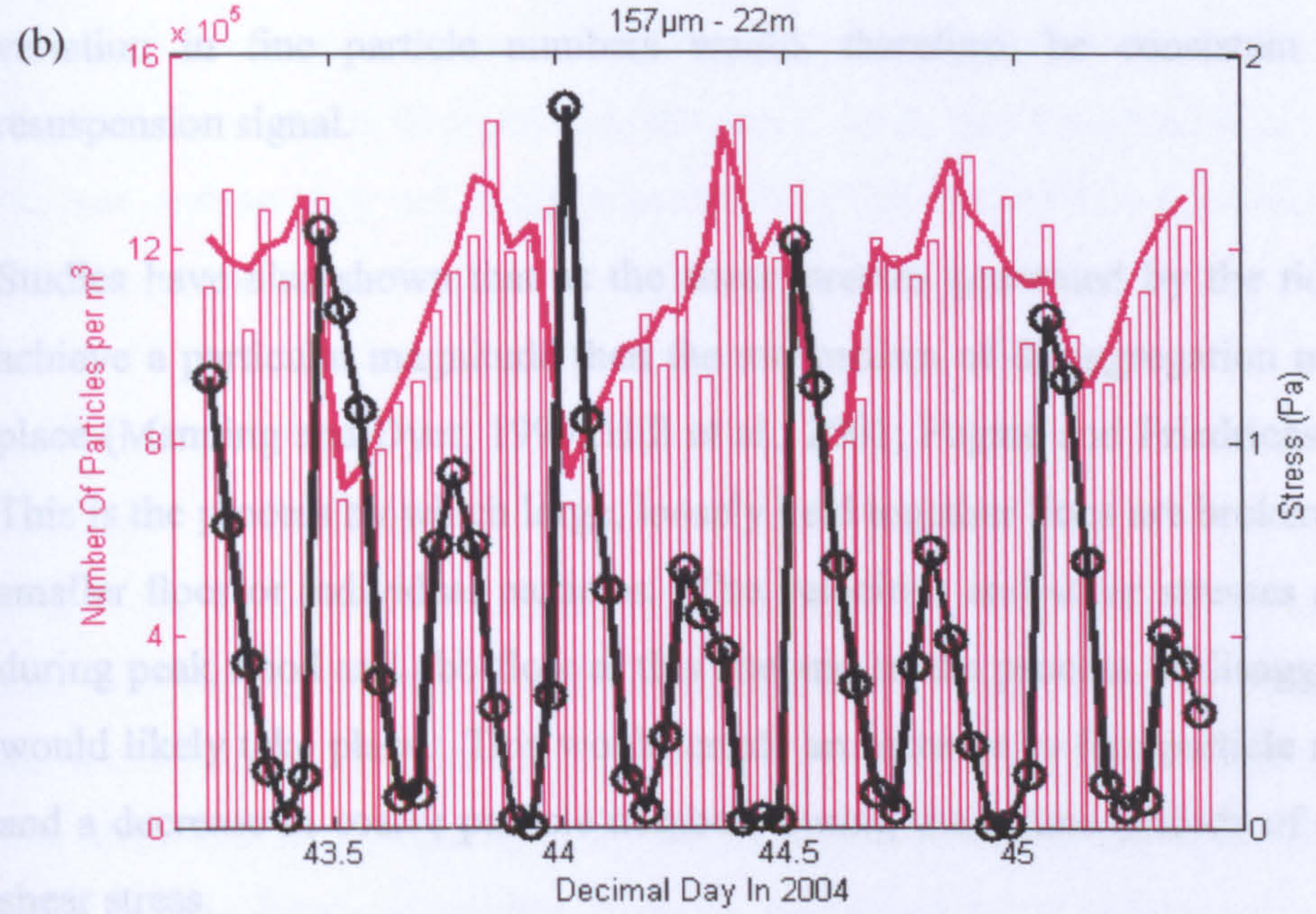

Fig. 6.04a and Fig. 6.04b show the times series of number of particles for the size classes 53.7µm and 157µm respectively. The particle numbers are plotted in red bars with a running-average red line and with the shear stress time series as measured at the same height in black. Note that the larger maximum stresses correspond to the flood tide and the smaller maximums correspond to the ebb tide.

6.4.2 Fine – 53.7µm.

6.4.2.1 Maxima.

Fig. 6.04a shows a quarter-diurnal signal in fine particle numbers. There is a large increase in fine particle numbers during the flood reaching a peak shortly after peak flood with a smaller maximum at approximately maximum ebb flow. This quarter-diurnal signal in peak particle numbers would appear to be related to the tidal flow and hence the variations in shear stress.

It is known that once a velocity reaches a critical value such that the shear stresses created also reach a critical value, then erosion of the bed takes place and resuspension of bed material takes place. The quarter-diurnal nature of the

variation in fine particle numbers would, therefore, be consistent with a resuspension signal.

Studies have also shown that as the shear stresses generated by the tidal flow achieve a particular magnitude then the mechanism of disaggregation may take place (Manning and Dyer, 1999; Hill et al., 2001; Fugate and Friedrichs, 2003). This is the process by which large, loosely held together flocs are broken up into smaller flocs or individual particles. The velocities and shear stresses are high during peak flood and ebb flow at this site and so the process of disaggregation would likely take place. This would create an increase in fine particle numbers and a decrease in coarse particle numbers during these time periods of elevated shear stress.

Advection of the turbid patch is another possible mechanism which would increase fine particle numbers during the flood. Harmonic analysis on the velocity time series showed that the tidal flow at this site was essentially west-east. Therefore, it follows that during the flood tide, as the tide floods from west to east, the turbid patch could be advected eastward by the tide, creating elevated fine particle numbers and reduced coarse particle numbers during the flood.

The range between the maximum and minimum number of fine particles over the study period reduces from approximately 1.4×10^7 particles at the beginning of observations to 0.9×10^7 particles. If the variation in particles is related to the tidal flow then this reduction in the range would be consistent with the reduction in the magnitude of the tidal currents as the tides change from springs to neaps over the observational period. As the tidal currents decrease in magnitude, the flow will exceed the critical values needed for resuspension and disaggregation for progressively shorter periods of time, which could result in a reduction in resuspension and disaggregation. Therefore, there would be a reduction in fine particle numbers overall. It is worth remembering however, that the high tidal velocities at the site mean that the critical values required for resuspension and disaggregation are exceeded for much of the tidal cycle. In addition to a possible

reduction in resuspension and disaggregation, if the turbid patch is advected by the flow, then as the flow reduces, the patch would not be advected as far over the site and so may not contribute as much fine material to the fine particle numbers at the site as during periods of higher tidal flows.

6.4.2.2 Minima.

Due to the quarter-diurnal nature of the variation in fine particle numbers, the time series shows that the minima are consistent with periods of low stress within the water column. Studies have shown that during periods of low tidal flow and low shear stress, aggregation may take place (Eisma, 1986; Xia et al., 2004). At times of low levels of mixing, particles can aggregate together to form larger flocs, such as by differential settling. As a result, numbers of fine particles would decrease whilst numbers of coarser particles would increase.

The pronounced minimum in fine particle numbers occurs at approximately low water slack. As a result of the west-east tidal flow, the turbid patch would be at its most westerly position due to advection processes, therefore, the fine particles introduced during the flood would now have been advected westward away from the observational site. This would produce a reduction in fine particle numbers and an increase in coarse particle numbers.

6.4.3 Coarse – 157µm.

6.4.3.1 Maxima.

Fig. 6.04b shows that overall particle numbers of coarse particles are over an order of magnitude lower than that of the fine particles and that there is a semi-diurnal signal in the coarse particles numbers. The lower magnitude of coarse particles may be due to the fact a single coarse floc may be composed of a number of fine 'particles' and so their numbers would be lower.

The main peak in coarse particle numbers occurs during the ebb tide; this is when the tidal flow is east to west. As the variation in particle numbers appears to be related to variations in the tidal flow, this would be consistent with the turbid patch being advected back towards the west by the flow. As a result there would be a reduction in fine particles numbers and an increase in coarse particle numbers as coarser particles from Liverpool Bay (in the east) are introduced.

6.4.3.2 Minima.

As a consequence of the semi-diurnal signal present in the coarse particle numbers the minimum occurs during the flood at approximately maximum shear stress. A possible explanation for this is that the high shear stresses could be disaggregating the large flocs into finer flocs or individual fine particles resulting in a reduction in coarse particle numbers and an increase in fine particle numbers.

Also, as a result of possible advection of the turbid patch, maximum flood tidal flow would be associated with the turbid patch being located over the study site and the coarser particles being out to the east of the site. The consequence of this would be a reduction in coarse particle numbers and an increase in fine particle numbers.

6.4.4 Total Particle Numbers.

The particle numbers of each size class at each height for each cast were calculated and so the total number of particles of all sizes at all heights for each cast were also be calculated (Fig. 6.05).

$$TNP(t) = \sum_{i=1}^{32} \sum_{j=1}^{N} NP_{ij} \qquad (Eq.\ 6.04)$$

where: $TNP(t)$ = total number of particles at time t

NP_{ij} = number of particles of size class i at height j.

Fig. 6.05 shows that the total number of particles co-varies with the state of the tide. Maximum total particle numbers occur at high water with minimum occurring at low water.

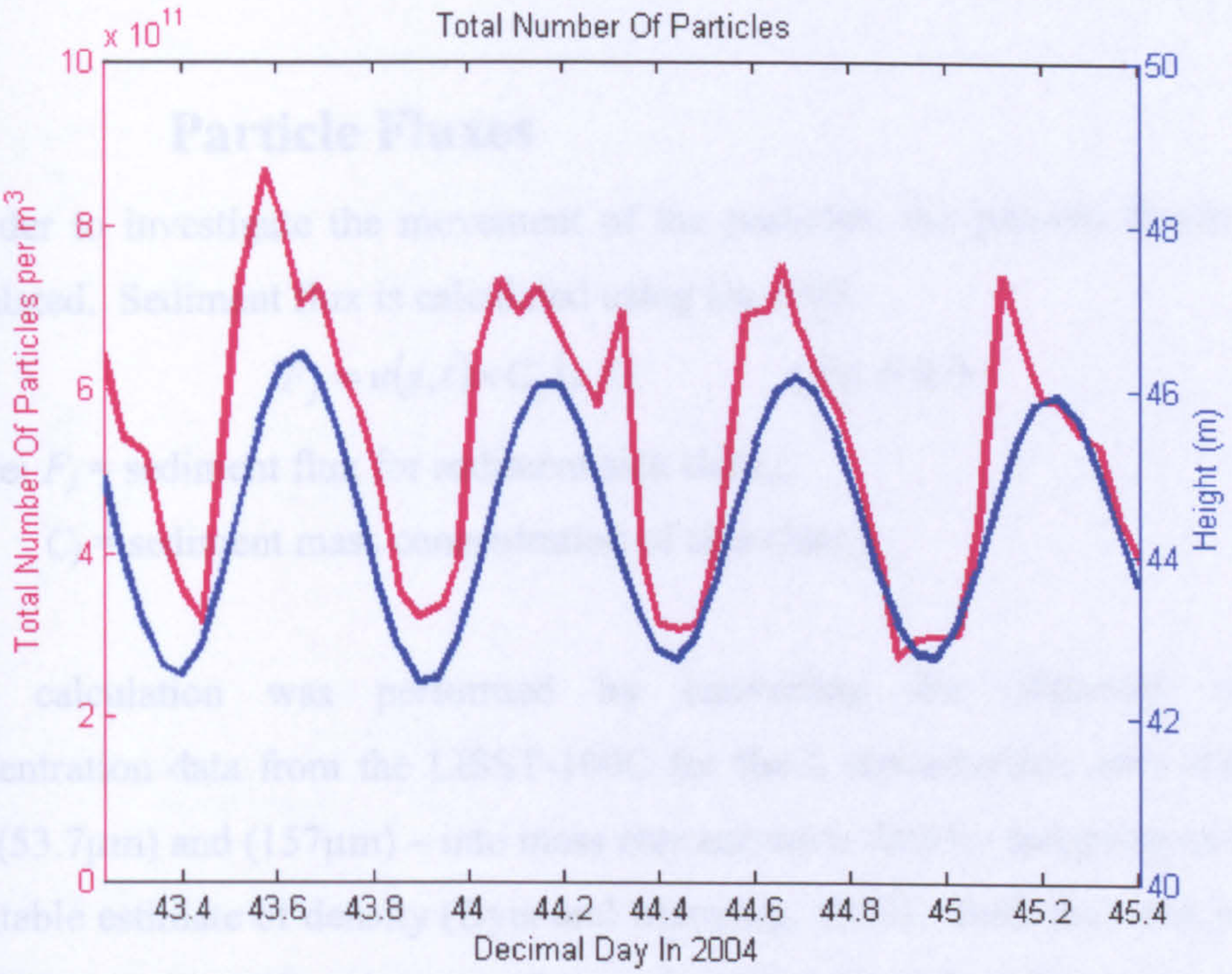

Fig. 6.05 Times series of total particle numbers within the water column (red). The free surface (blue) is also plotted for clarity.

As the sediment particle number variations seem to be associated with the tidal flow, the maximum total particle numbers at high water would be consistent with a large number of fine particles being introduced during the flood as a result of advection of the turbid patch eastward across the site. Similarly, the minimum total particle numbers at low water could be due to the removal of the fine particles by the reverse action of the advection of turbid patch westward during the ebb tide.

The range in total particle numbers is between 4.1 and 5.5×10^{11} particles per cubic metre. The range of the total particle numbers appears to be fixed between the upper and lower limits of the range; although the tidal cycle is decreasing from springs to neaps the maximum and minimum values do not fluctuate

greatly. Therefore, this implies that the SPM levels are in a steady (self sustaining) state which is not affected by the springs-neaps cycle.

6.5 Particle Fluxes

In order to investigate the movement of the particles, the particle fluxes were calculated. Sediment flux is calculated using Eq. 6.05.

$$F_j = u(z,t) \times C_j(z,t) \qquad (Eq.\ 6.05)$$

where: F_j = sediment flux for sediment size class j

C_j = sediment mass concentration of size class j.

This calculation was performed by converting the observed volume concentration data from the LISST-100C for the 2 characteristic size classes – fine (53.7μm) and (157μm) – into mass concentration data by assigning each size a suitable estimate of density (Dyer and Manning, 1999). Both the velocity data and SPM concentration data were interpolated to give values for every minute, rather than every hour. The slack waters in the interpolated velocity data were then found and full tidal cycles were identified. The sediment flux calculation was then performed for a tidal cycle at the beginning of the study period and again for a tidal cycle at the end of the study period (a tidal cycle being from low water to low water). The results are presented in Fig. 6.06.

Fig. 6.06 shows that the net flux of both particle sizes is toward the west both at the start of the study period (a) and at the end (b). The flux of the coarse particles (blue) is consistently greater than that of the fine (red). The flux of fine particles is greatest in the near bed region for both tidal cycles. However, for the coarse particles it is initially greater at the bed and then in the second tidal cycle it is greater toward the free surface.

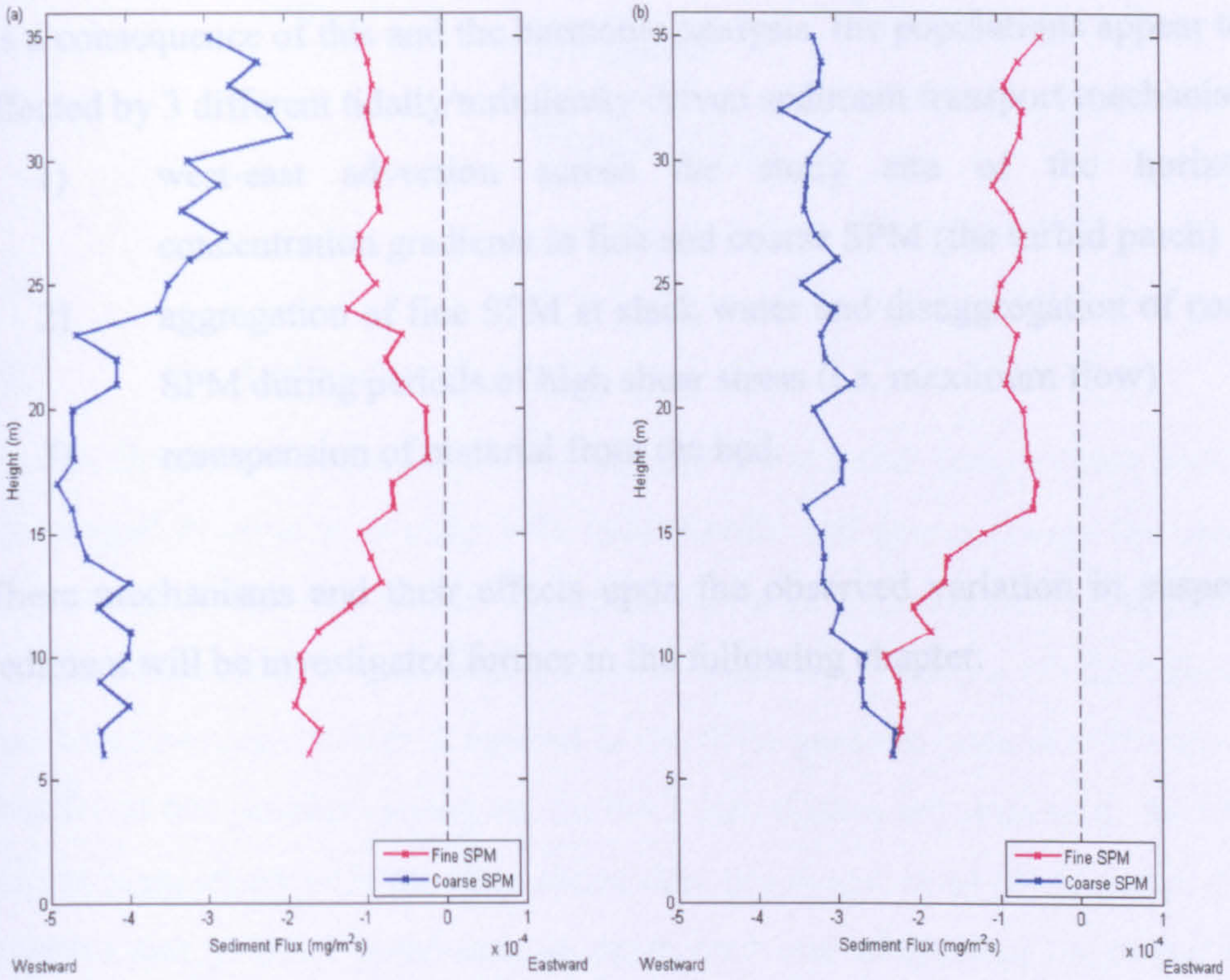

Fig. 6.06 Net flux of fine (red) and coarse (blue) SPM over a tidal cycle at the beginning of the study period (a), and at the end of the study period (b). The dashed vertical black line shows zero net flux.

6.6 Summary

The results of both the harmonic analysis and the entropy analysis indicate that the data may be simplified by considering only 2 distinct populations of suspended sediment – a fine and coarse size class. These populations show different variations during the tidal cycle and they differ in quantity.

Converting the volume concentration data into particle number data for each size classes was a useful exercise. Upon comparison with the shear stress time series, variability in the particle numbers of 2 representative size classes appear to be consistent with the variability in the tidal flow and the resulting shear stresses.

As a consequence of this and the harmonic analysis, the populations appear to be affected by 3 different tidally/turbulently-driven sediment transport mechanisms:

1) west-east advection across the study site of the horizontal concentration gradients in fine and coarse SPM (the turbid patch)
2) aggregation of fine SPM at slack water and disaggregation of coarser SPM during periods of high shear stress (i.e. maximum flow)
3) resuspension of material from the bed.

These mechanisms and their effects upon the observed variation in suspended sediment will be investigated further in the following chapter.

Chapter 7.

Modelling.

7.1 Introduction.

In this chapter the development of 2 models is discussed; these models have been developed in order to explain both qualitatively and quantitatively the observed variations in fine and coarse suspended sediment populations. In addition the results of the modelling are explained and discussed. Firstly a 1D tidal advection model is discussed which is applied to the SPM gradient present at the site. The results of this process carried out on the 2 size classes are presented. In order to allow comparison with the time series data the model must be corrected for the relative ship position at the time at which each cast of the time series was taken. This correction is explained and then the results presented.

The second model developed is again a 1D model which produces mass concentration time series for 2 size classes from prescribed velocity values. The model incorporates components for resuspension, aggregation/disaggregation and advection of the turbid patch. The model is described in detail with the driving equations presented. The results of the model are compared with the observed mass concentration time series for the equivalent 2 size classes and discussed. Sensitivity analysis of the tuneable parameters incorporated within the model is performed and the results discussed. To investigate the importance and roles of each of the sediment transport processes included within the model, sensitivity analysis is performed on each of these components with the results of this discussed.

7.2 Advection Model.

7.2.1 Description.

The results of the transect carried out across the study site showed that there is a gradient in suspended sediment concentration and size (Fig. 5.01 and Fig. 5.02). A turbid patch of fine SPM is present to the west of the observational site, which is consistent with other studies in this area, being a long-term, self-maintaining feature (Bowers et al., 2005; Ellis et al., 2004), and coarser SPM is present to the east of the study site. The tidal velocities around the study area are high, and, as suggested by the initial analysis of the data, advection of the turbid patch could be taking place. Therefore, as this feature appears to be a potentially important factor affecting the sediment characteristics and dynamics at this site, a model to simulate advection of the sediment gradient was developed.

The model developed was a conceptual 1D model to simulate the movement of the turbid patch by the observed tidal velocities. Each of the casts taken during the transect had its longitude and latitude position logged. As the transect was carried out along an approximately east-west line, the latitude measurements could be ignored; i.e. only the x-axis is considered. From the longitude measurements, it was possible to calculate the distances in metres of each cast of the transect from the location of the mooring site.

Initially the sediment volume concentration gradient as measured by the LISST was interpolated onto a higher resolution grid in order to decrease the interval between each measurement along the x-axis, i.e. in the distance from the mooring. It was interpolated such that there was a data point for every 39.12m (this split the gradient into approximately 1200 points).

At each time step, *dt*, the model calculates the distance travelled in that time step. As a result a new position within the sediment gradient is achieved, or alternatively, a new position within the sediment gradient is now positioned at the study site. The corresponding volume concentration value for this new position is found from the sediment gradient matrix and thus the new volume

concentration value at this time step, which is present purely as a result of advection of the sediment gradient, is determined (see equations below). The processes and effects of vertical mixing, resuspension, aggregation & disaggregation and settling are ignored in this model. The initial sediment concentration is the concentration taken from the gradient location at time t = 0.

$$dx(z,t) = u(z,t-1) \times dt$$
$$x(z,t) = x(z,t-1) + dx(z,t)$$
$$V_{adv}(z,t) = V_{grad}(z, x(z,t))$$

where: *dx(z,t)* = distance moved in the x-direction at height *z* and time *t*, by the east velocity, *u*, at height *z* and at the time between the previous time step and now, i.e. *t-1*.

dt = the time step, 600s

x(z,t) = the new location within the sediment gradient, V_{grad}, at height *z* and time *t*

x(z,t-1) = position within the sediment gradient at the previous time step, *t-1*

$V_{adv}(z,t)$ = the volume concentration of the purely advected gradient at height *z* and time *t*.

During initial runs of the model it was found that the transect did not extend far enough in the east direction and so the data had to be extrapolated eastward. For simplicity it was decided to assume that there was no change in volume concentration or median size for these additional data points.

7.2.2 Ship Position Corrected Model.

In order for the results of the advection model to be successfully compared with the collected sediment time series it was necessary to account for the movements of the ship. During the observational programme the ship was not anchored at the mooring site, rather the ship would attempt to reposition itself at the mooring site prior to each cast. As a result the ship was not exactly at the location of the

mooring site during each cast. The exact position of the ship at each cast was logged and so this data was used to apply a correction for the exact position of the ship from the mooring site (Fig. 7.01). This correction was incorporated into the model before calculation of the sediment concentration values.

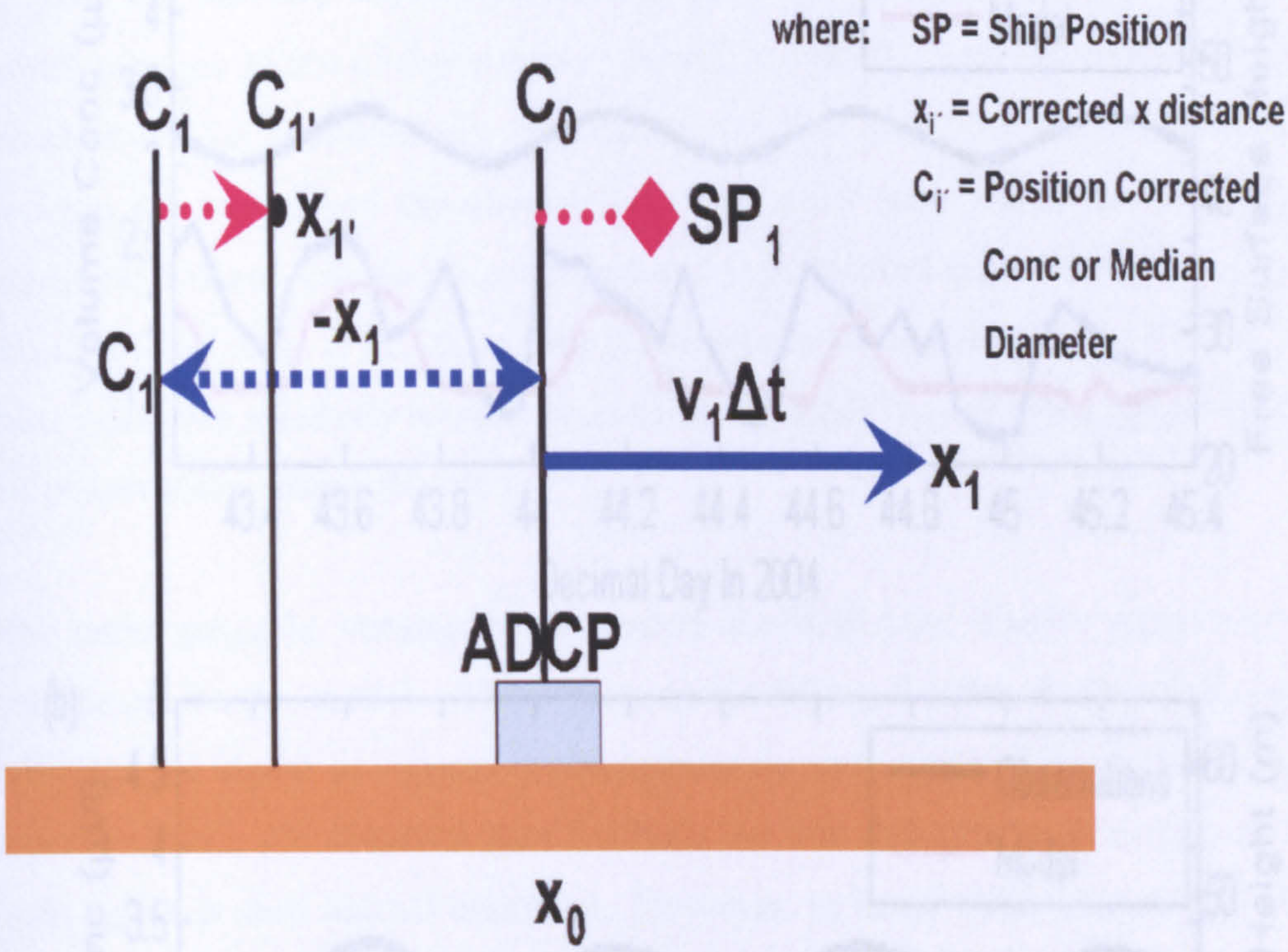

Fig. 7.01 A schematic of the ship position corrected advection model.

7.2.3 Model Results.

The model was run for the gradients in volume concentration of 2 sizes classes, a fine size class (53.7μm) and a coarse size class (157μm). Only 2 characteristic size classes were modelled as the results of the harmonic and entropy analysis showed that the suspended sediment at this site could be approximated by the behaviour of 2 distinct size classes. The observed velocity time series collected at all depths by the ADCP was used for the input velocity values and so the model was run for the duration of the observational period (Fig. 7.02).

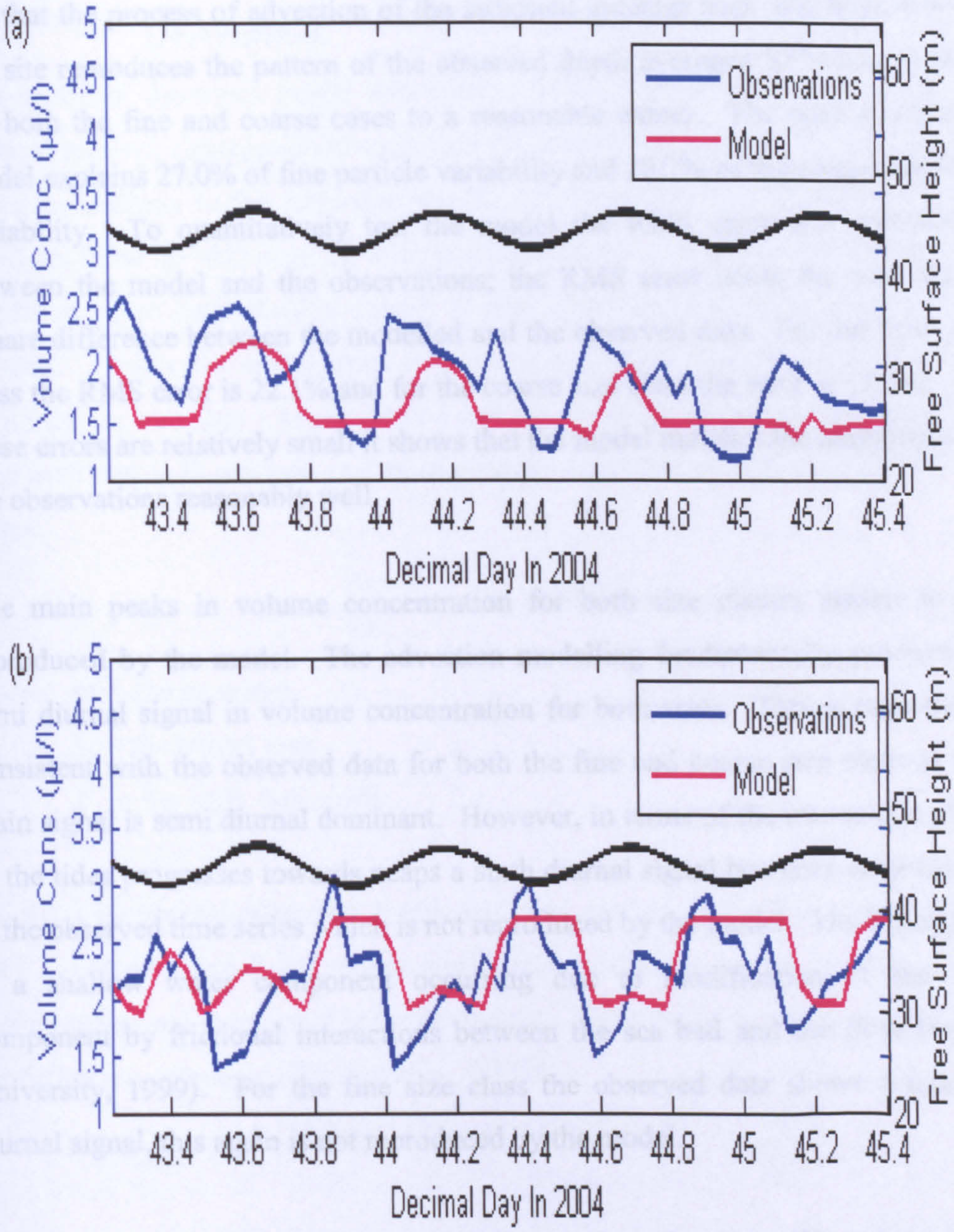

Fig. 7.02 Depth-averaged observed data for (a) the fine population (53.7µm) and (b) the coarse population (157µm) (blue) plotted against the results from the advection model for the same size class (red).

Initial conclusions from the depth averaged results of the advection modelling are that the process of advection of the sediment gradient back and forth across the site reproduces the pattern of the observed depth averaged SPM time series for both the fine and coarse cases to a reasonable extent. The pure advection model explains 27.0% of fine particle variability and 29.7% of the coarse particle variability. To quantitatively test the model the RMS error was calculated between the model and the observations; the RMS error being the root mean square difference between the modelled and the observed data. For the fine size class the RMS error is 22.1% and for the coarse size class the error is 17.1%. As these errors are relatively small it shows that the model matches the magnitude of the observations reasonably well.

The main peaks in volume concentration for both size classes appear to be reproduced by the model. The advection modelling fundamentally produces a semi diurnal signal in volume concentration for both sizes. This is reasonably consistent with the observed data for both the fine and coarse size class as the main signal is semi diurnal dominant. However, in terms of the coarse size class as the tides progresses towards neaps a sixth diurnal signal becomes emphasised in the observed time series which is not reproduced by the model. The M6 signal is a shallow water component occurring due to modification of the M2 component by frictional interactions between the sea bed and the flow (Open University, 1999). For the fine size class the observed data shows a quarter diurnal signal, this again is not reproduced by the model.

The results of the pure advection model suggest that advection, although it plays a role (over a quarter of the variability) in controlling the sediment characteristics and dynamics at this site, it is not the only process. This was also indicated by initial analysis of the observed data. In order to refine the model results another model was developed which included other possible sediment transport mechanisms.

7.3 Sediment Dynamics Model.

7.3.1 Description.

The sediment dynamics model was again a 1-dimensional model. It included vertical mixing, aggregation/disaggregation, erosion (resuspension) and settling terms in addition to the advection model. The boundaries were fixed so that there could be no exchange of sediment across them. At the bed an additional condition of an inexhaustible supply of sediment available for suspension was applied. Within the model mass is conserved. The modelled depth was 36m split into 1m bins (bin 1 being the bed and bin 36 being the surface). The time step used was 0.72 seconds as this adequately satisfied the CFL criterion which states:

$$\Delta t \leq \frac{\Delta z^2}{4K_z} \qquad (Eq.\ 7.01)$$

where: Δt = the time step

Δz = the height step

K_z = the eddy diffusivity.

Firstly, a resuspension/erosion component was created at the bottom boundary. This involved critical bed shear stress and erodibility terms to control the movement of sediment into the water column. The erosion rate was governed by the following equation (Aldridge et al., 2003).

$$Erosion = E_j = \begin{cases} \theta_j \gamma_0 (\tau / \tau_{cr} - 1), & \tau \geq \tau_{cr}, \\ 0, & \tau < \tau_{cr}, \end{cases} \qquad (Eq.\ 7.02)$$

where: θ_j = the fraction of the total erodible bed material that is in the class j

$= c_j / \sum_j c_j$, with c_j = sediment concentration of size class j

γ_0 = the erosion rate coefficient = 2.5×10^{-5} $kgm^{-2}s^{-1}$ (empirically derived by Aldridge et al. 2003 from their work in the Irish Sea)

τ = instantaneous bed shear stress = $C_D \rho \overline{U^2}$

τ_{cr} = critical bed shear stress.

Following this expression, the fraction of total erodible bed material for a particular size class would have to be calculated at each time step and for all size classes. However, as this model is only modelling 2 sizes classes this was not possible. Therefore, it was felt more appropriate to make an initial calculation of the variable (for both the fine and coarse size classes) utilising the observed data which contained all size classes. These values remained constant throughout the model run. The critical bed shear stress used was 0.2 Nm^{-2} (peak shear stress being approximately 6.9Nm^{-2} at this site).

The sediment continuity equation takes the following form:

$$\frac{\partial C_j}{\partial t} = w_{sj}\frac{\partial C_j}{\partial z} + \frac{\partial}{\partial z}\left(K_z \frac{\partial C_j}{\partial z}\right) \qquad \textit{(Eq. 7.03)}$$

where: $K_z = N_z = \kappa u_* z\left(1 - z/h\right)$

κ = von Karman's constant = 0.4

u_* = friction velocity (ms^{-1}) = $\sqrt{\tau_b/\rho}$

z = height above the bed (m)

h = water depth (m)

w_{sj} = particle settling velocity of size class j

C_j = mass concentration of the size class j = fine or coarse.

Therefore, we have a vertical mixing component and a settling component included in the model. The mixing component was consistent with the use of a logarithmic velocity profile assumption in formulating the profile of K_z, the vertical diffusivity. The profile of K_z has the shape of a vertical bell curve, i.e. there is a peak in vertical diffusivity in the middle of the water column. Sediment could therefore, be mixed up through the water column from the bed, with the settling component enabling sediment to drop out of the water.

The boundary conditions were set so that there can be no mixing across the boundaries, i.e:

$$K_z \frac{\partial C_j}{\partial z} + w_{sj} C_j = 0 \quad \text{at } z = h \text{ (i.e. the surface)}$$

$$K_z \frac{\partial C_j}{\partial z} = 0 \quad \text{at } z = 0 \text{ (i.e. the bed)} \qquad \textit{(Eq. 7.04)}$$

An aggregation/disaggregation component was included to enable fine particles to aggregate to create coarse particles and to allow coarse particles to disaggregate to create fine particles. This process was also a function of the shear stress at a particular location and time within the water column as developed by Bowers et al. (2005). The aggregation/disaggregation term is dependent upon the size class by the following expression.

$$\textit{Aggregation \& Disaggregation} = \begin{cases} -aC_f(z,t) + bC_c(z,t), & \text{for the fine term,} \\ +aC_f(z,t) - bC_c(z,t), & \text{for the coarse term.} \end{cases}$$

(Eq. 7.05)

where: C_f, C_c = mass concentration of the fine and coarse populations respectively

$$a = A - \alpha\tau = A\left(1 - \frac{\tau}{\tau_{max}}\right)$$

$$b = \alpha\tau = A\left(\frac{\tau}{\tau_{max}}\right)$$

A = constant coefficient of the order 10^{-5} s^{-1} (Bowers et al., 2005)

α = constant coefficient = A/τ_{max}

τ_{max} = the maximum shear stress value over the study/modelling period (approximately 6.9Nm^{-2} at this study site).

Bowers et al. (2005) conducted a study at several research sites in the Irish Sea including a site off the north-west coast of Anglesey (as in this study). They found that for the turbid patch considered in this study (of size of order 10km), A is of the order $10^{-5}s^{-1}$, i.e. one in every 100,000 particles is disaggregating every second in the centre of the turbid patch. They also derived the expression for α presented above.

The final component to be added was an advection term to account for the movement of the sediment gradient across this location. The volume concentration data collected during the transect was first converted into mass concentrations for the required size classes by assigning the populations a suitable estimate of density (Dyer and Manning, 1999). These gradients in mass concentration were then input into the advection model developed earlier. The advection component followed the same procedure as the advection model described previously.

The fine and coarse particle size classes are defined solely by assignment of 2 different settling velocities. Suitable settling velocities were estimated using Stokes law (Eq. 3.09). The fine size class has a slow settling velocity of order $0.01 mms^{-1}$, to provide a background particle population and the coarse size class has a fast settling velocity of order $1 mms^{-1}$ to provide a resuspendible population.

Therefore, the mass concentration of the fine and coarse populations at a given height in the water column is found by an expression of the following form:

$$C_j(z,t) = C_j(z,t-1) + \frac{\partial C_j(z,t)}{\partial t} + C_{advj}(z,t) \qquad (Eq.\ 7.06)$$

The $\partial C_j/\partial t$ term of the fine and coarse populations in the first bin of the model is given by:

$$\frac{\partial C_j}{\partial t}(z,t) = Vertical\ Mixing\ (less\ mixing\ from\ below) + Settling + Aggregation\ \&\ Disaggregation + Erosion \qquad (Eq.\ 7.07)$$

The boundary condition at the bed states that there can be no mixing through the bed which is why only the negative mixing term is used. Intuitively, the bed is the only part of the water column which includes the erosion term.

For the points between the bed and the surface the $\partial C_j/\partial t$ term is given by:

$$\frac{\partial C_j}{\partial t}(z,t) = Vertical\ Mixing + Settling + Aggregation\ \&\ Disaggregation$$

(*Eq. 7.08*)

The surface boundary condition states that there can be no vertical mixing or settling across the boundary, therefore, only the positive mixing term and the negative settling term are used in the expression for $\partial C_j/\partial t$:

$$\frac{\partial C_j}{\partial t}(z,t) = Vertical\ Mixing\ (less\ mixing\ to\ the\ level\ above) + Settling\ (less\ the\ settling\ from\ above) + Aggregation\ \&\ Disaggregation \quad (Eq.\ 7.09)$$

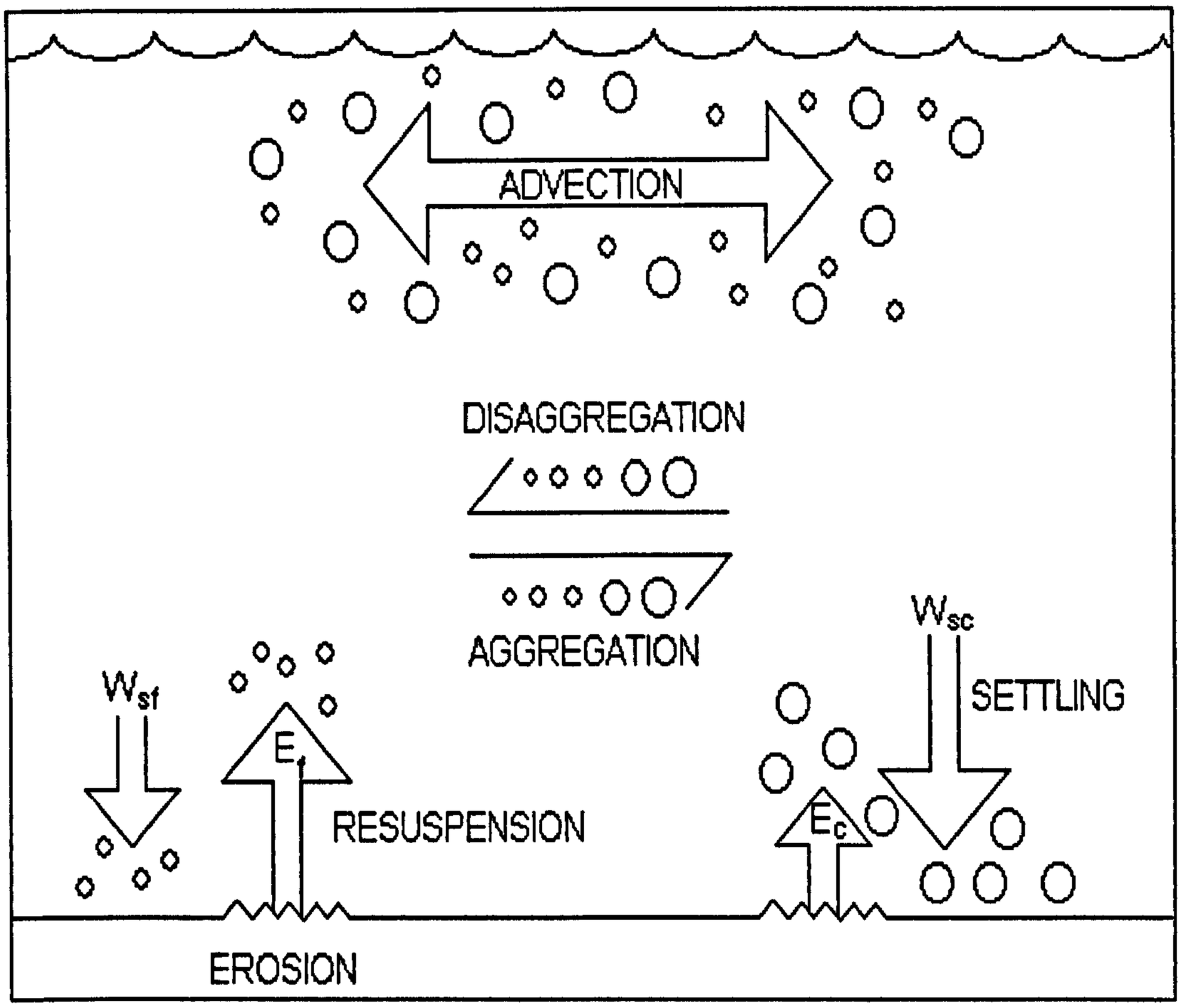

Fig. 7.03 A schematic describing the various components of the sediment dynamics model for the 2 size populations.

7.3.2 Model Results.

The model was run using the velocity time series obtained during the observational period. This was interpolated to provide data in accordance with the time step used. The initial mass concentrations for both the fine and coarse size classes were set to 0. The model makes calculations for all heights of the water column at the specified height interval of 1m. The results of the fine (Fig. 7.04) and coarse (Fig. 7.05) modelled profiles are presented with their corresponding observed profiles.

The results from the model were hourly averaged and depth averaged to enable clearer comparison between the model and the depth averaged observed data of the equivalent size fractions, i.e. 53.7 and 157μm (see Fig. 7.06).

Upon examination of Fig. 7.04, Fig. 7.05 and Fig. 7.06 it can be seen that there is a "spin-up" period of approximately 27 hours during which sediment is suspended from the bed by the model before reaching similar values to the observed data. Hereafter the model appears to reproduce the observed data reasonable well both qualitatively and quantitatively. The model explains 67.3% of the variability in the fine size class and 26.6% of the variability the coarse size class. The lower R^2 value for the coarse population is due to the fact that the high water mass concentration peak in the observed data is predicted early by the model. The RMS errors for the fine and coarse populations respectively are 9.2 and 16.4%. Therefore, in quantitative terms the model is of the same magnitude as the observed values. The results from the sediment dynamics model in general are promising.

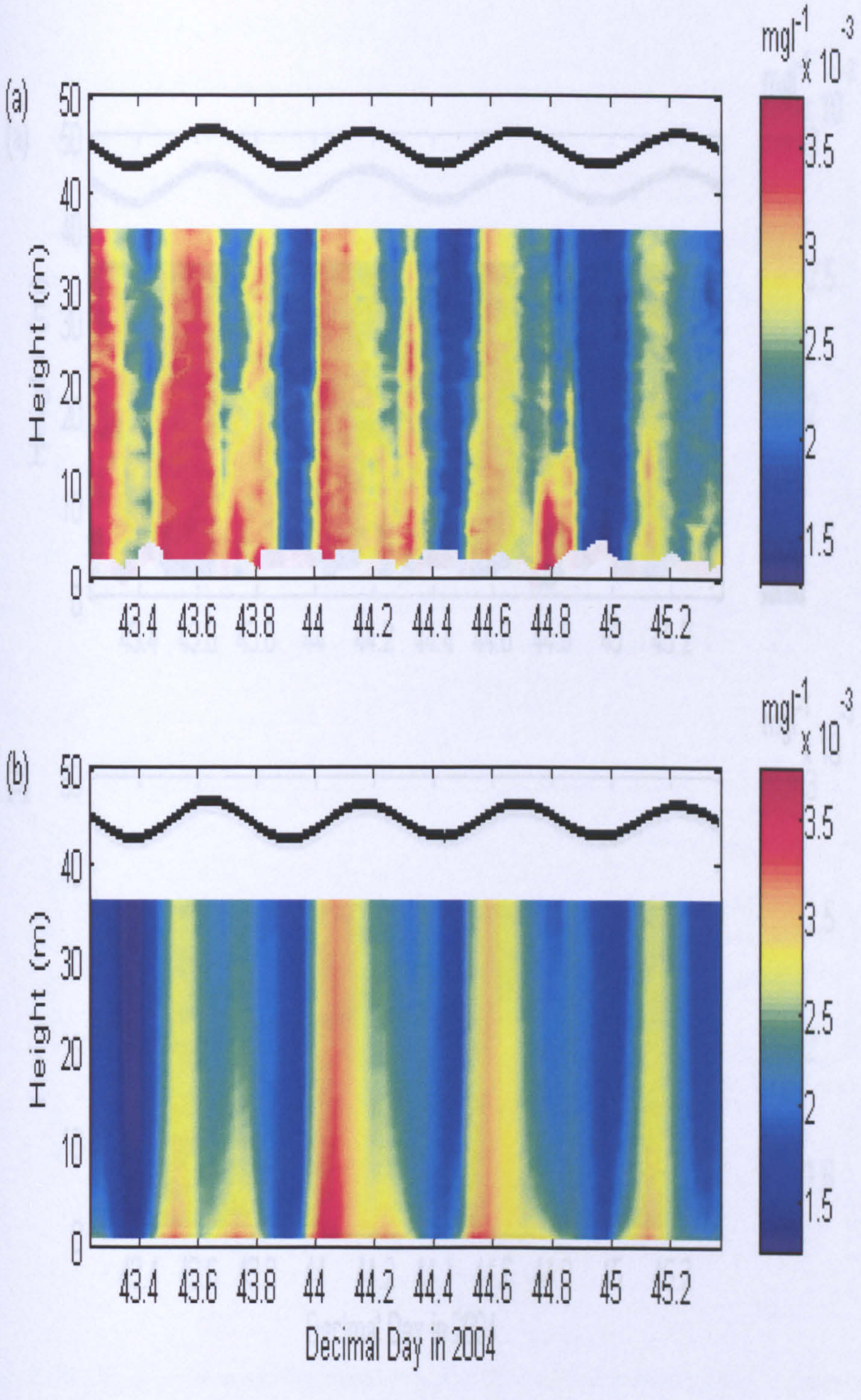

Fig. 7.04 Profiles of fine (53.7μm) SPM mass concentration (a) observed and (b) modelled. The solid black line is the free surface elevation to indicate the state of the tide.

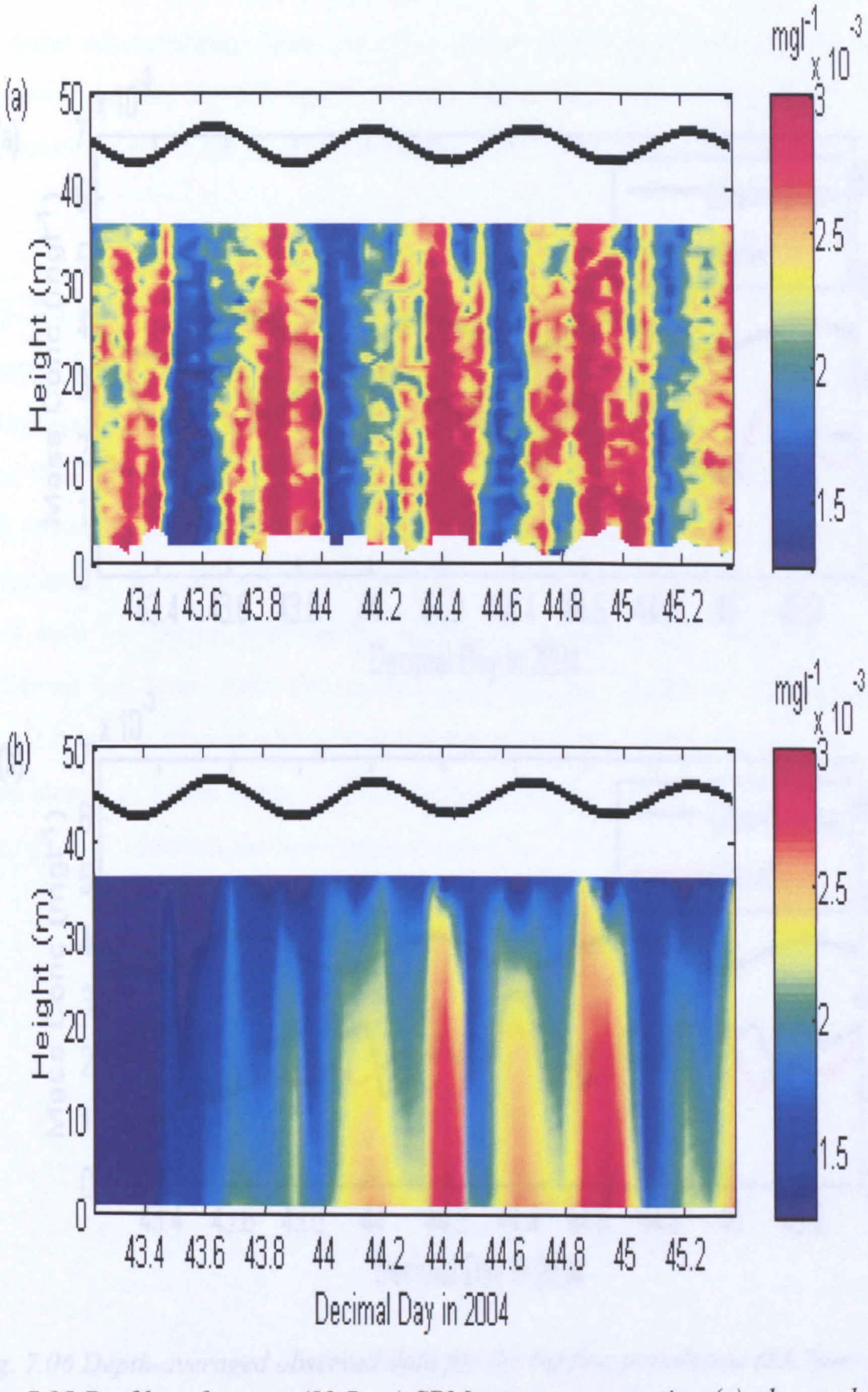

Fig. 7.05 Profiles of coarse (53.7μm) SPM mass concentration (a) observed and (b) modelled. The solid black line is the free surface elevation to indicate the state of the tide.

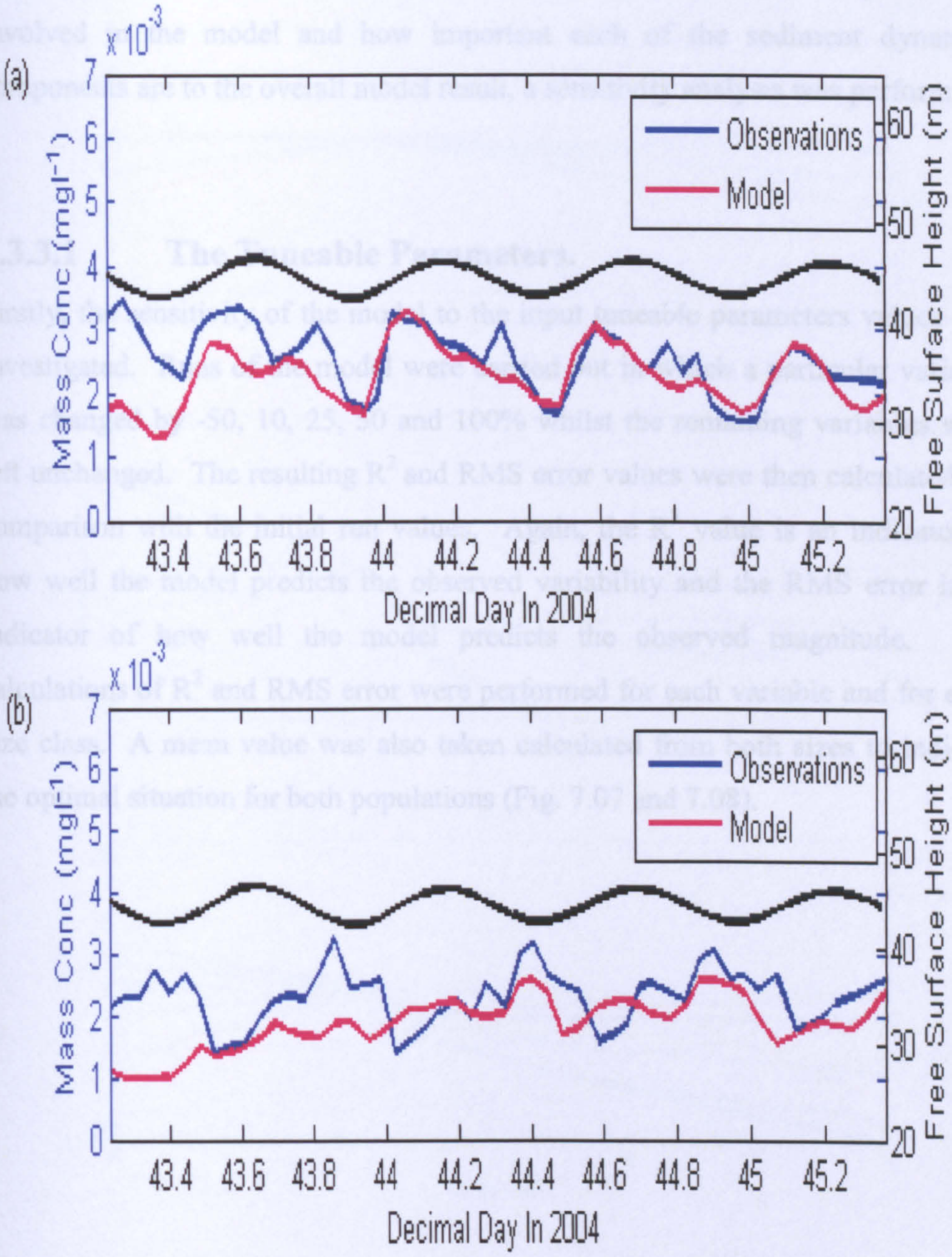

Fig. 7.06 Depth-averaged observed data for the (a) fine population (53.7μm) and (b) the coarse population (157μm) (blue) plotted against the results from the sediment dynamics model for the equivalent size class (red).

7.3.3 Sensitivity Analysis.

In order to determine how sensitive the model is to the tuneable parameters involved in the model and how important each of the sediment dynamics components are to the overall model result, a sensitivity analysis was performed.

7.3.3.1 The Tuneable Parameters.

Firstly, the sensitivity of the model to the input tuneable parameters values was investigated. Runs of the model were carried out in which a particular variable was changed by -50, 10, 25, 50 and 100% whilst the remaining variables were left unchanged. The resulting R^2 and RMS error values were then calculated for comparison with the initial run values. Again, the R^2 value is an indicator of how well the model predicts the observed variability and the RMS error is an indicator of how well the model predicts the observed magnitude. The calculations of R^2 and RMS error were performed for each variable and for each size class. A mean value was also taken calculated from both sizes to indicate the optimal situation for both populations (Fig. 7.07 and 7.08).

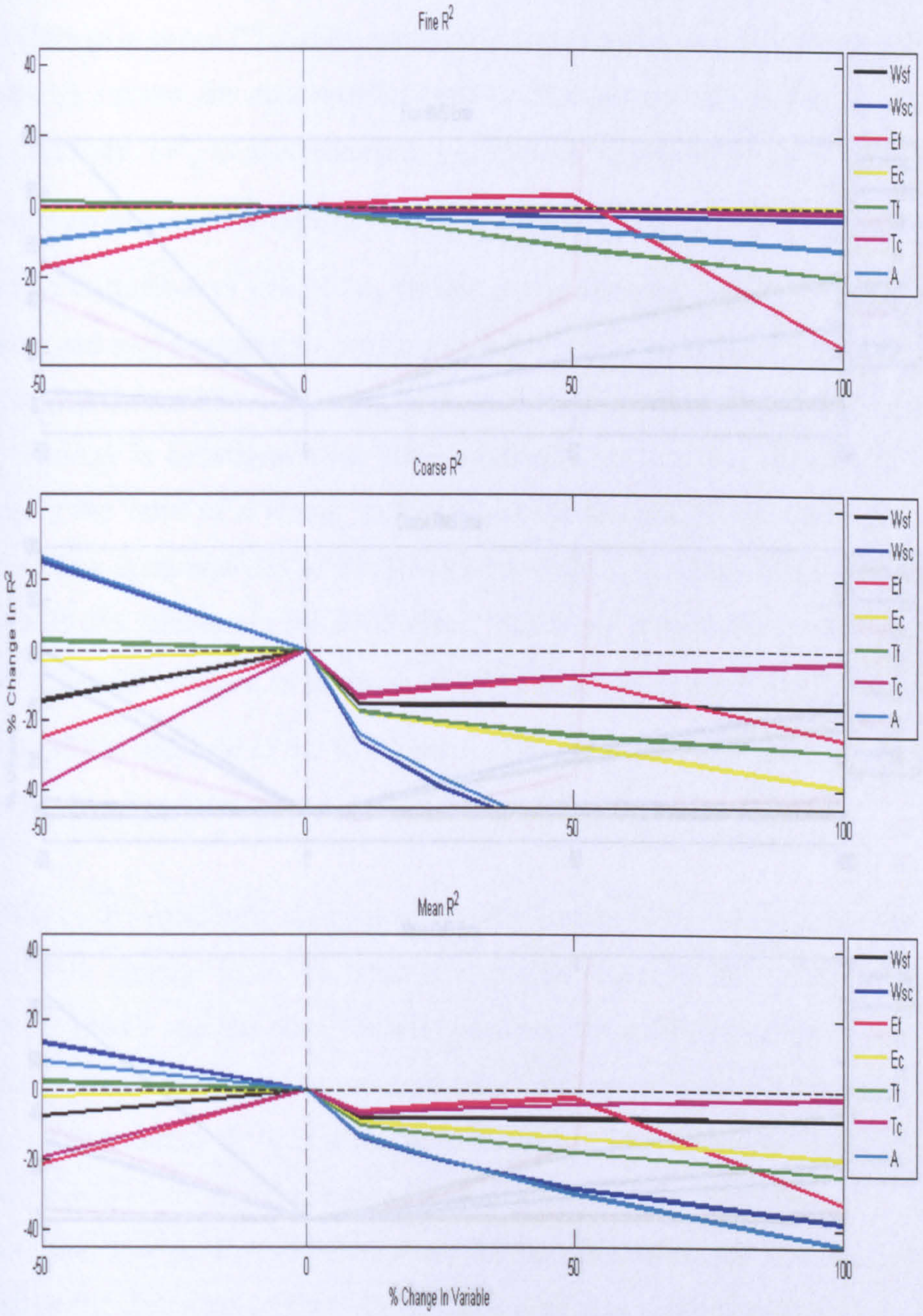

Fig. 7.07 Results of sensitivity analysis on the tuneable parameters, presenting how a percentage change of a particle variable alters the overall R^2 expressed as a percentage change from the R^2 found from the model run presented in Fig. 7.06.

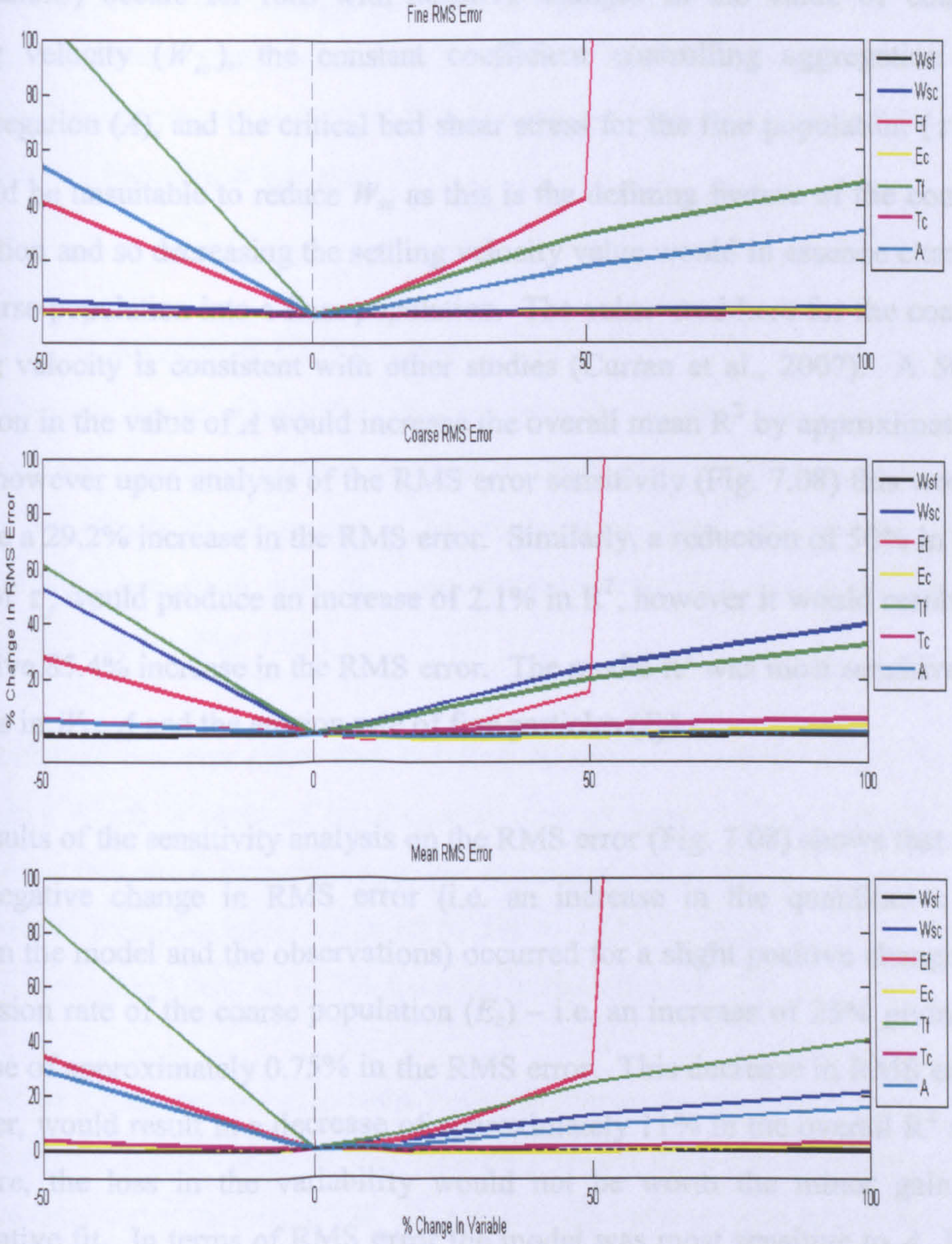

Fig. 7.08 Results of sensitivity analysis on the tuneable parameters, presenting how a percentage change of a particle variable alters the overall RMS error expressed as a percentage change from the RMS error found from the model run presented in Fig. 7.06.

The results of the sensitivity analysis on the R^2 (Fig. 7.07) shows that the only positive change in mean R^2 (i.e. an increase in the correlation of the model to the observations) occurs for runs with negative changes in the value of coarse settling velocity (W_{sc}), the constant coefficient controlling aggregation & disaggregation (A), and the critical bed shear stress for the fine population (τ_f). It would be unsuitable to reduce W_{sc} as this is the defining feature of the coarse population and so decreasing the settling velocity value would in essence change the coarse population into a finer population. The value used here for the coarse settling velocity is consistent with other studies (Curran et al., 2007). A 50% reduction in the value of A would increase the overall mean R^2 by approximately 8.2%, however upon analysis of the RMS error sensitivity (Fig. 7.08) this would produce a 29.2% increase in the RMS error. Similarly, a reduction of 50% in the value of τ_f would produce an increase of 2.1% in R^2, however it would result in a massive 85.4% increase in the RMS error. The model R^2 was most sensitive to changes in W_{sc}, A and the erosion rate of fine particles (E_f).

The results of the sensitivity analysis on the RMS error (Fig. 7.08) shows that the only negative change in RMS error (i.e. an increase in the quantitative fit between the model and the observations) occurred for a slight positive change in the erosion rate of the coarse population (E_c) – i.e. an increase of 25% giving a decrease of approximately 0.75% in the RMS error. This decrease in RMS error however, would result in a decrease of approximately 11% in the overall R^2 and therefore, the loss in the variability would not be worth the minor gain in quantitative fit. In terms of RMS error the model was most sensitive to A, W_{sc}, τ_f and E_f.

Therefore, the results of the sensitivity analysis on the R^2 and RMS error of the tuneable variables used within the model suggest that the values used here give the optimal level of performance both qualitatively and quantitatively.

7.3.3.2 The Model Components.

The sensitivity of the sediment dynamics model to the 3 main components of the model, i.e. the advection, the aggregation & disaggregation and the resuspension (erosion) processes, were tested and analysed. This was done in order to determine the importance and extent to which each of the components has upon the suspended sediment at this site.

7.3.3.2.1 Advection Component.

The model was run in exactly the same set up as the original run; however, the advection term was removed from the mass concentration calculations in order to remove the effects of advection. The results were again hourly and depth averaged for comparison with the observed equivalent fine and coarse depth averaged time series (Fig. 7.09).

The results of this run show that the fine population loses its flood biased asymmetry which is replaced by a quarter diurnal signal. This suggests that advection at this site is responsible for the asymmetry observed in the fines – the R^2 decreases from the initial value of 67.3% to 19.5%. There is only a slight increase in the RMS error to 14.7% from the initial value of 9.2%.

Removal of the advective component from the coarse modelled time series also has a dramatic effect. Most of the variability is lost from the modelled depth averaged time series indicating that advection is the main process controlling the variability in the coarse size class as advection provides the largest instantaneous change in SPM concentration. This point is highlighted in the R^2 as this reduces from the initial 26.6% value to just 1.9%. The RMS error shows little change being 16.7% from the original value of 16.4%, therefore, the mechanisms of aggregation and resuspension are able to provide the magnitude of coarse particles observed in the data.

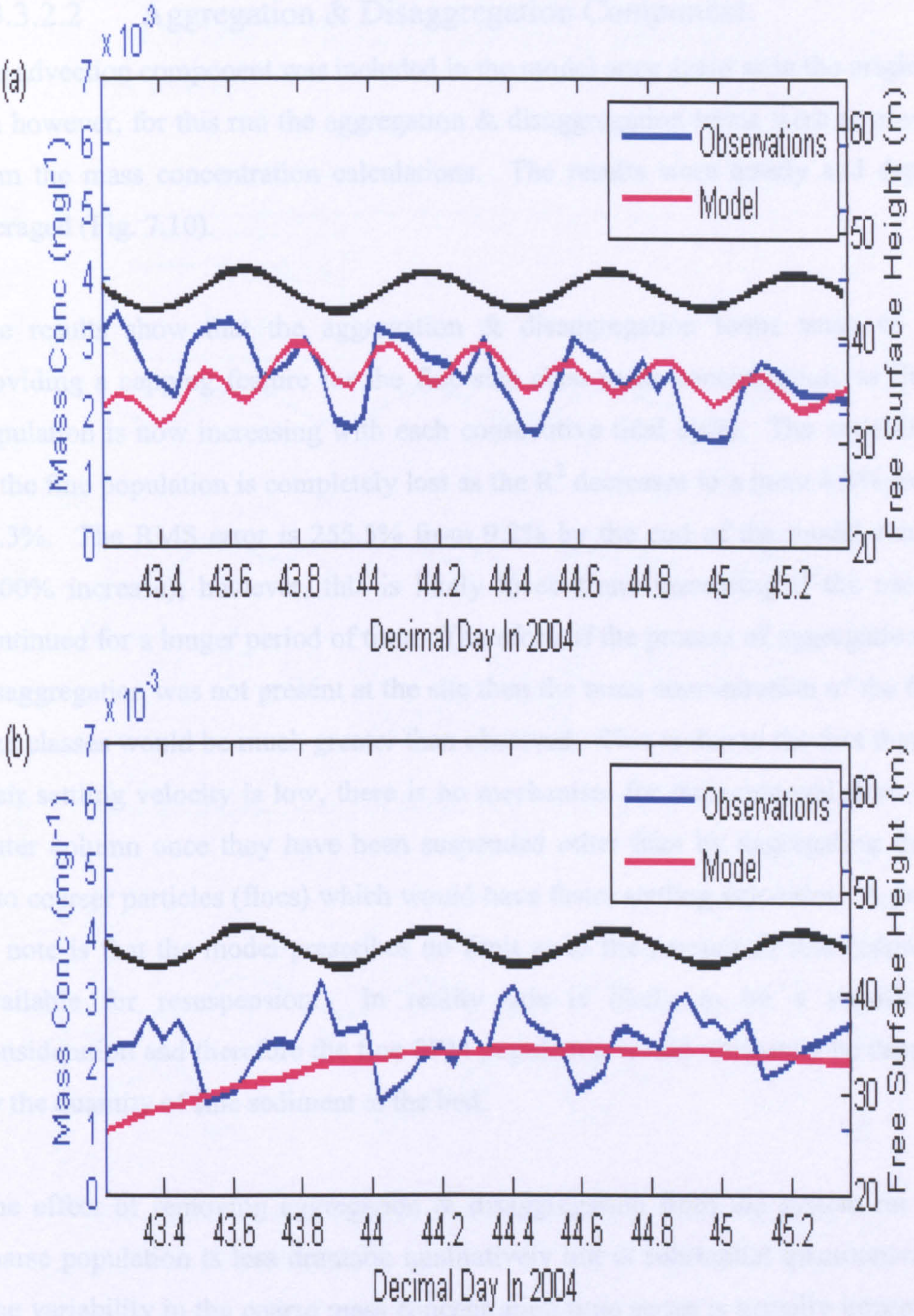

Fig. 7.09 Depth-averaged observed data for the (a) fine population (53.7μm) and (b) the coarse population (157μm) (blue) plotted against the results from the sediment dynamics model with the advection component turned off for the equivalent size class (red).

7.3.3.2.2 Aggregation & Disaggregation Component.

The advection component was included in the model once again as in the original run however, for this run the aggregation & disaggregation terms were removed from the mass concentration calculations. The results were hourly and depth averaged (Fig. 7.10).

The results show that the aggregation & disaggregation terms seem to be providing a capping feature for the fine size class mass concentration, as their population is now increasing with each consecutive tidal cycle. The variability in the fine population is completely lost as the R^2 decreases to a mere 4.8% from 67.3%. The RMS error is 255.5% from 9.2% by the end of the model run (a 2000% increase); however, this is likely to continue increasing if the model continued for a longer period of time. Therefore, if the process of aggregation & disaggregation was not present at the site then the mass concentration of the fine size classes would be much greater than observed. This is due to the fact that as their settling velocity is low, there is no mechanism for their removal from the water column once they have been suspended other than by aggregating them into coarser particles (flocs) which would have faster settling velocities. A point to note is that the model prescribes no limit as to the amount of fine sediment available for resuspension. In reality this is likely to be a significant consideration and therefore the fine SPM population would ultimately be capped by the quantity of fine sediment at the bed.

The effect of removing aggregation & disaggregation from the system on the coarse population is less dramatic qualitatively but is substantial quantitatively. The variability in the coarse mass concentration time series is actually improved by the removal of the aggregation & disaggregation mechanism. However, the concentration of the modelled coarse size class is not sufficiently high to match the observed concentration. The reduced concentration of coarse particles is due to the fact that the supply mechanism of aggregation, which produces coarse particles from fine particles, has been removed. The lower mass concentration is maintained by resuspension with the advection mechanism providing the

variability. This is reflected in the R^2 and RMS error. The R^2 is actually increased to 34.5% from 26.6%, but the RMS error is increased by a factor of 4 to 67.2% from 16.4%.

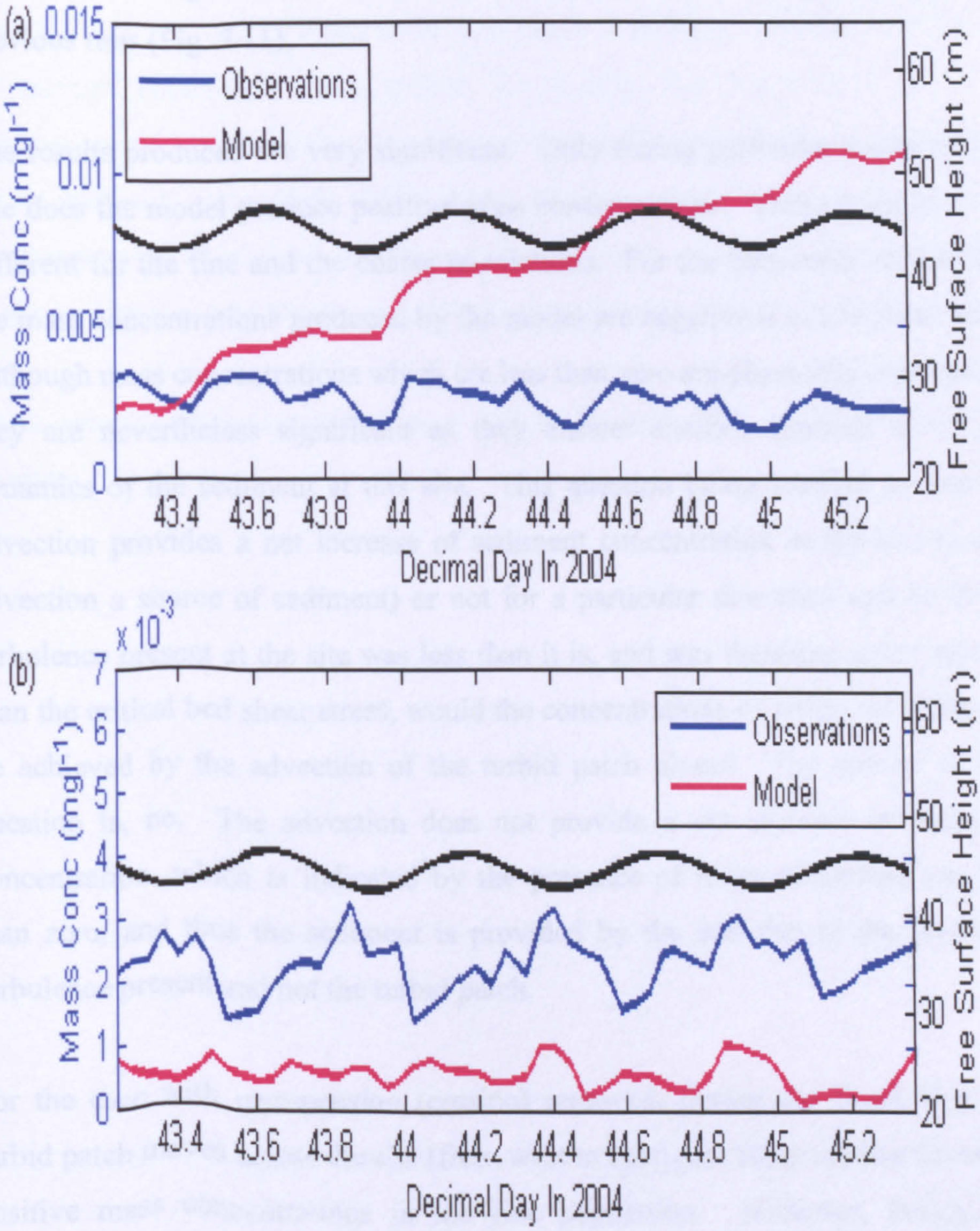

Fig. 7.10 Depth-averaged observed data for the (a) fine population (53.7μm) and (b) the coarse population (157μm) (blue) plotted against the results from the sediment dynamics model with the aggregation & disaggregation component turned off for the equivalent size class (red).

7.3.3.2.3 Resuspension (Erosion) Component.

The sediment dynamics model was run with the erosion of the bed component removed from the sediment mass concentration calculations and all the other terms included again. The results were hourly and depth averaged as with the previous runs (Fig. 7.11).

The results produced are very significant. Only during particular stages of the tide does the model produce positive mass concentrations. These occasions are different for the fine and the coarse populations. For the remainder of the time the mass concentrations produced by the model are negative (i.e. less than zero). Although mass concentrations which are less than zero are physically impossible, they are nevertheless significant as they answer another question as to the dynamics of the sediment at this site. This question being whether or not the advection provides a net increase of sediment concentration at the site (i.e. is advection a source of sediment) or not for a particular size class and so if the turbulence present at the site was less than it is, and was therefore never greater than the critical bed shear stress, would the concentrations of sediment at the site be achieved by the advection of the turbid patch alone? The answer to this question is, no. The advection does not provide a net increase in sediment concentration, which is indicated by the presence of mass concentrations less than zero, and thus the sediment is provided by the bed due to the levels of turbulence present and not the turbid patch.

For the case with resuspension (erosion) removed, during the flood, the fine turbid patch moves across the site (from west to east) providing the low levels of positive mass concentrations in the fine population. However, during the remainder of the time the turbid patch of fine particles is pushed back towards the west and the coarser particles from Liverpool Bay are pushed over the site resulting in mass concentrations less than zero in the fine population. This, however, is the time at which the only positive concentrations of coarse particles are produced by the model (i.e. during the ebb). Therefore, during the periods of negative mass concentration the input of sediment concentration by advection is

less than the output of sediment concentration by advection, settling and aggregation & disaggregation. The fine and coarse populations are inversely related due to the sediment concentration gradient present at the site. When the concentration of fine particles is positive the concentration of coarse particles is negative and vice versa. Without the turbulence eroding the bed there would not be enough sediment in the system to produce the magnitudes of mass concentrations present at the site and so although the advective component and the turbulence controlled aggregation & disaggregation component play important roles when there is sediment in suspension, it requires the turbulence controlled erosion and mixing to get the sediment in suspension in the first place.

These results and their consequences will be discussed further in the following chapter.

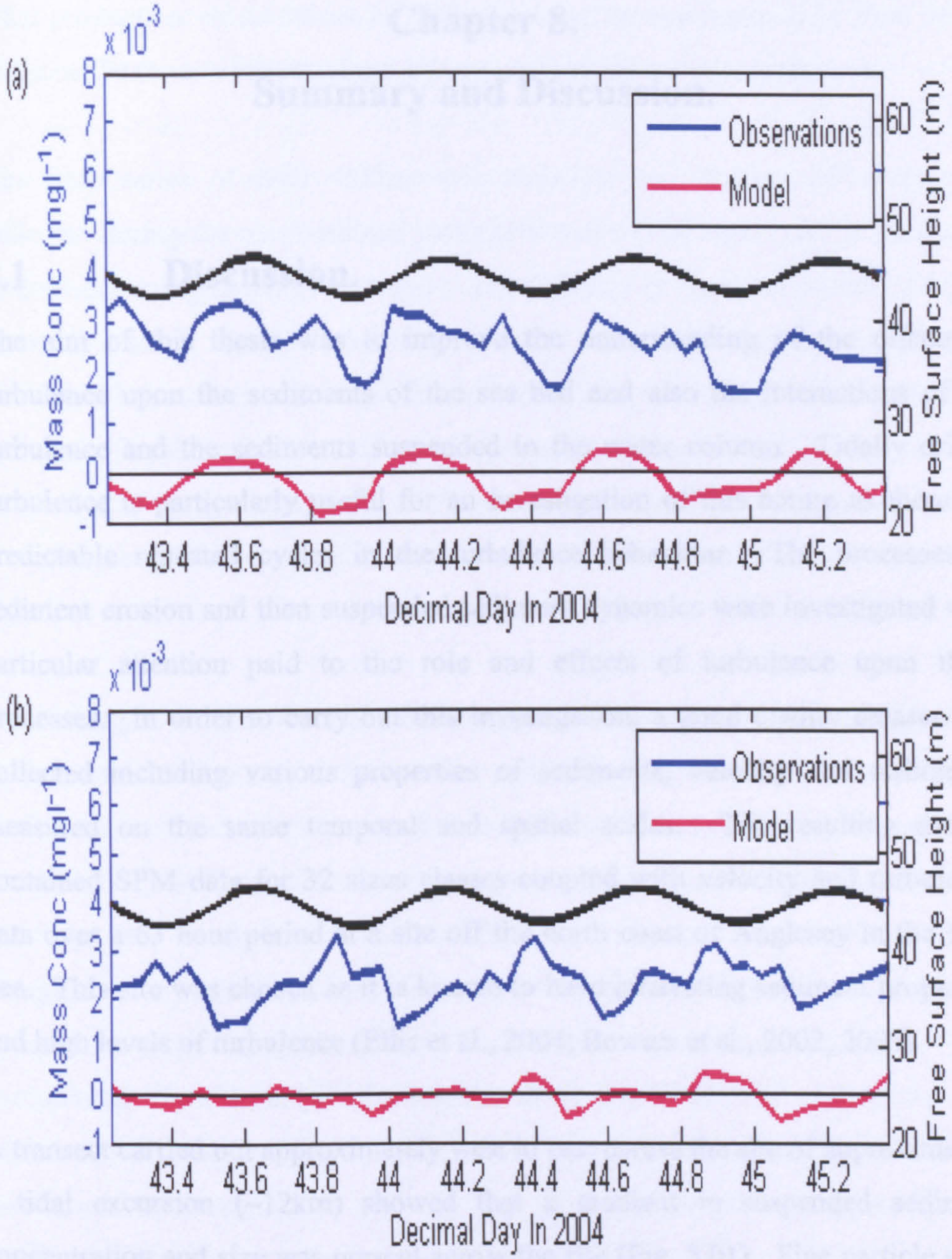

Fig. 7.11 Depth-averaged observed data for the (a) fine population (53.7μm) and (b) the coarse population (157μm) (blue) plotted against the results from the sediment dynamics model with the erosion component turned off for the equivalent size class (red).

Chapter 8.

Summary and Discussion.

8.1 Discussion.

The aim of this thesis was to improve the understanding of the effects of turbulence upon the sediments of the sea bed and also the interactions of the turbulence and the sediments suspended in the water column. Tidally driven turbulence is particularly useful for an investigation of this nature as there are predictable repeated cycles in the turbulence behaviour. The processes of sediment erosion and then suspended sediment dynamics were investigated with particular attention paid to the role and effects of turbulence upon these processes. In order to carry out this investigation, a good quality dataset was collected including various properties of sediments, velocity and turbulence measured on the same temporal and spatial scales. The resulting dataset contained SPM data for 32 sizes classes coupled with velocity and turbulence data over a 63 hour period at a site off the north coast of Anglesey in the Irish Sea. This site was chosen as it is known to have interesting sediment properties and high levels of turbulence (Ellis et al., 2004; Bowers et al., 2002, 2005)

A transect carried out approximately west to east across the site of approximately 1 tidal excursion (~12km) showed that a gradient in suspended sediment concentration and size was present across the site (Fig. 5.01). Fine particle sizes were present within a turbid patch in the west whilst coarser particles were present towards Liverpool Bay in the east. These observations were consistent with similar studies in this area (Ellis et al., 2004; Bowers et al., 2005, 2007).

The tide at the site was observed to be approximately rectilinear, with the velocity structure seen to be flood-biased. As a consequence, the TKE production time series showed flood-biased tidal asymmetry with the greatest

TKE production values observed at the bed during maximum tidal flow which was also the time of highest shear stresses within the water column.

The time series of total volume concentration and median SPM diameter collected during the observational period showed a tidal signal with a maximum in both occurring around low water. The maxima in fine and coarse SPM are inversely related; the fine maximum occurred during the maximum flood tidal current and thus during the maximum flood shear stress; the coarse maximum occurred after the maximum ebb tidal flow and so after the maximum ebb shear stress. Initial comparison of the SPM data and turbulence data suggested that the variation in the SPM signal is correlated with the variation in the turbulence signal.

To investigate the link between the turbulence and sediment signals, harmonic analysis was performed on the velocity and sediment data. This showed strong qualitative evidence for the correlation between the turbulence and sediment parameters. The harmonic analysis performed on the velocity data showed that the tide was semi-diurnal (M2) dominant with the quarter-diurnal (M4) component only 11.4% of the semi-diurnal amplitude, and that the M2 and M4 components were approximately in phase. Interactions between tidal components of different periods result in distortion of the tidal ellipse and tidal asymmetry (Open University, 1999). The relative contributions of the east and north velocity components showed that the tidal flow was approximately rectilinear aligned along the east-west axis.

In order to determine whether the suspended sediment population was behaving as a number of different size populations or as a smaller group of size populations, harmonic analysis and entropy analysis were performed on the sediment size distribution spectra. The method of the entropy analysis technique is to group similar size distribution spectra together to give information about the number of distinct size distributions within a given dataset.

The harmonic analysis showed a clear 2 size class split in the 32 size classes observed, the split occurring at approximately 90μm. There was a 6 hour phase difference in the semi-diurnal component (showing the flood-ebb asymmetry) between the 2 size populations and a 4 hour phase difference in the quarter-diurnal component (showing the flood and ebb stress maxima). Furthermore, the results of the entropy analysis confirmed that the variations in sediment at this site could be approximated by the behaviour of 2 distinct size classes with 2 distinct size distribution spectra; these being a fine population ~50μm and a coarse population ~150μm.

The quarter-diurnal signal present in the sediment data, particularly so in the fine size class (Fig. 6.04a), is consistent with a signal produced by resuspension and settling. Resuspension occurs once the shear stress has reached a critical magnitude. This would likely occur during the flood and during the ebb around maximum tidal flow and thus maximum shear stress, hence giving a quarter-diurnal signal. Whilst the stress is below the critical value, the settling component would be greater than the resuspension component.

The number of particles within the fine and coarse size classes was calculated in order to investigate the behaviour of 2 characteristic size classes. The variation in the particle numbers of the fine and coarse populations showed an inverse relationship between the maxima of the 2 size classes. This inverse relationship would be consistent with advection of the observed sediment gradient across the site by the tidal flow as this would give alternating maxima in fine and coarse sediment concentrations and numbers.

A further explanation for the inverse relationship between the maxima/minima of the 2 size classes could be aggregation and disaggregation processes; a mechanism for the transfer of particles between the 2 size classes. Aggregation of fine particles into coarser particles reduces the concentration and number of fine particles whilst at the same time increasing the concentration and number of coarser particles. Similarly, disaggregation of coarse flocs into finer particles

reduces the concentration/number of coarse flocs whilst at the same time increasing the concentration/number of finer particles.

The results of the harmonic and entropy analysis have provided some qualitative evidence for the relationships observed between the flow and the suspended sediment. In order to further investigate the observed variations in the fine (50μm) and coarse (150μm) size populations, and to provide some quantitative evidence for these variations, two models were developed.

To assess the role of advection of the turbid patch (or rather the sediment gradient as a whole) across the site by the tidal flow upon the variation in the sediment properties, a simple advection model was constructed. The simple advection model involved moving the measured SPM concentration gradient across the site as a result of the observed tidal flow. Settling, resuspension and all mixing factors were ignored; the value at each time step was as a result of the appropriate value taken from the SPM gradient (Fig. 7.02). Upon comparison with the observed data the purely advective approach explains 27% of the variation in the fine population and 29.7% of the variation in the coarse population. Therefore, the advection model explains almost a third of the variation observed in both the fine and coarse particle size populations. To quantify the results of the advection model the RMS error (the root mean square difference between the modelled and the observed data) was calculated. The results of this being 22.1% for the fine size class and 17.1% for the coarse size class; thus the model results quantitatively match the observed data reasonably well. Therefore, an important signal in both size classes appears to be advection of the SPM gradient.

To investigate the roles of the mixing, resuspension and aggregation/disaggregation processes that may be occurring at the site, the second model, an extension of the first to include a physically-based sediment dynamics model, included terms for advection, erosion (resuspension), vertical mixing, settling and aggregation/disaggregation (Figs. 7.04, 7.05 and 7.06). The

full sediment dynamics model explains 67.3% of the variability in the fine population and 26.6% of the variability in the coarse population. The R^2 for the coarse population has fallen; this being due to the early presence of the peak in concentration around high water. The R^2 for the fine size class shows that the model explains much of the variation in the fine size class. The RMS errors for the fine and coarse populations respectively are 9.2 and 16.4%; again the model quantitatively matches the observed data well. Therefore, the sediment dynamics model provides much more realistic estimates of the variability in the sediment transport of 2 size classes within the waters of this shelf sea study site and thus the additional processes included in this model must be present in the observed data.

The model was then used to assess the relative importance of the different processes which may be influencing the sediment properties. This was done by "turning off" particular terms in the model responsible for a particular process (such as the aggregation/disaggregation term) and then comparing the results from the model run with the observed data. The results of turning off the advection term show that the observed flood-biased asymmetry in the fine size class is no longer predicted and so advection is responsible for the flood-biased asymmetry seen in the fine population at this site. Without advection of the turbid patch the variation in fine SPM would be quarter diurnal (Fig. 7.09a). The resulting loss in variability decreases the R^2 to 19.5%. The impact upon the coarse size class was much more dramatic, with the removal of most of the variability observed in this size class; the R^2 decreased to just 1.9% (Fig. 7.09b). This indicates that the variation in the fine SPM is strongly influenced by the advection component and the variation in the coarse SPM is dominated by the advection.

The advection term was then included in the model calculations once more and the aggregation/disaggregation module was turned off so that its importance in the results could be assessed. Removal of the aggregation/disaggregation term from the full model provided dramatic results. All of the observed variability in

the fine size class was lost as the R^2 for the fine population fell to just 4.8% (Fig. 7.10a). It appears that the process of aggregation/disaggregation provides a capping effect upon the concentration of the fine SPM thus driving the variation in the fine particles. A model without this term therefore, would overestimate the concentration of fine SPM in the system. The impact upon the coarse size class was different to that of the fine size class. The variation in concentration was still present; however, the magnitude of the concentrations was lost (Fig. 7.10b). Without the supply mechanism of aggregating fine SPM into coarse SPM the concentration of the coarse size class would be significantly underestimated. Therefore, aggregation appears to be dominating the variation and magnitude of the fine population (the RMS error increased to 255.5% from 14.7%).

Finally the aggregation/disaggregation term was turned back on and the erosion of the bed term (or the resuspension term) was removed to show the importance of this process. The results of this were significant upon both size classes for the duration of the model run (Fig. 7.11). The results showed that erosion from the bed (and then the resulting vertical mixing) is the single most important mechanism for supplying the water column with sediment in the first place; therefore, the turbid patch does not act as a source of sediment. Without the turbulence-driven erosion at the bed resuspending sediment and the turbulent vertical mixing diffusing this sediment up through the water column, the magnitude of suspended sediment observed at this site would not be achieved by the other processes. Therefore, each of the terms included in the sediment dynamics model plays an important role. However, without a well defined erosion term, there would not be the sediment in the system with which the other terms can interact.

For reference the R^2 and RMS error values for the full model run and for the runs with the various components turned off are presented in Table 8.01. The data for the runs with the components turned off have been converted into pie charts (Fig. 8.01) in order to show the relative importance of each component upon the

variability (R^2) and magnitude (RMS error) of the fine and coarse mass concentrations. These plots show that for both size populations the 2 mechanisms controlling the magnitude of the SPM mass concentrations are erosion (resuspension) and aggregation/disaggregation, erosion being dominant for the coarse population and aggregation/disaggregation being dominant for the fine population. In terms of the variability, advection is by far the dominant mechanism for controlling the coarse population. However, for the fine population aggregation/disaggregation provides the capping feature, advection provides the flood-biased asymmetry while resuspension contributes less than a quarter (relatively speaking) of the variability.

Model	Fine		Coarse	
	R^2 (%)	RMS Error (%)	R^2 (%)	RMS Error (%)
Advection	27	22.1	29.7	17.1
Sediment Dynamics	67.3	9.2	26.6	16.4
Advection	19.5	14.7	1.9	16.7
Aggregation / Disaggregation	4.8	255.5	34.5	67.2
Erosion (Resuspension)	38.1	92.1	28.1	87.1

Table 8.01 The R^2 and RMS error values for the advection model and the sediment dynamics model. The R^2 and RMS error values for runs of the sediment dynamics model with various components removed (advection, aggregation/disaggregation and resuspension). All the models were regressed against the observed data.

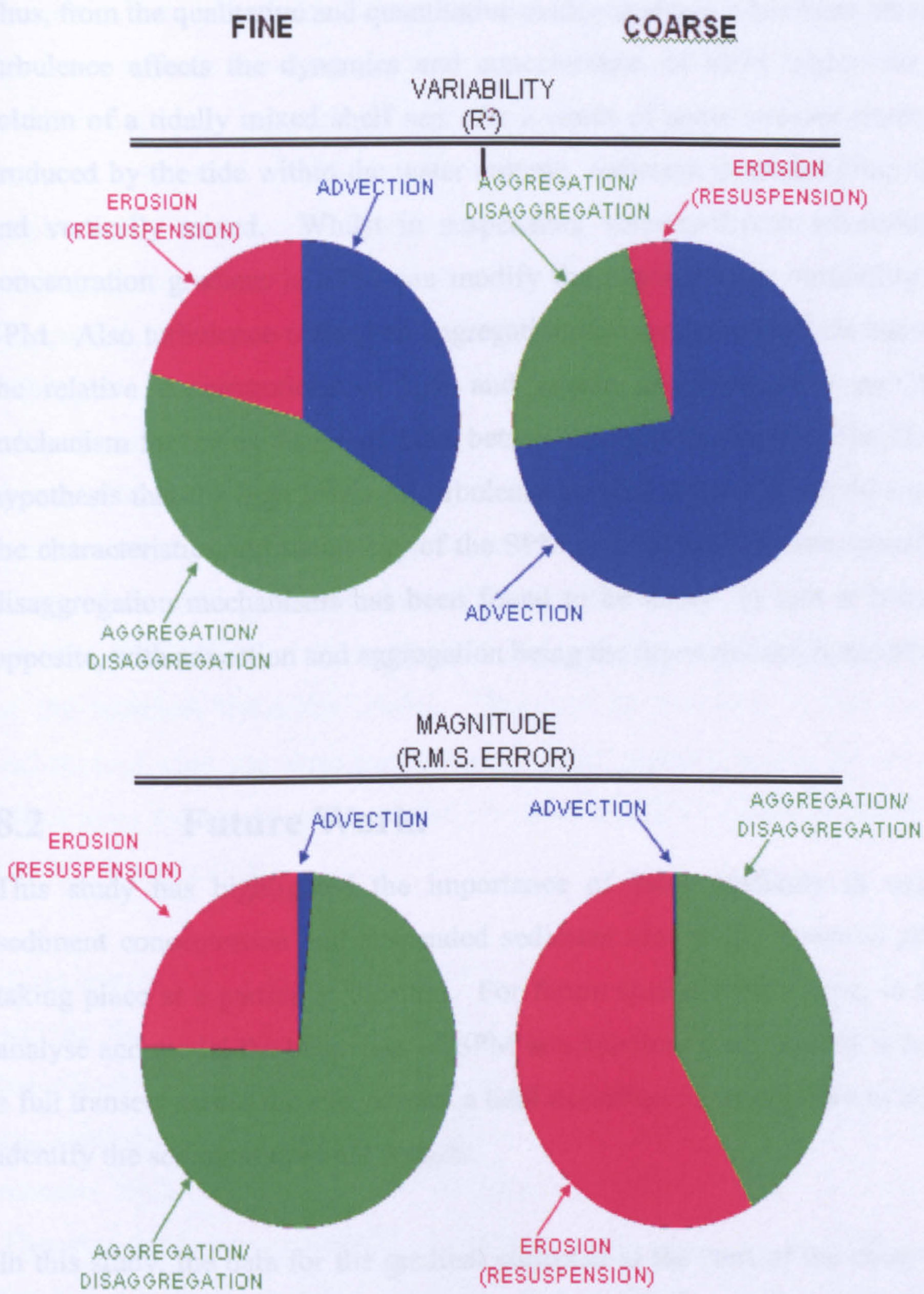

Fig. 8.01 The relative importance of the 3 main model components – erosion (resuspension), advection, aggregation/disaggregation, upon the variability (R^2) and magnitude (RMS error) of the fine and coarse mass concentrations.

Thus, from the qualitative and quantitative evidence above it has been shown that turbulence affects the dynamics and concentration of SPM within the water column of a tidally mixed shelf sea. As a result of shear stresses (turbulence) produced by the tide within the water column, sediment is eroded from the bed and vertically mixed. Whilst in suspension, velocity-driven advection of a concentration gradient in SPM can modify the concentration variability of the SPM. Also turbulence-controlled aggregation/disaggregation effects can control the relative concentrations of fine and coarse populations by providing a mechanism for the exchange of mass between the 2 populations. Therefore, the hypothesis that the high levels of turbulence present at the site would mean that the characteristics and variability of the SPM is dominated by resuspension and disaggregation mechanisms has been found to be false. In fact it is quite the opposite, with advection and aggregation being the dominant mechanisms.

8.2 Future Work.

This study has highlighted the importance of local gradients in suspended sediment concentration and suspended sediment size in the dynamic processes taking place at a particular location. For future studies of this type, in order to analyse and model the behaviour of SPM at a location, a top priority is to ensure a full transect across the site, at least a tidal excursion of spring tides in length, to identify the sediment gradient present.

In this study, the data for the gradient collected at the start of the observational programme was assumed to be representative of the gradient throughout the study period and so no short term evolution of the sediment gradient was included in the modelling process. This was taken to be a reasonable assumption as previous studies have shown the persistence of the gradient at this location (Ellis et al. 2004; Bowers, 2005). In addition, the satellite data for this period of study (such as Fig. 1.02) show the turbid patch to be present and stable. An interesting line of investigation which arises from this study is to test the seasonal and interannual variability in the turbidity at the study site; in particular

the seasonal and interannual variability of the sediment concentration gradient as this is an important feature at this site. Although the turbid patch is a well established feature it varies throughout the year in terms of total suspended matter concentration (Bowers et al., 1998). This variability can be seen in satellite data. As a result the advective term would evolve and vary and so the turbidity levels would also fluctuate throughout the year. Also, it has been observed that there is interannual variability in the turbidity in the Irish Sea (White et al., 2003), and so this could be investigated further, as the tidal influence is not greatly different. The work carried out by White et al. (2003) showed that the variability was correlated to wind stress. The effects of wind and so surface mixing were ignored from the model developed here; it was purely a tidal mixing investigation. Therefore, the addition of a term which takes into account wind stress and surface mixing would increase the modelling power of the sediment dynamics model. However, in the case of this study, the inclusion of wind and wave stirring in the model would not have had a profound effect upon the results as during the observational period there were low winds and low wave activity.

It has been noted by Le Hir et al. (2007) that very few sediment models take into account the effects of sensitivity to biota, particularly in terms of erodibility. Biological activity within the water column would also affect the aggregation/disaggregation mechanism (Eisma et al., 1991b) as biological material tends to make it easier for particles to stick together (i.e. aggregate). Therefore, the aggregation/disaggregation term could be modified to be a function of biological matter in addition to turbulence. The seasonal variation in the properties of the suspended sediments can be clearly seen in data that was collected at the same site in June 2004. Fig. 8.02 shows the median suspended particle diameters present between 30 May and 5 June 2004 at the study site. Upon comparison with the full profile median SPM diameter plot for February (Fig. 8.03) it can be seen that the signal is not as 'clean' as it was in February; this is thought to be potentially due to the fact that there was a phytoplankton bloom taking place whilst the measurements were taken in June. Another point

to notice between February and June is that the median SPM diameters in June were larger than in February, which is consistent with the idea that sticky biological material encourages aggregation (Eisma et al., 1991b).

The model developed here was only validated at one particular site, further validation of the sediment dynamics model could be carried out at another tidally mixed shelf sea site which also had a gradient in sediment concentration, e.g. off the east coast of Ireland at Arklow (White et al. 2003). In addition it would be of interest to test the model at a tidally mixed shelf sea site with little or no sediment concentration gradient present to investigate how important the resuspension and aggregation/disaggregation terms are at such a location. These 2 procedures would determine the validation of the tuneable parameters used within the model as further sensitivity analysis could be performed. As a result of these validation processes it may then be reasonable to assume that the model is suitable for general modelling of sediment dynamics in shelf seas.

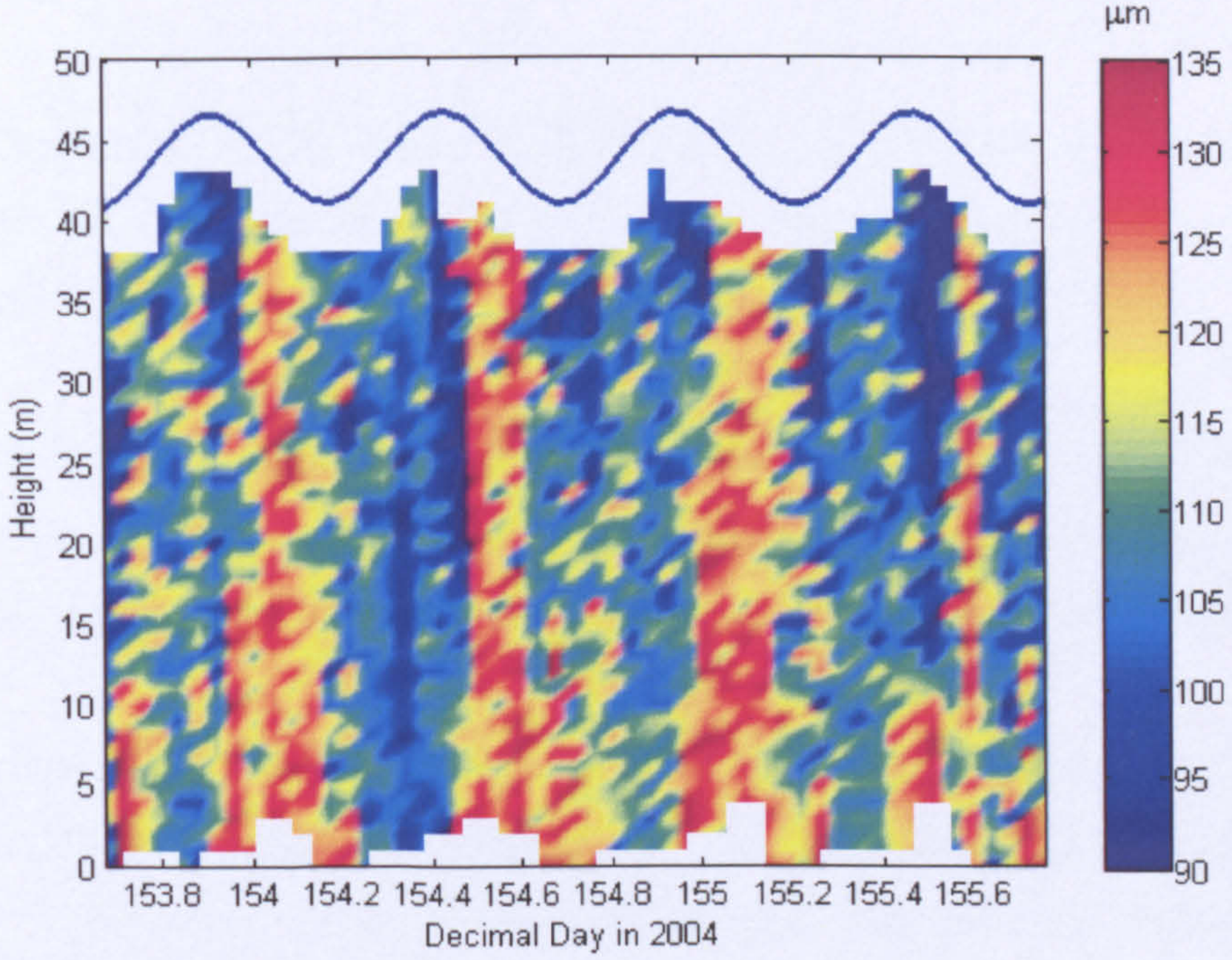

Fig. 8.02 The median suspended particle diameters present at the study site between 1 and 3 June 2004.

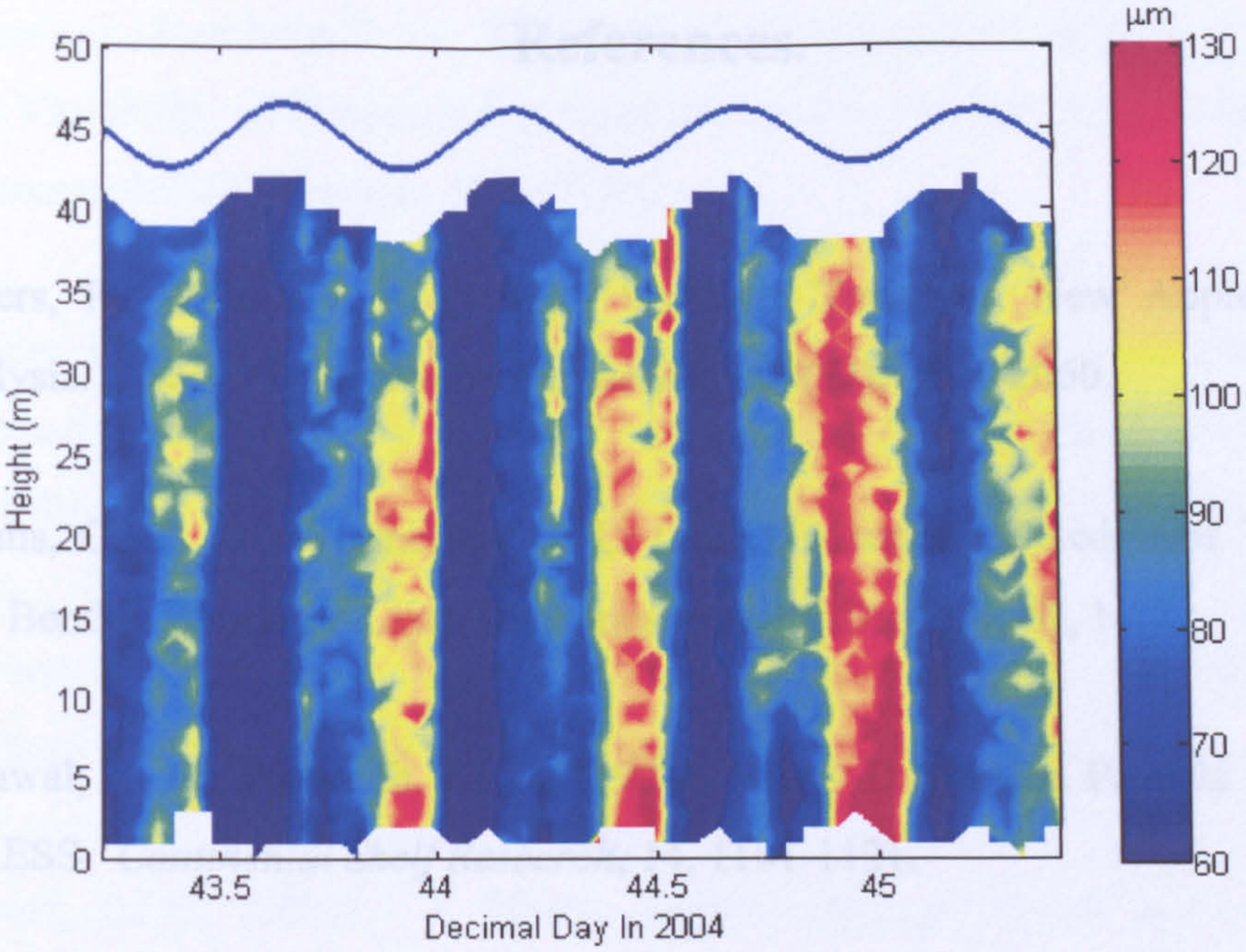

Fig. 8.03 The median suspended particle diameters present at the study site during the February cruise.

References.

Ackers, P., White, W. R. (1973). Sediment Transport: New Approach and Analysis. *Journal of Hydraulic Engineering*, **99(11)**, 2041-2060.

Adams, C. E., Jr., Weatherley, G. L. (1981). Suspended-Sediment Transport And Benthic Boundary-Layer Dynamics. *Marine Geology*, **42**, 1-18.

Agrawal, Y. C., Pottsmith, H. C., (1994). Laser Diffraction Particle Sizing In STRESS. *Continental Shelf Research*, **14**, 1101-1121.

Agrawal, Y. C., Pottsmith, H. C., (2000). Instruments for Particle Size and Settling Velocity Observations in Sediment Transport. *Marine Geology*, **168**, 89-114.

Al-Chalabi, S. A. M., Jones, A. R. (1993). Development of a Mathematical Model for Light Scattering by Statistically Irregular Particles. *Particle and Particle Systems Characterization*, **11**, 200-206.

Alldredge, A. L., Granata, T. C., Gotschalk, C. G., Dickey, T. D. (1990). The Physical Strength of Marine Snow and its Implications for Particle Dissaggregation in the Ocean. *Limnology and Oceanography*, **35**, 1415-1428.

Aldridge, J. N., Kershaw, P., Brown, J., McCubbin, D., Leonard, K. S., Young, E. F. (2003). Transport of Plutonium ($^{239/240}$Pu) and Caesium (^{137}Cs) in the Irish Sea: Comparison Between Observations and Results From Sediment and Contaminant Transport Modelling. *Continental Shelf Research*, **23**, 869-899.

Bale, A. J., Morris, A. W. (1987). In-Situ Measurements of Particle Size in Estuarine Waters. *Estuarine, Coastal and Shelf Science*, **24**, 253-263.

Berhane, I., Sternberg, R. W., Kineke, G. C., Milligan, T. G., Kranck, K. (1997). The Variability of Suspended Aggregates on the Amazon Continental Shelf. *Continental Shelf Research*, **17**, 267-285.

Bowers, D. G., Boudjelas, S., Harker, G. E. L. (1998). The Distribution of Fine Suspended Sediments in the Surface Waters of the Irish Sea and its Relation to Tidal Stirring. *International Journal of Remote Sensing*, **19**, 2789-2805.

Bowers, D. G., Gaffney, S., White, M., Bowyer, P. (2002). Turbidity in the Southern Irish Sea. *Continental Shelf Research*, **22**, 2115-2126.

Bowers, D. G. (2003). A Simple Turbulent-Energy Based Model of Fine Suspended Sediments in the Irish Sea. *Continental Shelf Research*, **23**, 1495-1505.

Bowers, D. G., Ellis, K. M., Jones, S. E. (2005). Isolated Turbidity Maxima in a Shelf Sea. *Continental Shelf Research*, **25**, 1071-1080.

Bowers, D. G., Binding, C. E., Ellis, K. M (2007). Satellite Remote Sensing of the Geographical Distribution of Suspended Particle Size in an Energetic Shelf Sea. *Estuarine, Coastal and Shelf Science*, **73**, 457-466.

Bradshaw, P. (1971). An Introduction to Turbulence and its Measurement, *Pergamon Press, Oxford.*

Bushell, G. C., Yan, Y. D., Woodfield, D., Raper, J., Amal, R. (2002). On Techniques for the Measurement of the Mass Fractal Dimension of Aggregates. *Advances in Colloid and Interface Science*, **95**, 1-50.

Campbell, A. R. (1996). Effects of Turbulence on Suspended Sediment Concentrations in a Tidal Flow, *Ph.D. Thesis, University of Wales, Bangor.*

Chen, S., Eisma, D., Kalf, J. (1994). In Situ Size Distribution of Suspended Matter During the Tidal Cycle in the Elbe Estuary. *Netherlands Journal of Sea Research*, **32**, 37-48.

Clifford, N. J., French, J. R., Hardisty, J. (1993). Turbulence: Perspectives on Flow and Sediment Transport, *John Wiley and Sons, Chichester, England.*

Curran, K. J., Hill, P. S., Milligan, T. G., Mikkelsen, O. A., Law, B. A., Durrieu de Madron, X., Bourrin, F. (2007). Settling Velocity, Effective Density, and Mass Composition of Suspended Sediment in a Coastal Bottom Boundary Layer, Gulf of Lions, France. *Continental Shelf Research*, **27**, 1408-1421.

Dewey, R. K., Crawford, W. R., Gargett, A. E., Oakey, N. S. (1987). A Microstructure Instrument for Profiling Oceanic Turbulence in Coastal Bottom Boundary Layers. *Journal of Atmospheric and Oceanic Technology*, **4**, 288-297.

Dyer, K. R. (1989). Sediment Processes in Estuaries: Future Research Requirements. *Journal of Geophysical Research*, **94**, 14327-14339.

Dyer, K. R, Cornelisse, J., Dearnaley, M. P., Fennessy, M. J., Jones, S. E., Kappenburg, J., McCave, I. N., Pejrup, M., Puls, W., van Leussen, W., Wolfstein, K. (1996). A Comparison of In-Situ Techniques for Estuarine Floc Settling Velocity Measurements. *Journal of Sea Research*, **36**, 15-29.

Dyer, K. R., Manning, A. J. (1999). Observation of the Size, Settling Velocity and Effective Density of Flocs and their Fractal Dimensions. *Journal of Sea Research*, **41**, 87-95.

Dyer, K. R., Christie, M. C., Manning, A. J. (2004). The Effects of Suspended Sediment on Turbulence within an Estuarine Turbidity Maximum. *Estuarine, Coastal and Shelf Science*, **59**, 237-248.

Einstein, H. A., Barbarossa, N. L. (1952). River Channel Roughness. *Transactions of the American Society of Civil Engineers*, **117**, 1121-1146.

Eisma, D., Kalf, J., Veenhuis, M. (1980). The Formation of Small Particles and Aggregates in the Rhine Estuary. *Netherlands Journal of Sea Research*, **14**, 172-191.

Eisma, D. (1986). Flocculation and Deflocculation of Suspended Matter in Estuaries. *Netherlands Journal of Sea Research*, **20**, 183-199.

Eisma, D., Irion, G. (1988). Suspended Matter and Sediment Transport. In: Salomons, W., Bayne, B. L., Duursma, E. K., Förstner, U. (Eds.). *Pollution of the North Sea – An Assessment*, Springer Verlag, Berlin, Heidelberg, New York, 20-35.

Eisma, D. (1991a). Particle Size of Suspended Matter in Estuaries. *Geo-Marine Letters II*, 147-153.

Eisma, D., Bernard, P., Cadee, G. C., Ittekkot, V., Kalf, J., Laane, R., Martin, J. M., Mook, W. G., Put, A., van Schuhmacher, T. (1991b). Suspended-Matter Particle Size in Some West-European Estuaries; Part 2: A Review on Floc Formation and Break-Up. *Netherlands Journal of Sea Research*, **28**, 215-220.

Ellis, K. M., Bowers, D. G., Jones, S. E. (2004). A Study of the Temporal Variability in Particle Size in a High-Energy Regime. *Estuarine, Coastal and Shelf Science*, **61**, 311-315.

Engelund, F., Hansen, E. (1967). A Monograph on Sediment Transport in Alluvial Streams. *Danish Technical Press, Copenhagen, Denmark.*

Fischbach, F. A., Brooks, S., Bond, J. (1985). Interpretation of Small-Angle Light Scattering Maxima of Single-Oriented Microparticles. *Optics Letters*, **10(11)**, 523-525.

Fisher, N. R., Simpson, J. H., Howarth, M. J. (2002). Turbulent Dissipation in the Rhine ROFI Forced by Tidal Flow and Wind Stress. *Journal of Sea Research*, **48**, 249-258.

Fredsøe, J., Deigaard, R. (1992). Mechanics of Coastal Sediment Transport, *Advanced Series on Ocean Engineering, Volume 3*, World Scientific Publishing Co, Singapore.

Fugate, D. C., Friedrichs, C. T. (2002). Determining Concentration and Fall Velocity of Estuarine Particle Populations Using ADV, OBS and LISST. *Continental Shelf Research*, **22**, 1867-1886.

Fugate, D. C., Friedrichs, C. T. (2003). Controls on Suspended Aggregate Size in Partially Mixed Estuaries. *Estuarine, Coastal and Shelf Science*, **58**, 389-404.

Gibbs, R. J. (1985). Estuarine Flocs: Their Size, Settling Velocity and Density. *Journal of Geophysical Research*, **90**, 3249-3251.

Gibbs, R. J., Tshudy, D. M., Konward, L., Martin, J. M. (1989). Coagulation and Transport of Sediments in the Gironde Estuary. *Sedimentology*, **36**, 987-999.

Glenn, S. M., Grant, W. D. (1987). A Suspended Sediment Stratification Correction for Combined Wave and Current Flows. *Journal of Geophysical Research*, **92**, 8244-8264.

Green, M. O., McCave, I. N. (1995). Seabed Drag Coefficient under Tidal Currents in the Eastern Irish Sea. *Journal of Geophysical Research*, **100**, 16057-16070.

Hearn, C. J. (1985). On the Value of the Mixing Efficiency in the Simpson-Hunter h/u^3 Criterion. *Ocean Dynamics*, **38(3)**, 133-145.

Hey, R. D. (1979). Flow Resistance in Gravel-Bed Rivers. *Journal of the Hydraulics Division, ASCE*, **89**, 365-379.

Hill, P. S., Nowell, R. M., Jumars, P. A. (1992). Encounter Rate by Turbulent Shear of Particles Similar in Diameter to the Kolmogorov Scale. *Journal of Marine Research*, **50**, 643-668.

Hill, P. S., Voulgaris, G., Trowbridge, J. H. (2001). Controls on Floc Size in a Continental Shelf Bottom Boundary Layer. *Journal of Geophysical Research*, **106**, 9543-9549.

Ittekkot, V., Haake, B., Bartsch, M., Nair, R. R., Ramaswany, V. (1992). Organic Carbon Removal in the Sea: the Continental Connection. *Geological Society, London, Special Publications 1992*, **64**, 167-176.

Jiang, Q., Logan, B. E. (1991). Fractal Dimensions of Aggregates Determined from Steady-State Size Distributions. *Environmental Science and Technology*, **25**, 2031-2038.

Jago, C. F., Bale, A. J., Green, M. O., Howarth, M. J., Jones, S. E., McCave, I. N., Millward, G. E., Morris, A. W., Rowden, A. A., Williams, J. J. (1993). Resuspension Processes and Seston Dynamics, Southern North Sea. *Phil. Trans. R. Soc. London*, **A343**, 475-491.

Jago, C. F., Jones, S. E. (1998). Observation and Modelling of the Dynamics of Benthic Fluff Resuspended from a Sandy Bed in the Southern North Sea. *Continental Shelf Research*, **18**, 1255-1282.

Jago, C. F., Jones, S. E., Sykes, P., Rippeth, T. (2006). Temporal Variation of Suspended Particulate Matter and Turbulence in a High Energy, Tide-Stirred, Coastal Sea: Relative Contributions of Resuspension and Disaggregation. *Continental Shelf Research*, **26**, 2019-2028.

Johnston, R. J., Semple, R. K. (1983). Classification Using Information Statistics. *Concepts and Techniques in Modern Geography No. 37, GeoBooks, Norwich*, 43.

Jones, A. R. (1987). Fraunhofer Diffraction by Random Irregular Particles. *Particle Characterization*, **4**, 123-127.

Jumars, P. A. (1993). Sediment Transport and Bottom Boundary Layer Structure. *Concepts in Biological Oceanography: An Interdisciplinary Primer*, Oxford University Press, Ch15, 265-279.

Kanda, H. (1999). Computerized Model of Transition in Circular Pipe Flows. Part 2. Calculation of the Minimum Critical Reynolds Number. *Proc. of ASME Fluids Engineering Division - 1999*, ASME FED-Vol. **250**, 197-204.

Kawanisi, K., Yokosi, S. (1997). Characteristics of Suspended Sediment and Turbulence in a Tidal Boundary Layer. *Continental Shelf Research*, **17**, 859-875.

Kim, S. C., Friedrichs, C. T., Maa, J. P. Y., Wright, L. D. (2000). Estimating Bottom Stress in Tidal Boundary Layer from Acoustic Doppler Velocimeter Data. *Journal of Hydraulic Engineering*, **126**, 399-406.

Kirk, J. T. O. (1994). Light and Photosynthesis in Aquatic Ecosystems. *2nd Edition, Cambridge University Press*, New York, 256.

Klamer, J. C., Hull, R. N., Laane, R. W. P. M., Eisma, D. (1990). The Distribution of Heavy Metals and Polycyclic Aromatic Hydrocarbons in the Sediments of the Oyster Grounds (North Sea). *Netherlands Journal of Sea Research*, **26**, 83-87.

Knebel, H. J., Signell, R. P., Rendigs, R. R., Poppe, L. J., List J. H. (1999). Seafloor Environments in the Long Island Sound Estuarine System. *Marine Geology*, **155**, 277-318.

Knight, P. J., Howarth, M. J., Rippeth, T. P. (2002). Inertial Currents in the Northern North Sea. *Journal of Sea Research*, **47**, 269-284.

Kranck, K. (1973). Flocculation of Suspended Sediment in the Sea. *Nature*, **246**, 348-350.

Krank, K., Milligan, T. G. (1992). Characteristics of Suspended Particles At An 11-hour Anchor Station in San Francisco Bay, California. *Journal of Geophysical Research*, **97**, 11373-11382.

Kranenburg, C. (1994). The Fractal Structure of Cohesive Sediment Aggregates. *Estuarine, Coastal and Shelf Science*, **39**, 451-460.

Kundu, P. K. (1990). Fluid Dynamics, *Academic Press Inc., London.*

Lavelle, J. W., Mofjeld, H. O., Baker, E.T. (1984). An In-Situ Erosion Rate For A Fine Grained Marine Sediment. *Journal of Geophysical Research*, **89**, 6543-6552.

Law, D. J., Bale, A. J., Jones, S. E. (1997). Adaptation of Focused Beam Reflectance Measurement to In-Situ Particle Sizing in Estuaries and Coastal Waters. *Marine Geology*, **140**, 47-59.

Le Hir, P., Monbet, Y., Orvain, F (2007). Sediment Erodibility in Sediment Transport Modelling: Can We Account for Biota Effects? *Continental Shelf Research*, **27**, 1116-1142.

Li, D. H., Ganczarczyk, J. (1989). Fractal Geometry of Particle Aggregates Generated in Water and Wastewater Treatment Process. *Environmental Science and Technology*, **23**, 1385-1389.

Li, D. H., Ganczarczyk, J. (1990). Structure of Activated Sludge Flocs. *Biotechnology and Bioengineering*, **35**, 57-65.

Li, D. H., Ganczarczyk, J. (1992). Advective Transport in Activated Sludge Flocs. *Water Environment Research*, **64**, 236-240.

Lick, W. (1982). Entrainment, Deposition and Transport of Fine-Grained Sediments in Lakes. *Hydrobiologia*, **91-92**, 31-40.

Lick, W., Huang, H., Jepsen, R. (1993). Flocculation of Fine-Grained Sediments Due to Differential Settling. *Journal of Geophysical Research*, **98**, 10279-10288.

Lohrmann, A., Hackett, B., RØed, L. P. (1989). High Resolution Measurements of Turbulence, Velocity and Stress Using a Pulse-to-Pulse Coherent Sonar. *Journal of Atmospheric and Oceanic Technology*, **7**, 19-37.

Lu, Y., Lueck, R. G. (1999a). Using a Broadband ADCP in a Tidal Channel. Part I: Mean Flow and Shear. *Journal of Atmospheric and Oceanic Technology*, **16**, 1556-1567.

Lu, Y., Lueck, R. G. (1999b). Using a Broadband ADCP in a Tidal Channel. Part II: Turbulence. *Journal of Atmospheric and Oceanic Technology*, **16**, 1568-1579.

Lunven, M., Gentien, P. (2000). Suspended Sediments in a Macrotidal Estuary: Comparison and Use of Different Sensors. *Oceanologica Acta*, **23**, 245-260.

Lynch, J. F., Agrawal, Y. C., (1991). A Model-Dependent Method for Inverting Vertical Profiles of Scattering to Obtain Particle Size Spectra in Boundary Layers. *Marine Geology*, **99**, 387-401.

McCave, I. N. (1984). Size Spectra and Aggregation of Suspended Particles in the Deep Ocean. *Deep Sea Research*, **31**, 329-352.

Mahmood, K. (1971). Flow in Sand-Bed Channels. *Water Management Technical Report*, **11**, Colorado State University, Fort Collins, CO.

Manning, A. J., Dyer, K. R. (1999). A Laboratory Examination of Floc Characteristics With Regard To Turbulent Shearing. *Marine Geology*, **160**, 147-170.

McLean, S. R., Yean, J. (1987). Velocity and Stress in the Deep-Ocean Boundary Layer. *Journal of Physical Oceanography*, **17**, 1356-1365.

Meade, R. H. (1972). Sources and Sinks of Suspended Matter on Continental Shelves. In: Swift, D. J. P., Duane, D. B., Pilkey, O. H. (Eds.). *Shelf Sediment Transport: Processes and Patterns*, Dowden, Hutchinsons and Ross, Stroudsburg, Pa

Meakin, P. (1988). Fractal Aggregates. *Advances in Colloid and Interface Science*, **28**, 249-331.

Mehta, A. J. (1988). Laboratory Studies on Cohesive Sediment Deposition and Erosion. In: W. van Leussen, (Ed.), *Physical Processes in Estuaries*, Springer Verlag, Berlin, 427–445.

Mehta, A. J. (1991). Review Notes on Cohesive Sediment Erosion. *Coastal Sediments 1991*, 40-53.

Michallet, H., Mory, M. (2004). Modelling Of Sediment Suspensions in Oscillating Grid Turbulence. *Fluid Dynamics Research*, **35**, 87-106.

Mikkelsen, O. A., Curran, K. J., Hill, P. S., Milligan, T. G. (2007). Entropy Analysis of In-Situ Particle Size Spectra. *Estuarine, Coastal and Shelf Science*, **72**, 615-625.

Milligan, T. G., Kineke, G. C., Blake, A. C., Alexander, C. R., Hill, P. S. (2001). Flocculation and Sedimentation in the ACE Basin, South Carolina. *Estuaries*, **24**, 734-744.

Moody, J. A., Butman, B., Bothner, M. H. (1987). Near Bottom Suspended Matter Concentration on the Continental Shelf during Storms: Estimates Based on the In-Situ Observations of Light Transmission and a Particle Size Dependent Transmissometer Calibration. *Continental Shelf Research*, **7**, 609-628.

Mühlenweg, H., Hirleman, E. D. (1998). Laser Diffraction Spectroscopy Influence of Particle Shape and Shape Adaption Technique. *Particle and Particle Systems Characterisation*, **15**, 163-169.

Munk, W., Wunsch, C. (1998). Abyssal Recipes II: Energetics of Tidal and Wind Mixing. *Deep Sea Research I*, **45**, 1977-2010.

Namer, J. and Ganczarczyk, J. (1993). Settling Properties of Digested Sludge Particle Aggregates. *Water Research*, **27**, 1285-1294.

Nielsen, P. (1992). Coastal Bottom Boundary Layers and Sediment Transport, *Advanced Series on Ocean Engineering, Volume 4*, World Scientific Publishing Co, Singapore.

Nowell, A. R. M., Jumars, P. A., Eckman, J. E. (1980). Effects of Biological Activity on the Entrainment of Marine Sediments. *Marine Geology*, **42**, 133-153.

Odd, N. M. V., Cooper, A. J. (1989). A Two Dimensional Model of the Movement of Fluid Mud in a High Energy Turbid Estuary. *Journal of Coastal Research*, **5**, 185-194.

O'Melia, C. R. (1980). Aquasols: The Behaviour of Small Particles in Aquatic Systems. *Environmental Science and Technology*, **14**, 1052-1060.

Open University (1999). Waves, Tides and Shallow Water Processes. *Butterworth-Heinemann, Oxford.*

Parchure, T. M., Mehta, A. J. (1985). Erosion of Soft Cohesive Sediment Deposits. *Journal of Hydraulic Engineering,* **111**, 1308–1326.

Pedocchi, F., García, M. H. (2006). Evaluation of the LISST-ST Instrument for Suspended Particle Size Distribution and Settling Velocity Measurements. *Continental Shelf Research*, **26**, 943-958.

Prandtl, L. (1925). Bericht über Untersuchungen zur ausgebildeten Turbulenz. *Z. Angew. Math, Meth.*, **5**, 136-139.

Raudkivi, A. J. (1998). Loose Boundary Hydraulics. *Taylor and Francis.*

Reynolds, O. (1883). An Experimental Investigation of the Circumstances Which Determine Whether the Motion of Water in Parallel Channels Shall Be Direct or Sinuous and of the Law of Resistance in Parallel Channels. *Philos. Trans. R. Soc*, **174**, 935-982.

Richardson, L.F. (1922). Weather Predictions by Numerical Process. *Cambridge University Press, Cambridge.*

Rippeth, T. P., Fisher, N. R., Simpson, J. H. (2001). The Cycle of Turbulent Dissipation in the Presence of Tidal Straining. *Journal of Physical Oceanography*, **31**, 2458-2471.

Rippeth, T. P., Williams, E., Simpson, J. H. (2002). Reynolds Stress and Turbulent Energy Production in a Tidal Channel. *Journal of Physical Oceanography*, **32**, 1242-1251.

Rippeth, T. P., Simpson, J. H., Williams, E., Inall, M. E. (2003). Measurement of the Production and Dissipation of Turbulent Kinetic Energy in an Energetic Tidal Flow: Red Wharf Bay Revisited. *Journal of Physical Oceanography*, **33**, 1889-1901.

Sanford, L. P., Panageotou, W., Halka, J. P. (1991). Tidal Resuspension of Sediments in Northern Chesapeake Bay. *Marine Geology*, **97**, 87-103.

Shannon, C. E. (1948). A Mathematical Theory of Communication. *The Bell System Technical Journal*, **27**, 379-423, 623-656.

Simpson, J. H., Crawford, W. R., Rippeth, T. P., Campbell, A. R., Cheok, J. V. S. (1996). The Vertical Structure of Turbulent Dissipation in Shelf Seas. *Journal of Physical Oceanography*, **26**, 1579-1590.

Simpson, J. H., Fisher, N. R., Wiles, P. (2004). Reynolds Stress and TKE Production in an Estuary with a Tidal Bore. *Estuarine, Coastal and Shelf Science*, **60**, 619-627.

Simpson, J. H., Hughes, D. G., Morris, N. C. G. (1977). The relation of Seasonal Stratification to tidal Mixing on the Continental Shelf. In: A Voyage of Discovery (Ed. M. Amgel). *Deep Sea Research (Suppl.)*, 327-340.

Simpson, J. H., Hunter, J. R. (1974). Fronts in the Irish Sea. *Nature*, **250**, 404-406.

Soulsby, R. L. (1981). Measurement of the Reynolds Stress Components Close to a Marine Sand Bank. *Marine Geology*, **42**, 35-47.

Soulsby, R. L. (1983). The Bottom Boundary Layer of Shelf Seas. In: John, B. (Eds), *Physical Oceanography of Coastal and Shelf Seas*, Elsevier Oceanography Series, **35**, Amsterdam, 189-266.

Soulsby, R. (1997). *Dynamics of Marine Sands*, Thomas Telford Publications, London.

Stacey, M. T., Monismith, S. G., Burau, J. R. (1999). Measurements of Reynolds Stress Profiles in Unstratified Tidal Flow. *Journal of Geophysical Research*, **104**, 10933-10949.

Sternberg, R. W., Berhane, I., Ogston, A. S. (1999). Measurement of Size and Settling Velocity of Suspended Aggregates on the Northern California Continental Shelf. *Marine Geology*, **154**, 43-53.

Stow, D. A. V., Bowen, A. J. (1980). A Physical Model for the Transport and Sorting Of Fine-Grained Sediment by Turbidity Currents. *Sedimentology*, **27**, 31-46.

Tambo, N., Watanabe, Y. (1979). Physical Characteristics of Flocs – I. The Floc Density Function and Aluminium Floc. *Water Research*, **13**, 409-419.

Taylor, G. I. (1921). Diffusion by Continuous Movements. *Proc. of the London Mathematical Society*, **20**, 196.

Tennekes, H., Lumley, J. L. (1972). A First Course in Turbulence, *The MIT Press, Cambridge, Massachusetts.*

Thomas, H., Bozec, Y., Elkalay, K., de Baar, H. J. W. (2004). Enhanced Open Ocean Storage of CO2 from Shelf Sea Pumping. *Science*, **304**, 1005-1008.

Traykovski, P., Latter, R. J., Irish, J. D. (1999). A Laboratory Evaluation of the Laser In Situ Scattering and Tranmissometry Instrument Using Natural Sediments. *Marine Geology*, **159**, 355-367.

Trent, J. D., Shanks, A.L., Silver, M. W. (1978). In Situ and Laboratory Measurements on Macroscopic Aggregates in Monterey Bay, California. *Limnology and Oceanography*, **23**, 626-635.

Van Leussen, W. (1988). Aggregation of Particles, Settling Velocity of Mud Flocs-A Review. In: Dronkers, J., van Leussen, W. (Eds), *Physical Processes in Estuaries*, Springer-Verlag, New York, 348-403.

Van Leussen, W and Winterwerp, JC, (1990). Laboratory Experiments on Sedimentation of Fine-Grained Sediments: A State-of-the-art Review in the Light of Experiments with the Delft Tidal Flume. In: Cheng, RT (Ed), Residual currents and long-term transport. Coastal and Estuarine Studies 38. Springer-Verlag, New York. 241–259.

Van Leussen, W. (1997). The Kolmogorov Microscale as a Limiting Value for the Floc Sizes of Suspended Fine-Grained Sediments in Estuaries. In: Burt, N., Parker, R., Watts, J. (Eds.), *Cohesive Sediments*, John Wiley & Sons Ltd., New York, 45-62.

Von Karman, T (1930). Mechanische Ähnlichkeit und Turbulenz, Nachrichten der Akademie der Wissenschaften, Göttingen, Maths-Phys. Klasse, **58**.

Voulgaris, G., Meyers, S. T. (2004). Temporal Variability of Hydrodynamics, Sediment Concentration and Sediment Settling Velocity in a Tidal Creek. *Continental Shelf Research*, **24(15)**, 1659-1683.

White, M., Gaffney, S., Bowers, D. G., Bowyer, P. (2003). Interannual Variability in Irish Sea Turbidity and Relation to Wind Strength. *Biology and Environment: Proceedings of the Royal Irish Academy*, **103B(2)**, 83-90.

Wiesner, M. R. (1992). Kinetics of Aggregate Formation in Rapid Mix. *Water Research*, **26**, 379-387.

Williams, E., Simpson, J. H. (2004). Uncertainties in Estimates of Reynolds Stress and TKE Production Rate Using the ADCP Variance Method. *Journal of Atmospheric and Oceanic Technology*, **21**, 347-357.

Winterwerp, J. C. (1998). A Simple Model for Turbulence Induced Flocculation of Cohesive Sediment. *Journal of Hydraulic Research*, **36**, 309-326.

Winterwerp, J. C. (2002). On The Flocculation and Settling Velocity of Estuarine Mud. *Continental Shelf Research*, **22**, 1339-1360.

Wollast, R. (1998). Evaluation and Comparison of the Global Carbon Cycle in the Coastal Zone and in the Open Ocean. In Brink, K. H., Robinson, A. R. (Eds.), *The Global Coastal Ocean*, John Wiley & Sons, 213-252.

Wu, R. M., Lee, D. J. (1998). Hydrodynamic Drag Force Exerted on a Moving Floc and its Implication to Free-Settling Tests. *Water Research*, **32**, 760-768.

Wunsch, C. (1998). The Work Done By the Wind on the Oceanic General Circulation. *Journal of Physical Oceanography*, **28**, 2332-2340.

Xia, X. M., Li, Y., Yang, H., Wu, C. Y., Sing, T. H., Pong, H. K. (2004). Observations on the Size and Settling Velocity Distributions of Suspended Sediment in the Pearl River Estuary, China. *Continental Shelf Research*, In Press.

Zabawa, C. (1978). Microstructure of Agglomerated Suspended Sediments in Northern Chesapeake Bay Estuary. *Science*, **202**, 49-51.

Ziervogel, K., Bohling, (2003). Sedimentological Parameters and Erosion Behaviour of Submarine Coastal Sediments in the South-Western Baltic Sea. *Geo-Marine Letters*, **23**, 43-52.